

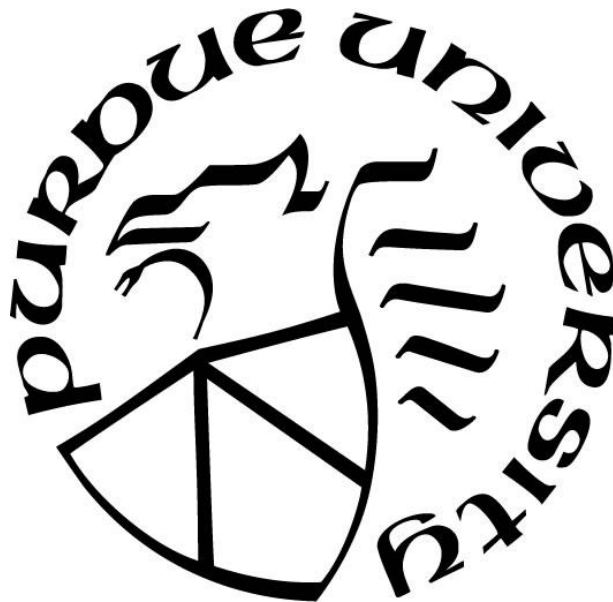
**THE DESIGN OF CONTINUOUS CHROMATOGRAPHY FOR
SEPARATION AND PURIFICATION**

by
David Harvey

A Dissertation

*Submitted to the Faculty of Purdue University
In Partial Fulfillment of the Requirements for the degree of*

Doctor of Philosophy



Davidson School of Chemical Engineering

West Lafayette, Indiana

May 2020

**THE PURDUE UNIVERSITY GRADUATE SCHOOL
STATEMENT OF COMMITTEE APPROVAL**

Dr. Nien-Hwa Linda Wang, Chair

Davidson School of Chemical Engineering

Dr. Sangtae Kim

Davidson School of Chemical Engineering

Dr. Raj Gounder

Davidson School of Chemical Engineering

Dr. Mary Wirth

Department of Chemistry

Approved by:

Dr. John Morgan

Dedicated to Christ my rock, Miranda my love, and my family who has supported me

ACKNOWLEDGMENTS

I would first like to acknowledge Prof. Nien-Hwa Linda Wang for her patience and guidance through my PhD. Without her tutelage the following dissertation would not have been possible. I would also like to thank Dr. Nicholas Soepriatna, Dr. George Weeden, Dr. Hoon Choi, Dr. Grace Chen, Mr. Yi Ding, Mr. Kai Jin, Mr. Clayton Gentilcore, and Mr. Zihao Liang for their input, discussions, and support. I am grateful to have worked in such an excellent research group.

I would like to thank Prof. Sangtae Kim, Prof. Raj Gounder, and Dr. Mary Wirth for serving on my committee. I appreciate your guidance and interest in my research.

I would also like to thank Dr. Michael Cordon, Mr. Garrett Mitchell, and Mr. Daniel Wilcox for their friendship and professional insight. Your insight and advice was valuable.

Funding for the research in this dissertation was provided by the National Science Foundation (CBET 1403854), the Purdue Process Safety and Assurance Center, the Davidson School of Chemical Engineering, and the Arvind and Karen Varma Fellowship.

TABLE OF CONTENTS

LIST OF TABLES	8
LIST OF FIGURES	10
ABSTRACT	13
1. INTRODUCTION	15
1.1 Background	15
1.2 Research Objectives	16
1.3 Research Approach	17
1.4 Outline of Dissertation	17
2. SPEEDY STANDING WAVE DESIGN AND SIMULATED MOVING BED SPLITTING STRATEGIES FOR THE SEPARATION OF TERNARY MIXTURES WITH LINEAR ISOTHERMS	19
2.1 Introduction to SMB	19
2.2 Theory	24
2.2.1 Standing wave design	24
2.2.2 Speedy standing wave design equations and dimensionless groups	27
2.2.3 Ideal Systems	34
2.2.4 Dispersion limited case	35
2.2.5 Diffusion limited case	35
2.3 Case study and simulation parameters	36
2.4 Results and Discussion	38
2.4.1 Verification of SSWD yields and effectiveness of splitting using rate model simulations	39
2.4.2 Effect of Retention Factors on Productivity	41
2.4.3 Effect of Retention Factors on Solvent Efficiency	45
2.4.4 Ring 2 of the Case Study	46
2.4.5 Effect of Column Configuration on Productivity and Solvent Efficiency	49
2.4.6 Design Rules Derived from SSWD Equations	50
2.5 Conclusions	52

3. STANDING-WAVE DESIGN OF THREE-ZONE, OPEN-LOOP NON-ISOCRATIC SMB FOR PURIFICATION	54
3.1 Introduction and Background for Non-Isocratic SMB	54
3.2 Methods.....	60
3.2.1 Adsorption Isotherms.....	63
3.2.2 Standing-Wave Design for Ideal, Linear, or Non-Linear Systems.....	64
3.2.3 Standing Wave Design for Non-Ideal Systems	65
3.2.4 Example Systems.....	69
3.2.5 Rate Model Simulations	74
3.3 Results.....	75
3.3.1 Results for Example 1.....	75
3.3.2 Results for Example 2.....	78
3.4 Discussion.....	80
3.4.1 Discussion of Example 1: Comparison with Optimal Batch Stepwise Elution.....	80
3.4.2 Discussion of Example 2: Comparison with Literature SMB	81
3.5 Conclusions.....	83
4. CONTINUOUS LIGAND-ASSISTED DISPLACEMENT FOR THE SEPARATION OF TWO OR THREE RARE EARTH ELEMENTS	84
4.1 Introduction and Background	84
4.2 Theory.....	88
4.2.1 Constant Pattern Design of Ligand-Assisted Displacement.....	89
4.2.2 Optimal Productivity	93
4.2.3 Continuous Chromatography Configuration	93
4.2.4 Multizone Design for Separation of Complex Mixtures	96
4.3 Materials and Methods.....	97
4.3.1 Materials	97
4.3.2 Column Loading and Preparation.....	97
4.3.3 Experiment 1 Separation of 2 Rare Earth Elements Using Continuous LAD.....	97
4.3.4 Experiment 2 Separation of 3 Rare Earth Elements Using Continuous LAD.....	99
4.3.5 Experiment 3 Separation of REEs from magnet simulant.....	102
4.3.6 Robustness Study.....	108

4.4	Results and Discussion	108
4.4.1	Experiment 1.....	108
4.4.2	Experiment 2.....	111
4.4.3	Stricter Purity Requirements.....	113
4.4.4	Separation and Purification of REEs from a Simulated Crude Magnet Mixture using a Two Zone Continuous LAD	114
4.4.5	Robustness Analysis	119
4.4.6	Advantages of Continuous LAD compared to Batch LAD and Liquid-Liquid Extraction.....	121
4.5	Conclusions.....	122
5.	CONCLUSIONS AND RECOMMENDATIONS	124
5.1	Conclusions.....	124
5.2	Recommendations.....	125
	APPENDIX A. STANDING WAVE EQUATIONS AND THE RELATION BETWEEN THE DECAY FACTOR β_{ij} AND THE YIELD Y_i	127
	APPENDIX B. IMPLEMENTATION OF SSWD	128
	APPENDIX C. OPERATING CONDITIONS FOR THE CASE STUDIES.....	132
	APPENDIX D. IMPLEMENTATION OF THE STANDING-WAVE DESIGN FOR NON-ISOCRATIC SYSTEMS	133
	APPENDIX E. ASPEN CHROMATOGRAPHY MODEL	136
	REFERENCES	137
	VITA.....	146
	PUBLICATIONS.....	147

LIST OF TABLES

Table 2.1 Summary of Steady State Multi-Component SMB Systems in Literature	21
Table 2.2 Summary of Dimensionless Groups used for SSWD	29
Table 2.3 Key SSWD Equations.....	31
Table 2.4 Summary of Intrinsic Parameters, System Parameters, and Simulation Parameters for Amino Acid Case Study in VERSE.....	37
Table 2.5 Description of Splitting Options: Ring 1 and Ring 2	37
Table 2.6 Case Specific Productivity and Solvent Efficiency Equations for Ternary Case Study	38
Table 2.7 Summary of Ring 1 Rate Model Simulation Results.....	39
Table 2.8 Comparison of Solvent Efficiency with Ideal Cases for Ring 1	45
Table 2.9 Summary of Ring 2 Rate Model Simulation Results. *Note: Feed values are based on the initial feed concentrations from Ring 1 (8 g/L)	46
Table 2.10 Differences Between Binary and Ternary Systems	51
Table 3.1 Chapter Notation Table of All Variables	62
Table 3.2 column and Simulation Parameters for Examples 1 and 2. All other parameters not shown in table can be found in Appendix E. Different Lumped resistance film modes were used based on the available data from the literature sources. Parameters taken from Candy et al. [1] and Cristancho and Seidel-Morgenstern [26].....	72
Table 3.3 Results for Example 1: Comparison with Optimal Batch. No pressure limit was set in Case 3. The pressure was calculated in Cases 1 and 2 using the Ergun Equation [42].	76
Table 3.4 Results for Example 2: Comparison with Literature pH-SMB for the Separation of Target antibody fragments from a competitive adsorbing impurity. *Length of 2.5 cm was selected due to commercial availability of this column size. The inner diameter of the columns in both cases was 0.7 cm.	78
Table 4.1 Simulation and Experimental Parameters.....	98
Table 4.2 Summary of Inlets, Outlets and Cycle Times for 2 Component LAD Separation of Sm and Nd. Column 2 was preloaded with copper at the beginning of cycle 1.	99
Table 4.3 Summary of Inlets, Outlets, Flowrates, and cycle times for ternary separation of REEs. In Table Detect refers to the outlet going to the detector. All flowrates are in mL/min, and MB refers to the mixed band solution.....	101
Table 4.4 Simulation parameters for Zone I of separation of REEs from magnet simulant.....	103

Table 4.5 Summary of Inlets, Outlets, Flowrates, and cycle times for separation of REEs from crude magnet feed. In Table Detect refers to the outlet going to the detector. All flowrates are in mL/min.....	104
Table 4.6 Simulation parameters for Zone IIa of the separation of REEs from magnet simulant	105
Table 4.7 Summary of Inlets, Outlets, Flowrates, and cycle times for separation of REEs from crude magnet feed in Zone IIa. Water washing and Copper regeneration steps done at 20 mL/min. All other flowrates set to 7.54 mL/min.....	106
Table 4.8 Simulation parameters for Zone IIb of the separation of REEs from magnet simulant	107
Table 4.9 Summary of Inlets, Outlets, Flowrates, and cycle times for separation of REEs from crude magnet feed in Zone IIa. Water washing and Copper regeneration steps done at 20 mL/min. All other flowrates set to 3.9 mL/min.....	107
Table 4.10 Binary Continuous LAD Separation Results. Minimum Target Yield of 73%	111
Table 4.11 Ternary Continuous LAD Separation Results Minimum Target Yield 69%.....	113
Table 4.12 Summary of Zone I Experimental Results.....	115
Table 4.13 Summary of Cycles 1 and 2 from Continuous Zone IIa using 2 Columns.....	116
Table 4.14 Summary of Cycle 1 from Continuous Zone IIb using 2 Columns	118
Table 4.15 Summary of yield and purity of Nd with a variety of concentrations. Target yield 78% with a breakthrough cut of 0.05 and a dead volume of 2 mL was used in all cases. Loading was held constant and the safety factor was based on the flowrate. The highlighted concentrations (red) are the concentrations that have been changed compared to the base case.	120
Table 4.16 Comparison of safety factors on the yield and purity of Nd with a variety of concentrations. Target yield 78% with a breakthrough cut of 0.05 and a dead volume of 2 mL. Loading was held constant. Safety factor was achieved by reducing the design column length.	121
Table 4.17 Comparison between conventional liquid-liquid extraction and Purdue technology	122

LIST OF FIGURES

Figure 2.1 (a) Binary ideal standing wave design profile (b) Ternary ideal standing wave profile. (c) Ternary standing wave profile with wave spreading. Waves are for Histidine (His), Phenylalanine (Phe), and Tryptophan (Trp). Example taken from the end of a step in Split 2. *Denotes a pinched wave.....	20
Figure 2.2 Overview of SSWD.....	28
Figure 2.3 Column profile at the beginning of a step for Ring 1 (a) Split 1, (b) Split 2, (c) Split 3, (d) Split 4, and (e) Split 5. Standing waves in each zone are labeled. *Denotes a pinched wave.....	40
Figure 2.4 (a) Dimensionless productivity as a function of $NDL, 3 *$ from case study. Solution curves for different splitting options. (b) Solvent efficiency as a function of $NDL, 3 *$ from case study.....	42
Figure 2.5 (a) Effect of Heavy Key Retention Factor when the Heavy Key is not the most Retained (Split 1). (b) Effect of Heavy Key Retention Factor when the Heavy Key is Most Retained (Split 2).....	44
Figure 2.6 Column profiles at the end of a step for Ring 2 at cyclic steady state. (a) Split 1, (b) Split 2, (c) Split 3, (d) Split 4a, € Split 4b, and (f) Split 5. Standing waves in each zone are labeled.	48
Figure 2.7 (a) Productivity as a function of $NDL, 3 *$ for different column configurations with 12 columns for Split 2. (b) Solvent efficiency as a function of $NDL, 3 *$ for different column configurations with 12 columns for Split 2. Similar Trends were observed in Split 1.....	50
Figure 3.1 Example of 3 column periodic counter current separation. In Zone III, the feed is loaded into the column. Zone II assures that the less retained component is contained so that it does not leak into the extract product. In Zone I, the desorbent is fed into the column to collect the more retained product as extract. The colors in this figure are the same as Fig. 3.1.	55
Figure 3.2 3-zone open-loop simulated moving bed	57
Figure 3.3 Overview of Standing Wave Design Inputs and Outputs. Complete list of variable definitions found in Table 3.1	60
Figure 3.4 Example column profile from 3-zone open-loop SMB. The plateau concentrations are denoted with the p and s subscripts. The * denotes the concentration before the feed port. Subscript R and E denotes raffinate concentration and extract concentration respectively. The concentrations with a numeral superscript denote the concentration of the feed into that zone which in both cases listed here is zero. Concentrations shown in middle step. Profile from Example 1 Case 1.	67
Figure 3.5 Langmuir “a” value for target protein for Example 1. The isotherm parameter for the impurity is not shown on this figure because it is a constant 1.6 and would not be easily visible on the scale shown in the figure. Adsorption done at pH 7.4 and desorption done at 5.4.....	70

Figure 3.6 Isotherm parameters for the fragment and impurity for Example 2. Adsorption will take place at a pH value of 7.0 and desorption will take place at a pH value of 3.8. The selectivity is greater at pH 7.0.....	73
Figure 3.7 Example profiles for SMB designed for Case 1 of Example 1 using SWD.....	77
Figure 3.8 Example profiles for SMB designed for Case 1 of Example 2 using SWD. Profiles shown at the middle of a step.....	79
Figure 4.1 Example of batch LAD Process Cycle. After Step 4, the cycle is repeated	85
Figure 4.2 Example of a Continuous LAD Process with 2 columns; recycle of the mixed bands is not shown for simplicity	87
Figure 4.3 General Map for Non-Ideal LAD Design for the Constant Pattern Design Method...	89
Figure 4.4 Detailed overview of 2 component continuous Ligand-Assisted Displacement Chromatography	94
Figure 4.5 Detailed overview of 3 component continuous Ligand-Assisted Displacement Chromatography	95
Figure 4.6 Cycle 1 of Experiment 1; Continuous Separation of Nd and Sm with VERSE simulations	109
Figure 4.7 Cycle 2 of Experiment 1: Continuous Separation of Nd and Sm. Time is based on total run time	110
Figure 4.8 Cycle 3 of Experiment 1: continuous Separation of Nd and Sm. Time started at the elution stage	110
Figure 4.9 Cycle 1 of Experiment 2: Continuous Separation of Sm, Nd, and Pr. The difference in concentration for Pr between the simulated and experimental Pr is likely due to the pH difference shifting the ligand efficiency during the experiment. This can also be seen in Fig. 4.10.....	112
Figure 4.10 Cycle 2 of Experiment 2: Continuous separation of Sm, Nd, and Pr.....	112
Figure 4.11 Chromatograph of Cycle 1 of Separation of Nd from Simulated Magnet Crude. The break at around 104 minutes is due to a temporary pause in the script due to instrument error. Dy fractions were collected every minute.	114
Figure 4.12 Chromatograph of Cycle 1 of Separation of Nd from Simulated Magnet Crude. Dy fractions were collected every thirty seconds.	115
Figure 4.13 Chromatograph of Dy Nd separation simulation (dotted line) with experimental data (solid line) for Cycle 1. The Capacity used in the simulation was 1.4 meq./mL for a 78.5 cm column (1.16 cm ID). The elution ligand was 0.09 M EDTA at pH 9. The row up of Dy is an artifact due to the pH change that occurs between the elution of copper and dysprosium.....	116
Figure 4.14 Chromatograph of Dy Nd separation simulation (dotted line) with experimental data (solid line) for Cycle 2. The Capacity used in the simulation was 1.4 meq./mL for a 78.5 cm column (1.16 cm ID). The elution ligand was 0.09 M EDTA at pH 9. The row up of Dy is an artifact due to the pH change that occurs between the elution of copper and dysprosium.....	117

Figure 4.15 Chromatograph of Nd and Pr separation simulation (dotted line) with experimental data (solid line) for Cycle 1. The Capacity used in the simulation was 1.35 meq./mL for a 78.5 cm column (1.16 cm ID). The elution ligand was 0.09 M EDTA at pH 9. The row up of Nd is an artifact due to the pH change that occurs between the elution of copper and neodymium. It is also possible that the detector had not stabilized after being hooked up further exaggerating the row up. This is because copper is also visible on the same wavelength as Nd meaning that the copper signal must be removed to see the Nd signal. 119

ABSTRACT

Continuous chromatography is an attractive alternative to traditional batch chromatography because it can have higher productivity, solvent efficiency, and product concentrations. However, several barriers prevent further use of continuous chromatography. There are many operating parameters that must be determined when designing continuous systems making it difficult to achieve high purity, yield, and productivity. Through the identification and strategic combination of the key dimensionless groups that control a continuous separation, it is possible to design highly productive systems that produce products with high yield and high purity. In this dissertation, three examples were selected to demonstrate the significance of a model-based method when designing continuous chromatography systems. (1) The Speedy Standing Wave Design and simulated moving bed splitting strategies for the separation of ternary mixtures with linear isotherm. (2) The Standing-wave Design of Three-Zone open-loop non-isocratic SMB for purification. (3) The Continuous Ligand-Assisted Displacement for the separation of Rare Earth Elements.

In the first example, the Speedy Standing Wave Design equations were developed for multicomponent separations with linear isotherms and a systematic splitting strategy was developed for the design of multiple sequential Simulated Moving Beds (SMBs). By performing the easiest split first, the overall productivity and solvent efficiency can be significantly improved. Rate model simulations were used to verify that the SSWD equations achieved target yields and purities. In systems where only one component is desired, the sorbent should be selected such that this component is the most or least retained so that it can be separated in a single SMB.

In the second example, the Standing Wave Design Method was extended to non-isocratic three zone open loop SMBs. The standing wave design equations were derived and then verified using rate model simulations. In two case studies it was shown that non-isocratic SMBs designed using the standing wave design show an order of magnitude higher productivity than a comparable batch system when the impurities are weakly adsorbing. When the impurities are competitive, the SWD method produces SMB systems with 2 orders of magnitude higher productivity than comparable batch systems. Because the design is based on dimensionless groups, the resulting designs are easily scalable and no rate model simulations are required to design high yield, high purity, and high productivity SMBs.

In the third example, the constant pattern design method was extended to continuous LAD systems. A continuous operation mode was developed that reduced the cycle time of LAD systems to further increase the productivity. In cases where the feed was equimolar, the continuous configuration increased the productivity between 20-50%. A multizone continuous LAD configuration was developed for the separation of a complex mixture of Dy, Nd, and Pr that simulated a crude magnet feed. The resulting overall productivity for this system was 190 kg/m³day which was two orders of magnitude higher than a single column batch system and 70% higher than a multizone batch system. The robustness of the constant pattern design method was demonstrated through a simulated case study and it was determined that adding a safety factor through the reduction of the flowrate was more effective than reducing the design length.

Using a model-based design allows for the consistent design of continuous chromatography systems. The effects of a change in a feed or operating condition can be more easily understood through the lens of the model. This means that adjustments can be made pre-emptively when necessary and the new designs can be tested with virtual experiments before being implemented. The understanding of key dimensionless groups allows for designs that meet key design criteria at all scales of operation and thus allows for the easy transition from one scale to another.

1. INTRODUCTION

1.1 Background

Chromatography is a technique that is used to a variety of separation and purification applications. In liquid chromatography, a mixture is fed into a column packed with a stationary phase. The stationary phase provides adsorption sites for the different components in the feed mixture. Components with lower affinities for the stationary phase elute earlier because they spend less time adsorbed on the stationary phase, and those with higher affinities elute later. In the batch configuration, the feed is loaded at the top of the column and the separated products are collected as they exit the column. This batch configuration is widely used in the chemical and pharmaceutical industry. However, in many applications it is limited by low sorbent utilization, low product concentration, and low solvent efficiency. Continuous chromatography has been introduced to address these limitations.

One common type of continuous chromatography is the simulated moving bed (SMB). Simulated moving bed chromatography was created by UOP in the 1960s. SMB has been shown to have higher productivity and solvent efficiency than comparable batch systems [1,2]. However, use of SMB has been limited due to the large number of parameters that must be determined and optimized to achieve a separation with high productivity, high purity and high yield. When designing a two SMB system for the separation of 3 components, there are 27 parameters that must be set. In cases where there are multicomponent separations, the design is further complicated by the variety of splitting options available. To address the large number of operating parameters that must be determined, this dissertation proposes using the strategic combination of variables and analysis using dimensionless groups. Utilizing these strategies can reduce the number of variables that require optimization. Using dimensionless parameters, a design method and splitting strategy were developed by extending the Speedy Standing Wave Design method to multicomponent separations with linear isotherms. A splitting strategy based on the key dimensionless groups that control the separation was also developed. Additionally, using a dimensionless basis for design means that solutions are easily scalable.

In cases where the SMB are non-isocratic, for example SMB systems with a pH step change, there are even more design parameters. When using a traditional closed SMB configuration, it

becomes difficult to control the pH in each of the SMB zones. In such cases, it becomes beneficial to use an open configuration. In an open configuration, the solvent is not recycled back through the loop. Instead, fresh solvent is used in each zone. This gives added flexibility in the zone velocity and the pH in each section or Zone of the SMB. Similarly, these systems are best designed using a strategic combination of variables and by analyzing the dimensionless groups that control the separation. This dissertation extends the standing wave design method to non-isocratic systems. The standing wave design equations provide a framework to design cost-effective separations that have high productivity, low solvent consumption, and high product concentration.

Ligand-assisted displacement chromatography is another chromatographic method that requires the determination of many operating parameters for the design of high purity, high yield, and high productivity separations. Before a systematic design method was developed for the design of LAD, experiments took as anywhere from days to months and suffered from low productivities and product concentrations [3]. Recently, the constant pattern design method was developed for batch LAD systems. This design method utilized strategic combination of variables and dimensionless groups analysis to determine the minimum column length to reach a constant pattern isotachic train in non-ideal systems. In this dissertation, the constant pattern design method was adapted to continuous systems to improve the column utilization and ultimately increase the overall productivity of LAD systems.

1.2 Research Objectives

Specifically, the objectives of this research are as follows: (1) Extend the Speedy Standing Wave design method to multicomponent linear and nonideal systems and develop a systematic splitting strategy for the design of tandem SMB systems. (2) Derive the Standing Wave equations for non-isocratic three zone SMB systems and develop a method based on the equations that allows for the design of high productivity, high yield, and high purity systems. (3) Extend the constant pattern design method for LAD systems to the continuous configuration to improve the productivity of LAD purifications while also testing the robustness of such LAD systems for real REE feeds.

1.3 Research Approach

The approach taken in each of these cases is to first collect preliminary data through either literature search or screening experiments. Then based on the information, a model using key dimensionless groups was developed for the design of chromatography systems. Next, rate model simulations were used to verify the model design. If possible, experiments were then performed to verify the accuracy of the model and rate model simulations. Corrections to the model were made to account for inconsistencies with either the rate model simulations or experiments.

1.4 Outline of Dissertation

This dissertation is divided into three separate sections. In each section, a different continuous chromatography application will be explored. In each case, the key dimensionless groups were identified through literature search or through screening experiments and then applied in a design method. Each chapter will discuss one of these different applications.

In Chapter 2, the speedy standing wave design method was extended for the design of SMB systems for the separation of ternary mixtures with linear isotherms. In this chapter, the speedy standing wave design is used to determine the optimal configuration, operating parameters, and splitting strategy for the separation of ternary mixtures with linear isotherms using SMB. The SSWD allows all the designs that meet purity and yield requirements to be solved simultaneously. Each design can then be compared in terms of productivity and solvent efficiency. In this chapter, the separation of amino acids is used as an example case study to demonstrate the effectiveness of the SSWD method.

In chapter 3, the standing wave design method was extended to non-isocratic 3-zone open loop separations with linear and Langmuir isotherms. The standing wave design equations were derived which allow for the design of non-isocratic SMB systems by solving algebraic equations with no rate model simulations or “trial and error”. The SMB systems designed using this method was compared to batch systems, and SMB systems designed using Triangle theory. Purification of antibodies and antibody fragments are used as example separation systems in this chapter. This study demonstrated that separations designed using The SWD method had an order of magnitude higher productivity than batch systems when the impurities are not competitively adsorbed on the

solid phase, and two orders of magnitude higher productivity when there was a competitive impurity.

In chapter 4, the constant pattern design method was extended to continuous LAD systems. This chapter shows the first demonstration of the continuous configuration for a LAD separation. This configuration was first demonstrated on binary and ternary equimolar mixtures. Then the continuous configuration was applied to the two-zone purification of rare earth elements from a complex mixture of Dy, Nd, and Pr that mimic the composition in a magnet crude. Compared to the single zone batch systems, the resulting separation has two orders of magnitude higher productivity compared to a single column batch system that gives similar productivity and yield.

The final chapter, (chapter 5) will give a summary of the major conclusions of this dissertation as well as recommendations for future work in the field of continuous chromatography related the projects discussed in the contained studies.

2. SPEEDY STANDING WAVE DESIGN AND SIMULATED MOVING BED SPLITTING STRATEGIES FOR THE SEPARATION OF TERNARY MIXTURES WITH LINEAR ISOTHERMS

Results in this chapter are reprinted from *J. of Chromatogr. A*, 1530 Speedy standing wave design and simulated moving bed splitting strategies for the separation of ternary mixtures with linear isotherms, 152-170 Copyright (2017), with permission from Elsevier.

2.1 Introduction to SMB

Simulated moving bed (SMB) chromatography was developed by UOP in 1961. It is an attractive alternative to traditional batch chromatography because it can have an order of magnitude higher productivity or solvent efficiency, and consequently much lower separation costs [4–7]. A simulated moving bed consists of a series of columns, which are connected to form a loop. Traditionally, a simulated moving bed has a feed port, a desorbent port, an extract port, and a raffinate port. The inlet and outlet ports divide the loop into four zones with different flow rates. The positions of these ports move at a regular interval to follow the migrating bands so that the feed is consistently added in a mixed band region and pure products can be drawn from the non-mixed band regions (Fig. 2.1).

SMB for the separation of a mixture of three or more components has been proposed and tested at lab scale in applications for betaine separation from sugars and molasses, purifications of sugars, separation of propylene glycol, recycling of ionic liquid, and separation of flame retardants from polymers as well as others [5,8–13]. It has also been developed and tested for the separation of multi- component mixtures in medical and pharmaceutical applications such as the purification of insulin [7,14,15]. This study is focused on steady state SMB systems. A summary of previous studies on the separation of three or more components using SMB can be found in Table 2.1. More complex unsteady state operations such as the JO system are not included in Table 2.1 [16].

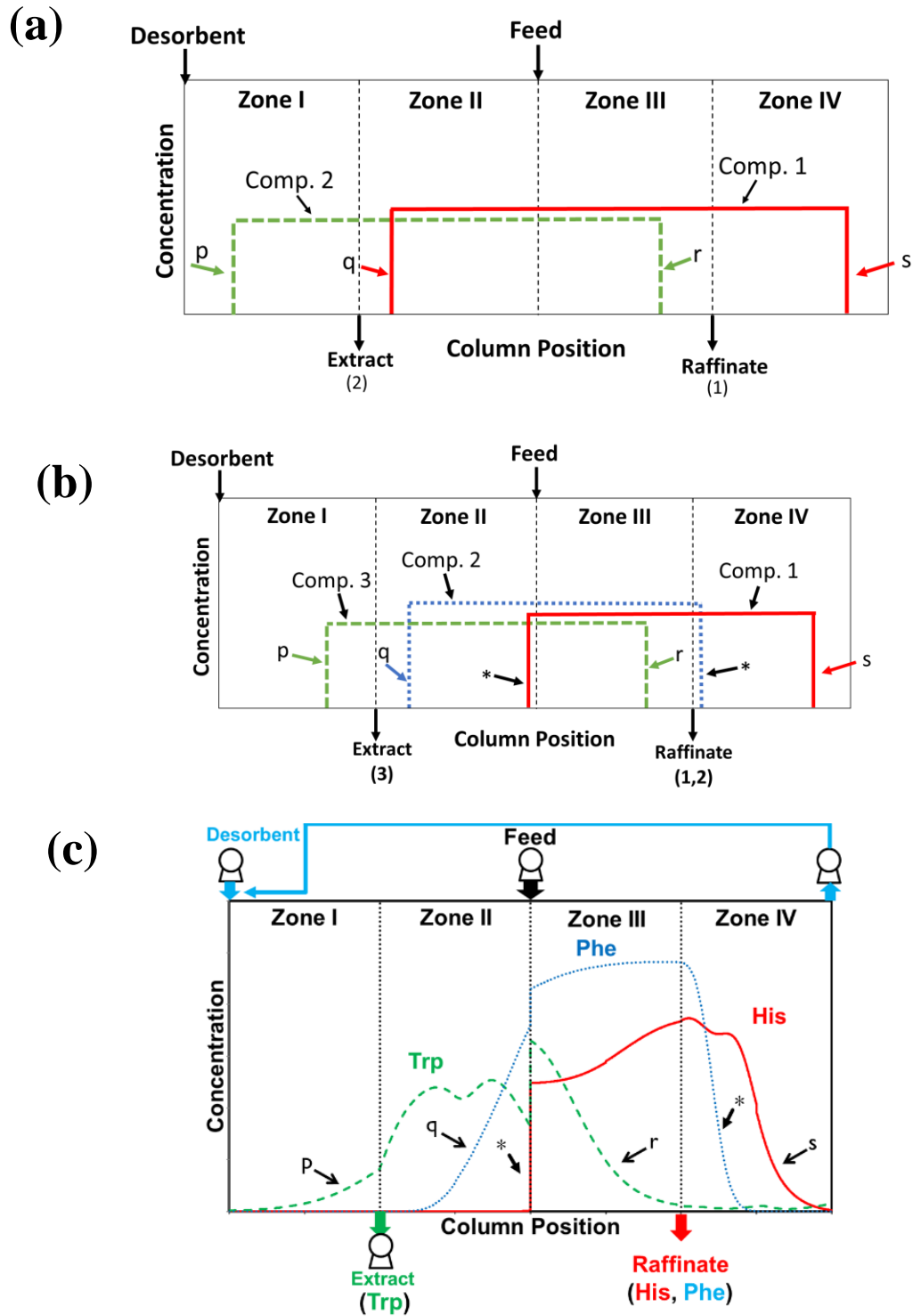


Figure 2.1 (a) Binary ideal standing wave design profile (b) Ternary ideal standing wave profile. (c) Ternary standing wave profile with wave spreading. Waves are for Histidine (His), Phenylalanine (Phe), and Tryptophan (Trp). Example taken from the end of a step in Split 2. *Denotes a pinched wave

Table 2.1 Summary of Steady State Multi-Component SMB Systems in Literature

First Author/Citation	Year	Components	Mechanism	Design Method	Process Description	Comments
Keikki Heikkila [8]	1992	Betaine, Sucrose, Molasses	Cation Exchange	Not Disclosed	Tandem Periodic Simulated Moving Bed	Separation of Sucrose and Betaine from Molasses
Benjamin Hritzko [13]	2002	Sulfuric Acid, Glucose, Xylose, Acetic Acid	Adsorption	Standing Wave Design	Tandem 4 zone SMB	Purification of sugars from acid impurities
Yi Xie [7]	2002	Insulin, High Molecular Weight Proteins, Zinc Chloride	Size Exclusion	Standing Wave Design	Tandem 4 zone SMB	Purification on Insulin from Protein and Zinc Chloride impurities
Yi Xie [9]	2005	Arabinose, Mannose, Xylose, Galactose, Glucose, Cellobiose, Sulfuric Acid, Acetic Acid, Furfural, Hydroxymethyl Furfural	Adsorption	Standing Wave Design	Single closed loop 5 zone SMB or tandem 4 zone SMB	Separation of 6 sugars from the 4 impurities
Thomas Binder [10]	2008	Propylene glycol, Ethylene glycol, Methanol, 2-propanol, Glycerol, Lactic acid, Glyceric acid, Butanediols, Sodium lactate, Sodium glycate	Ion Exclusion	Not Disclosed	Unspecified	Separation of propylene glycol and ethylene glycol from impurities
Ngoc Mai [11]	2012	Glucose, Xylose, Ionic Liquid	Ion Exclusion	Triangle Theory	Single Closed loop	Separation of ionic liquid from 2 sugars
George Weeden Jr. [5]	2015	2 Flame Retardants and a polymer (styrene acrylonitrile)	Size Exclusion	Speedy Standing Wave Design for SEC-SMB	Single Closed loop	Separation of 1 polymer from 2 flame retardants

Several barriers often hinder applications of SMB systems. Both binary and ternary systems have complex transient and cyclic steady state phenomena. The equipment is more complex than in batch chromatography, and experiments can be expensive and time-consuming. More importantly, for a four-zone SMB for ternary separation there are 27 design parameters, which include yields, equipment parameters, material properties, and operating parameters (see Section 2.2.2)., it is unclear how solvent consumption and sorbent productivity are related to the design parameters. Furthermore, because SMB only separates a mixture into two products, for ternary systems there are many ways to distribute the three components between the extract and the raffinate products (defined as the “splits” in this study). It is unclear how the splits will affect the productivity and solvent efficiency.

Even in cases with fixed feed composition, equipment parameters, yields, and material properties, there are still five operating parameters (four zone velocities and the average port velocity) that must be specified in the design. Several methods have been developed for determining these operating parameters for binary separation in SMB systems. One of the most widely used design methods is the “triangle” theory. Triangle theory works well for binary separation when mass transfer effects can be ignored (ideal systems). It utilizes adsorption parameters to define a triangular separation region in the plane of dimensionless zone II and III velocities [17–19]. This method has been extended to include zone I and zone IV dimensionless velocities as well [18,20]. Alternatively, the flow rate in zone I can be found using the separation volume method which takes mass transfer effects into account but requires simulations similar to that of the triangle method [21].

Because the triangle method is derived from ideal systems, for binary and ternary systems with significant mass transfer effects (non-ideal systems), a combination of numerous rate model simulations and a search program are required to find the operating parameters in the triangular region which can achieve a desired purity or yield [20,22]. Another weakness of the triangle method is that it does not give the solvent efficiency or productivity for non-ideal systems. Furthermore, the triangle method was developed for binary separation of an ideal system, and thus provides no guidance on how to split a ternary mixture for a non-ideal system.

An alternative method for determining the operating parameters for non-ideal systems is Standing Wave Design (SWD) developed by Ma and Wang in 1997 for linear binary systems [23]. SWD considers mass transfer effects and does not require rate model simulations to find the

operating conditions to achieve desired purity and yield for non-ideal systems. Given a fixed feed flow rate, yields, material properties, and equipment properties, SWD solves the five operating parameters from five algebraic equations, instead of searching for the operating conditions that satisfy the desired yield or purity using rate model simulations, which require solving differential equations or partial differential equations.

This method has been paired with a variety of optimization techniques such as grid search, genetic algorithms, and simulated annealing to find the optimal yields, zone lengths, or particle size [14,24–26]. It has been extended to non-linear systems and non-isothermal systems [27–30]. Pressure limits have also been considered using the SWD method [29,31,32]. SWD has been extended to three or more components in several applications [7,12–15,33]. The major advantage of SWD for multi-component splits is that it controls the yields of the components in the raffinate and extract products. This allows for a component that is either most retained or least retained to be recovered with high purity and high yield in one SMB, thus saving on both equipment and solvent costs. Basic splitting rules have also been developed for SWD, allowing for targeted distribution of products in the extract and raffinate streams [13].

Speedy Standing Wave Design (SSWD) method for size exclusion systems was developed by Weeden and Wang in 2015 [6]. This method utilizes dimensionless groups to reduce the number of variables and the design parameters and to elucidate how the design parameters are related to productivity or solvent efficiency. In SSWD, the dimensionless zone velocities (or zone velocities normalized by port velocity) were solved as functions of yields, dimensionless equipment parameters, material parameters, and for diffusion-controlled systems, a key dimensionless design parameter, which is the ratio of cycle time to a characteristic diffusion time. If yields, equipment parameters, and material properties are fixed, the operating parameters that give the minimum cost, the maximum productivity, or the maximum solvent efficiency can be calculated very quickly. The solutions also enable SSWD to show an overview of sorbent productivity, solvent efficiency, or separation costs for many viable designs over the entire range of port velocities. The SSWD method has been developed for binary systems with linear isotherms, but in ternary systems, only size exclusion systems have been considered [2,6].

The objectives of this chapter are: (1) to extend SSWD to systems with three or more adsorptive components with linear isotherms, (2) derive equations relating productivity (P_R) and solvent efficiency (F/D) to the design parameters, (3) explain how SSWD theory can be utilized

to design SMB for various splitting options, (4) verify, using rate model simulations, that the operating conditions solved from the SSWD equations can achieve target yields for the separation of three amino acids, (5) compare the PR and F/D for various splitting strategies using the ternary example system, and (6) to develop general guidelines for multicomponent splitting strategies to achieve high productivity or solvent efficiency for ternary systems. To fulfill the objectives, we first derive the SSWD equations for multicomponent systems with linear adsorption isotherms in terms of key dimensionless properties and dimensionless groups. We then obtain the general solutions for the solvent efficiency and productivity as functions of yields, equipment, material, and operating parameters. The limiting cases of ideal systems, dispersion limited systems, and diffusion limited systems will be discussed. The diffusion-controlled case is especially useful because in cases of high Peclet number ($P_{eb,i}^j$) the dispersion terms can be ignored. Attention will be given to the implementation of SSWD to demonstrate the methodology of utilizing the design method. Finally, a case study of a ternary example system will be used to show the effects of design parameters and splitting strategies on productivity and solvent efficiency. Larger differences in the retention factors of the heavy key and light key components, whose concentration waves confined to zones III and II respectively, are shown to give higher productivity and solvent efficiency. Minimizing the over- all range of retention factors can significantly improve the solvent efficiency. These insights will be used to develop general guidelines for designing SMB systems for the separation of ternary mixtures. If multiple splits are required for the separation, the easiest split should be done first for higher productivity or solvent efficiency

2.2 Theory

2.2.1 Standing wave design

The standing wave design equations are derived from the steady state solutions for a true moving bed system. For an ideal, binary system, the key wave velocity in each zone is matched with the port velocity (v). Because the ports move at the same velocity of the waves, the waves appear to be “standing” relative to the ports (Fig. 2.1a). For an ideal ternary system, components 1 (the least retained component) and 2 can be recovered in the raffinate and component 3 (the most retained component) can be recovered in the extract. To achieve this split, the desorption wave of component 3 is standing in zone I, the desorption wave of component 2 is standing in zone II, the

adsorption wave of component 3 is standing in zone III, and the adsorption wave of component 1 is standing in zone IV (Fig. 2.1b). A ternary feed mixture is split into two products in SMB, as a feed mixture is split into a light product and a heavy product in distillation. The terms “heavy key” and “light key” are borrowed from distillation to describe the components between which the split will occur. In this case component 3 is the heavy key and component 2 is the light key. In this study, “p” will refer to the component standing in zone I, “q” is the component standing zone II also referred to as the light key component because it is prevented from eluting in the extract product, “r” is the component standing in zone III also known as the heavy key component because it is prevented from eluting in the raffinate stream, and “s” is the component standing in zone IV.

In addition to standing waves, binary, ternary, and other multi-component SMB systems can have “pinched waves” [34,35]. Pinched waves are waves that are “pinched” at a boundary between two zones. An example of pinched waves can be seen in Fig. 2.1b (indicated by the *). The adsorption wave for component 2 is pinched at the zone boundary between zones III and IV. Component 2 cannot migrate faster than component 1 in zone IV because it has a higher affinity for the sorbent, and it must migrate faster than component 3 in zone III. Thus, the adsorption wave of component 2 is “pinched” at the zone boundary between the two zones. The desorption wave of component 1 is “pinched” at the boundary between zones II and III. Because the desorption wave of component 2 is “standing” in zone II, the desorption wave of component 1 is forced to the boundary since it migrates faster than component 2. At the same time, the desorption wave of component 1 cannot exist stably in zone III because it would migrate faster than component 2 which is standing. Therefore, the stable solution is for it to be pinched at the boundary. In the pinched wave design method, the flow rates are selected to “pinch” the waves to increase the robustness of the process. In ternary systems, pinched waves occur naturally based on the retention factors of components relative to the retention factors of the standing components in those zones [34,35].

For ideal systems, Eqs. (1a)–(1d) the wave velocity of each standing component is set equal to the port velocity, where $u_{w,i}^j$ is defined as the wave velocity of the key component “i” in zone “j”. For linear adsorption isotherms, these wave velocities are also expressed in terms of the zone velocity (u_0^j) for zone “j” by using the retention factor (δ) and phase ratio (ϕ). The phase ratio is defined as $(1 - \varepsilon_b)/\varepsilon_b$, where ε_b is the bed void fraction. Eq. (2), which is based on the mass

balance around zone II, zone III, and the feed port, is paired with Eq. (1) to solve for the four zone velocities (u_0^j) and the port velocity (v). u_F is the feed velocity.

$$u_{w,p}^I = v = \frac{u_0^I}{1 + \phi \delta_p} \quad (1a)$$

$$u_{w,q}^{II} = v = \frac{u_0^{II}}{1 + \phi \delta_q} \quad (1b)$$

$$u_{w,r}^{III} = v = \frac{u_0^{III}}{1 + \phi \delta_r} \quad (1c)$$

$$u_{w,s}^{IV} = v = \frac{u_0^{IV}}{1 + \phi \delta_s} \quad (1d)$$

$$u_F = u_0^{III} - u_0^{II} \quad (2)$$

In non-ideal systems, the adsorption and desorption waves spread because of mass-transfer effects (see Fig. 2.1c). Wave spreading can lead to breakthrough into adjacent zones if it is not accounted for when determining zone velocities. One can focus the waves toward the zone boundaries if the zone I and zone II wave velocities are higher than the port velocity, whereas the zone III and zone IV wave velocities are lower than the port velocity. For this reason, a mass-transfer correction term (Δ_i^j) is added to Eq. (1) to counter wave spreading, as seen in Eqs. (3a)–(3d).

$$u_0^I = (1 + \phi \delta_p)v + \Delta_p^I \quad (3a)$$

$$u_0^{II} = (1 + \phi \delta_q)v + \Delta_p^{II} \quad (3b)$$

$$u_0^{III} = (1 + \phi \delta_q)v + \Delta_p^{III} \quad (3c)$$

$$u_0^{IV} = (1 + \phi \delta_q)v + \Delta_p^{IV} \quad (3d)$$

The mass transfer correction terms have been derived previously and are shown in Eq. (4) [29–32]. The results of substituting Eq. (4) into Eq. (3) are shown in Appendix A.

$$\Delta_i^j \equiv \frac{\beta_i^j}{L^j} \left(E_{b,i}^j + \frac{\phi \delta_i^2 v^2}{K_i^j} \right) \quad (4)$$

In this equation, δ_i is the retention factor for linear adsorption isotherms defined in Eq. (5), β_i^j is the decay factor, defined as the natural log of the ratio of the maximum concentration of I in zone j to the minimum concentration of I in zone j (more detailed definition is in Appendix A),

$E_{b,i}^j$ is the axial dispersion coefficient, L^j is the zone length, and K_i^j is the overall mass transfer coefficient, which is related to other parameters in Eq. (6) for linear systems.

$$\delta_i = \varepsilon_p K_{se,i} + (1 - \varepsilon_p) a_i + \frac{DV}{1 - \varepsilon_b} \quad (5)$$

$$\frac{1}{K_i^j} = \frac{R_p^2}{15 K_{se,i} \varepsilon_p D_{p,i}} + \frac{R_p}{3 k_{f,i}^j} \quad (6)$$

In these equations, DV is the dimensionless dead volume (in terms of column volume), a_i is the Langmuir “a” or linear term in terms of solid volume, $K_{se,i}$ is the size exclusion factor, $D_{p,i}$ is the pore diffusivity, ε_p is the particle porosity, R_p is the particle radius, and $k_{f,i}^j$ is the film mass transfer resistance of component i. In most systems with large particles, the film mass transfer resistance is negligible so the second term in Eq. (3) is assumed to be zero. Although Eq. (1) is strictly for linear adsorption isotherms, it can be used as an approximation for nonlinear systems in preliminary analysis.

2.2.2 Speedy standing wave design equations and dimensionless groups

SSWD reduces the total number of variables in the SWD equations through a combination of dimensionless variables and dimensionless groups (see Fig. 2.2) to reduce the total variables in a ternary system from 27 to 16. For a ternary system, the four dimensionless SWD equations (see Eq. (11), Table 2.3) reduce the number of variables by four. The number of variables is reduced by three because of the nondimensionalization. Furthermore, the combination of variables reduces the number of variables by four. This is done by combining the Langmuir “ a_i ” terms with the dead volume and the three size exclusion factors in the form of the effective retention factors (see Eq. (5)). A summary of the dimensionless variables and groups can be found in Table 2.2.

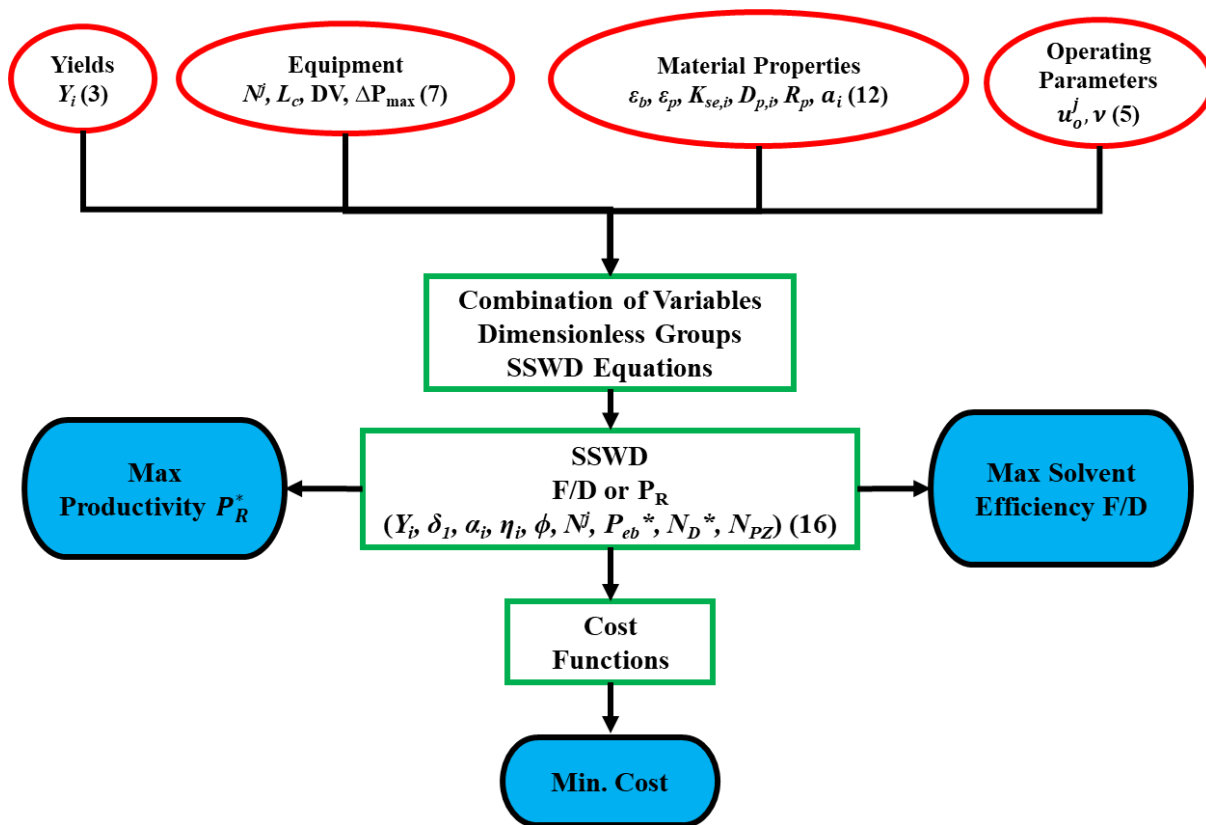


Figure 2.2 Overview of SSWD

Table 2.2 Summary of Dimensionless Groups used for SSWD

Symbol	Name	Definition	Description
α_i	Selectivity	$\frac{\delta_i}{\delta_1}$	Ratio of retention factor to retention factor of component 1
η_i	Diffusivity Ratio	$\frac{K_{se,i}D_{p,i}}{K_{se,1}D_{p,1}}$	Ratio of intraparticle diffusivity multiplied by ratio of size exclusion ratios
$N_{D,i}$	-	$\frac{\phi \varepsilon_p K_{se,i} D_{p,i} L_c}{\nu R_p^2}$	Step time relative to diffusion time
$N_{DL,i}$	-	$N_{D,i} N$	Cycle time relative to diffusion time
$P_{eb_i}^j$	Peclet Number	$\frac{\nu L_c}{E_{b,i}^j}$	Ratio of dispersion time to cycle time
$\frac{1}{\Gamma^j}$	Resistance to mass transfer	$\frac{P_{eb_i}^j}{P_{eb_p}^j} = \frac{\frac{\nu L_c}{E_{b,i}^j}}{\frac{\nu L_c}{E_{b,p}^j}} = \frac{E_{b,p}^j}{E_{b,i}^j}$	Ratio of axial dispersion coefficients from zone 1 to zone j
$N_{DL,n}^*$	-	$\frac{t_{cy}}{t_{D,n} \phi \delta_n} = \frac{N_{D,i} N}{\phi \delta_n}$	Modified $N_{DL,i}$
$P_{eb_l}^*$	-	$\phi \delta_n P_{eb}^j N$	Modified Peclet Number
N_{PZj}	-	$f^j \delta_n N_{DL,n}^* \left[\frac{u_0^j}{\nu} \right]^{-1}$	Cycle time relative to diffusion time at pressure limit
f^j	Zone Fraction	$\frac{N^j}{N}$	Fraction of total columns within a specific zone

Among the key dimensionless groups are $N_{D,i}$ and $N_{DL,n}^*$. Eq. (7) shows that $N_{D,i}$ multiplied by the number of columns (N) is the ratio of the cycle time to the diffusion time. Whereas $N_{DL,n}^*$ normalizes this dimensionless group by the product of the retention factor of the most retained component (n , $n=3$ for ternary separations) and the phase ratio (see Eq. (8)).

$$N_{D,i}N = \frac{\phi \varepsilon_p K_{se,i} D_{p,i} L_c N}{\nu R_p^2} = \frac{t_{cy}}{t_D} \quad (7)$$

$$N_{Dl,n}^* = \frac{N_{D,i}N}{\phi \delta_n} = \frac{t_{cy}}{t_D \phi \delta_n} \quad (8)$$

Another key dimensionless group is the Peclet number for the components in different zones $P_{eb_i}^j$ which is defined in Eq. (9a).

$$P_{eb_i}^j = \frac{\nu L_c}{E_{b,i}^j} \quad (9a)$$

$$E_b^j = 10 \varepsilon_b R_p u_0^j \quad (9b)$$

According to the Chung and Wen correlation, the axial dispersion coefficient ($E_{b,i}^j$) reduces to Eq. (9b) for low Reynolds number systems [36]. $E_{b,i}^j$ is independent of the component or $E_{b,i}^j = E_b^j$. This means that Peclet number is also the same for all components in each zone and thus can be written as P_{eb}^j . In the SSWD equations it is useful to put all the equations in terms of the Peclet number for the first zone. This is accomplished using the axial dispersion ratio as defined in Table 2.2. Additionally, the zone I Peclet number is modified to give P_{ebt}^* as defined in Eq. (10).

$$P_{ebt}^* = \phi \delta_n P_{eb}^j N \quad (10)$$

When put in terms of $N_{D,i}$ and $P_{eb_i}^j$ the dimensionless zone velocities equations are expressed in Eq. (11a)-(11d) (See Table 2.3), where η_i is the ratio of the interparticle diffusivity multiplied by the ratio of the size exclusion ratios.

Table 2.3 Key SSWD Equations

General	Eq.	Diffusion Controlled	Eq.
$\frac{u_0^I}{\nu} = 1 + \phi\delta_p + \frac{\beta_p^I}{P_{eb}^I N^I} + \frac{\phi^2 \delta_p^2 \eta_n \beta_p^I}{15 N_{D,n} \eta_p N^I}$	(11a)	$\frac{u_0^I}{\nu} = 1 + \phi\delta_p + \frac{\phi^2 \delta_p^2 \eta_n \beta_p^I}{15 N_{D,n} \eta_p N^I}$	(23a)
$\frac{u_0^{II}}{\nu} = 1 + \phi\delta_q + \frac{\beta_q^{II} \Gamma^{II}}{P_{eb}^{II} N^{II}} + \frac{\phi^2 \delta_q^2 \eta_n \beta_q^{II}}{15 N_{D,n} \eta_q N^{II}}$	(11b)	$\frac{u_0^{II}}{\nu} = 1 + \phi\delta_q + \frac{\phi^2 \delta_q^2 \eta_n \beta_q^{II}}{15 N_{D,n} \eta_q N^{II}}$	(23b)
$\frac{u_0^{III}}{\nu} = 1 + \phi\delta_r - \frac{\beta_r^{III} \Gamma^{III}}{P_{eb}^{III} N^{III}} - \frac{\phi^2 \delta_r^2 \eta_n \beta_r^{III}}{15 N_{D,n} \eta_r N^{III}}$	(11c)	$\frac{u_0^{III}}{\nu} = 1 + \phi\delta_r - \frac{\phi^2 \delta_r^2 \eta_n \beta_r^{III}}{15 N_{D,n} \eta_r N^{III}}$	(23c)
$\frac{u_0^{IV}}{\nu} = 1 + \phi\delta_s - \frac{\beta_s^{IV} \Gamma^{IV}}{P_{eb}^{IV} N^{IV}} - \frac{\phi^2 \delta_s^2 \eta_n \beta_s^{IV}}{15 N_{D,n} \eta_s N^{IV}}$	(11d)	$\frac{u_0^{IV}}{\nu} = 1 + \phi\delta_s - \frac{\phi^2 \delta_s^2 \eta_n \beta_s^{IV}}{15 N_{D,n} \eta_s N^{IV}}$	(23d)
$P_R^* = \frac{1}{N_{DL,n}} \left[\phi(\delta_r - \delta_q) - \frac{1}{P_{eb}^I N} \left(\frac{\beta_r^{III} \Gamma^{III}}{f^{III}} + \frac{\beta_q^{II} \Gamma^{II}}{f^{II}} \right) - \frac{\phi^2}{15 N_{DL,1}} \left(\frac{\beta_r^{III} \delta_r^2}{f^{III} \eta_r} + \frac{\beta_q^{II} \delta_q^2}{f^{II} \eta_q} \right) \right] \quad (14)$			
$\frac{F}{D} = \frac{\phi(\delta_r - \delta_q) - \frac{1}{P_{eb}^I N} \left(\frac{\beta_r^{III} \Gamma^{III}}{f^{III}} + \frac{\beta_q^{II} \Gamma^{II}}{f^{II}} \right) - \frac{\phi^2}{15 N_{DL,1}} \left(\frac{\beta_r^{III} \delta_r^2}{f^{III} \eta_r} + \frac{\beta_q^{II} \delta_q^2}{f^{II} \eta_q} \right)}{\phi(\delta_p - \delta_s) + \frac{1}{P_{eb}^I N} \left(\frac{\beta_p^I}{f^I} + \frac{\beta_s^{IV} \Gamma^{IV}}{f^{IV}} \right) + \frac{\phi^2}{15 N_{DL,1}} \left(\frac{\beta_p^I \delta_p^2}{f^I \eta_p} + \frac{\beta_s^{IV} \delta_s^2}{f^{IV} \eta_s} \right)} \quad (17)$			
$P_R^* = \frac{1}{N_{DL,n}} \left[\phi(\delta_r - \delta_q) - \frac{\phi^2}{15 N_{DL,1}} \left(\frac{\beta_r^{III} \delta_r^2}{f^{III} \eta_r} + \frac{\beta_q^{II} \delta_q^2}{f^{II} \eta_q} \right) \right] \quad (24)$			
$\frac{F}{D} = \frac{\phi(\delta_r - \delta_q) - \frac{1}{P_{eb}^I N} \left(\frac{\beta_r^{III} \Gamma^{III}}{f^{III}} + \frac{\beta_q^{II} \Gamma^{II}}{f^{II}} \right) - \frac{\phi^2}{15 N_{DL,1}} \left(\frac{\beta_r^{III} \delta_r^2}{f^{III} \eta_r} + \frac{\beta_q^{II} \delta_q^2}{f^{II} \eta_q} \right)}{\phi(\delta_p - \delta_s) + \frac{1}{P_{eb}^I N} \left(\frac{\beta_p^I}{f^I} + \frac{\beta_s^{IV} \Gamma^{IV}}{f^{IV}} \right) + \frac{\phi^2}{15 N_{DL,1}} \left(\frac{\beta_p^I \delta_p^2}{f^I \eta_p} + \frac{\beta_s^{IV} \delta_s^2}{f^{IV} \eta_s} \right)} \quad (25)$			

In the evaluation of SMB systems, both sorbent productivity and solvent efficiency are key to process cost. Productivity of component “I” is defined as the amount produced per unit mass sorbent over a time, Eq. (12), where S is the cross-sectional area of the column, and ρ_p is the particle density.

$$P_{R,i} = \frac{S \varepsilon_b u_F Y_i C_{F,i}}{SNL_C (1 - \varepsilon_b) \rho_p} = \frac{S \varepsilon_b (u_0^{III} - u_0^I) Y_i C_{F,i}}{SNL_C (1 - \varepsilon_b) \rho_p} \quad (12)$$

Through the substitution of Eq. (11) into Eq. (12) and simplification of variables, the following form of productivity is derived in Eq. (13).

$$P_{R,i} = \frac{\nu Y_i C_{F,i}}{NL_C \phi \rho_p} \left[\phi(\delta_r - \delta_q) - \frac{1}{P_{eb}^I N} \left(\frac{\beta_r^{III} \Gamma^{III}}{f^{III}} + \frac{\beta_q^{II} \Gamma^{II}}{f^{II}} \right) - \frac{\phi^2}{15 N_{DL,1}} \left(\frac{\beta_r^{III} \delta_r^2}{f^{III} \eta_r} + \frac{\beta_q^{II} \delta_q^2}{f^{II} \eta_q} \right) \right] \quad (13)$$

Productivity is then put into dimensionless form in terms of P_R^* by substituting ν with the expression for $N_{DL,n}$ and then dividing Eq. (13) by the rest of the term outside the bracket to give Eq. (14) in Table 2.3.

This form of the productivity elucidates the relationship between material properties and productivity, Eq. (13). A larger difference in heavy key and light key retention factors gives a higher productivity. For a non-ideal system, the mass transfer correction terms are related to diffusion resistances and proportional to δ^2/η which is the square of the retention factors of the heavy key and light key components divided by their effective diffusivity relative to that of the fastest solute. The larger the magnitude of the retention factors, the more pronounced the diffusion correction terms become. Eq. (13) suggests that the best possible case is for the light key retention factor (δ_q) to be 0. This would maximize the difference between the light and heavy key retention factors and eliminate the diffusion terms for that component. It is interesting to note that because productivity is dependent on the difference between the heavy key and light key retention factors, there is no difference in productivity if the target product is the heavy key or light key component.

One measure of solvent efficiency is the ratio of volumetric feed flow rate to volumetric desorbent flow rate (F/D). Feed flow rate can be calculated using Eq. (15), and desorbent flow rate can be calculated using Eq. (16).

$$F = \varepsilon_b S(u_0^{III} - u_0^{II}) \quad (15)$$

$$D = \varepsilon_b S(u_0^I - u_0^{IV}) \quad (16)$$

When the SSWD equations for zone flow rate are substituted into Eq. (15) and Eq. (16) and the ratio is taken of the two equations, the expression for solvent efficiency is derived in Eq. (17), Table 2.3. This equation shows that solvent efficiency is related to the retention factors and diffusivity of the components in every zone. Solvent efficiency can also be increased with a large difference in heavy key and light key retention factors. For a set difference in heavy key and light key retention factors, the total range of retention factors should then be minimized to reduce the denominator of Eq. (17). Additionally, larger retention factors increase the mass transfer correction terms, decreasing the solvent efficiency. Large effective diffusivities improve the solvent efficiency by decreasing the mass transfer correction terms.

The forms of the productivity and solvent efficiency equations given previously are useful for explaining the relationship between physical properties and performance. The SSWD equations can also be placed in terms of both $N_{DI,n}^*$ and P_{ebl}^* . When this is done, the retention factors are converted to selectivities. These new forms, seen in Appendix B, provide the additional advantages of easing convergence in extreme cases (i.e. $K_{se,1} = 0$) and using a normalized $N_{DI,n}^*$, which allows

for comparisons across applications. This form is also consistent with the binary SSWD method reported previously [31].

It should be noted that all the designs are subject to pressure limits. The pressure through each zone can be calculated using the simplified Ergun equation (without the term due to turbulence) shown in Eq. (18) [37].

$$\Delta P = \frac{37.5\mu L_c u_0^1 \phi^2 N^j}{R_p^2} \quad (18)$$

ΔP is the pressure drop across the column, and μ is the viscosity of the fluid in the column. This can be used given a maximum pressure determined from equipment available. Any designs that do not meet the pressure requirements should not be considered. The pressure limited ratio of convection time of component j to the most retained component is defined as N_{PZj} and can be found in Table 2.2.

While material properties have a major effect on SMB productivity, the column configuration of the SMB can also have a major effect. The SSWD equations allow for the optimization of distribution of columns across zones for productivity by optimizing zone fractions. In Eq. (14), it is evident that the zone fractions for zones I and IV have no effect on the column productivity. Therefore, like in binary systems, the number of columns in those zones should be minimized. The optimal zone fractions for zones II and III can be solved by taking the partial derivative of Eq. (14) with respect to f^{II} , bearing in mind that f^{III} is a function of f^{II} , and then setting the resulting expression equal to zero. The result is Eqs. (19a)–(19d). The zone lengths thus can be adjusted to improve the productivity of an SMB by matching the optimal zone fractions as closely as possible with the number of available columns. It should be noted, in systems with large mass transfer effects, more than one column may be necessary per zone due to differences between the true moving bed solution and simulated moving bed.

$$f^I = \frac{1}{N} \quad (19a)$$

$$f^{II} = \sqrt{\frac{\beta_q^{II} \eta_r (NP_{eb}^I \delta_q^2 \phi^2 + 15N_{DL,1} \eta_q \Gamma^{II})}{\beta_r^{III} \eta_q (NP_{eb}^I \delta_r^2 \phi^2 + 15N_{DL,1} \eta_r \Gamma^{III})}} f^{III} \quad (19b)$$

$$f^{III} = \frac{1 - f^I - f^{IV}}{1 + \sqrt{\frac{\beta_q^{II} \eta_r (NP_{eb}^I \delta_q^2 \phi^2 + 15N_{DL,1} \eta_q \Gamma^{II})}{\beta_r^{III} \eta_q (NP_{eb}^I \delta_r^2 \phi^2 + 15N_{DL,1} \eta_r \Gamma^{III})}}} \quad (19c)$$

$$f^{IV} = \frac{1}{N} \quad (19d)$$

2.2.3 Ideal Systems

For an ideal system, the zone flow rates are given by Eq. (1). In these cases, the diffusion rate is infinite meaning that $N_{DL,n}$ has no physical meaning. The productivity cannot be nondimensionalized into P_R^* in the same way as non-ideal systems. Because there are no diffusion effects, the productivity is proportional to the port velocity that is selected. This means that for maximum productivity, the port velocity should be increased to the pressure limit. The expression for the productivity is Eq. (20).

$$P_{R,i} = \frac{(\delta_r - \delta_q) \nu Y_i C_{F,i}}{NL_C} \quad (20)$$

Larger differences in heavy key and light key retention factors predict higher productivity at a given port velocity. The mass transfer terms in the solvent efficiency equation (Eq. (17), Table 2.3) can be ignored in the ideal case as well. The simplified solvent efficiency equation is Eq. (21).

$$\left(\frac{F}{D}\right)_{ideal} = \frac{\delta_r - \delta_q}{\delta_p - \delta_s} \quad (21)$$

Eq. (21) indicates that solvent efficiency is not only dependent on $(\delta_r - \delta_q)$, but also $(\delta_p - \delta_s)$. Unlike in a two-component case, the solvent efficiency for an ideal system is not always one. Furthermore, it is beneficial to have a smaller difference in $(\delta_p - \delta_s)$ for higher solvent efficiency. Because the differences determine the value for solvent efficiency, the target compound can be either the heavy key or light key component without penalty. The ideal solvent efficiency (Eq. (21)) can be used as a crude estimate for comparing between multiple splitting options, as will be seen in the case study in Section 4.3. Higher solvent efficiency results in higher extract product concentrations.

2.2.4 Dispersion limited case

If the Peclet number is small, the dispersion term becomes large relative to the diffusion term in Eq. (14), Table 2.3. In this case, dispersion has the dominant effects on wave spreading. The Chung and Wen correlation estimate of the axial dispersion term is shown in Eq. (9b). When this is substituted into the Peclet number definition and multiplied by N, Eq. (22) is the result:

$$P_{eb}^I N = \frac{Nv}{u_0^I \varepsilon_b} 10 \left(\frac{L_C}{R_p} \right) \quad (22)$$

If the ratio of column length to particle radius is 1000 or higher, then the $1/P_{eb}^I N$ will generally be on the order of 10^{-3} . The coefficient of the diffusion term of Eq. (14) is typically on the order of 10^{-1} meaning that the dispersion effects are negligible compared to the diffusion effects. For this reason, the dispersion limited case will not be discussed at length here. The general SSWD equations with dispersion are useful in sugar separations, where viscous fingering results in large dispersion of the concentration waves [32].

2.2.5 Diffusion limited case

In cases where the Peclet number is very large ($L_C/R_p > 1,000$), the dispersion term can be ignored, leading to the zone velocity equations, Eqs. (23a)–(23d) in Table 2.3. Eqs. (23a)–(23d) can then be substituted into the definitions of productivity and solvent efficiency given in Eqs. (12), (15), and (16) to give Eqs. (24) and (25) in Table 2.3. These forms of the productivity and solvent efficiency equations are particularly useful because they apply whenever a sufficiently long column is used. The equations simplify significantly when the dispersion terms are negligible, and they were used in the case study.

Optimal column configuration for productivity for diffusion limited cases

The same procedure performed to optimize column configuration in the general case can be done using the equations simplified for the diffusion limited case. Eqs. (26a)–(26d) are the result. These equations can be used to optimize the number of columns in each zone, thus further improving productivity. Because of the simplified nature of these equations compared to those in the general case, they can provide a crude estimation of optimal column configuration before more extensive calculations.

$$f^I = \frac{1}{N} \quad (26a)$$

$$f^{II} = \sqrt{\frac{\beta_q^{II} \eta_r \delta_q^2}{\beta_r^{III} \delta_r^2 \eta_q}} f^{III} \quad (26b)$$

$$f^{III} = \frac{1 - f^I - f^{IV}}{1 + \sqrt{\frac{\beta_q^{II} \eta_r \delta_q^2}{\beta_r^{III} \delta_r^2 \eta_q}}} \quad (26c)$$

$$f^{IV} = \frac{1}{N} \quad (26d)$$

2.3 Case study and simulation parameters

This section will describe the ternary example and the simulation parameters used in the study. The example selected is the separation of a mixture of Histidine (His), Phenylalanine (Phe), and Tryptophan (Trp). A summary of the intrinsic parameters, system parameters, and simulation parameters are given in Table 2.4. The adsorption parameters for Phe and Trp were taken from Wu et al. [38]. Histidine was estimated as a non-adsorbing component. The column configuration and column length were fixed. The operating parameters were optimized using the SSWD method for maximum productivity at 99% yield of each component. The operating parameters are summarized in Table B1 in Appendix B. All simulations were performed using the VERSE program developed in 1991 for batch chromatography and extended to SMB in 2002 [13,39]. The VERSE simulations for SMB have been verified with experimental data in more than 10 different systems [5,7,9,13,29,31–33,38,40]. In this case study, the target yields and intended splits of the SMB processes design using the diffusion controlled SSWD method were verified using VERSE simulations.

Table 2.4 Summary of Intrinsic Parameters, System Parameters, and Simulation Parameters for Amino Acid Case Study in VERSE

L_c (cm)	Column Diameter (cm)	R_p (μm)	ε_b	ε_p	φ	DV	Y	$E_{b,i}^j$	Film Mass Transfer Coefficient
25	5	160	0.37	0.55	1.60	0.017	0.99	Chung and Wen	Wilson and Geankoplis
Component		K_{se}	a (per SV)	D_p (cm^2/min)		δ	α	η	C_F (g/L)
Histidine (His)		1.0	0.00	6.55×10^{-5}		0.58	1.00	1.0	8.0
Phenylalanine (Phe)		1.0	1.61	6.55×10^{-5}		1.30	2.25	1.0	8.0
Tryptophan (Trp)		1.0	10.73	6.55×10^{-5}		5.41	9.36	1.0	8.0
Axial Elements	Step Size	Collocation Points				Tolerance			
101	0.01	Axial		Particle		Absolute		Relative	
		4		2		0.0001		0.001	

When the desired component is either the most retained or least retained component, only one SMB is needed. If the middle component is a desired product, then two SMBs in series (tandem SMB) will be needed. In a 3-component system, there are 5 possible splitting options. A full summary of the splitting options is listed in Table 2.5. In Split 1 the least retained is separated from the rest, while in Split 2, most retained is separated and removed in its pure form. If all three components are desired products, then Ring 2 of Splits 1 and 2 can be used to purify the mixed products from Ring 1. If the middle component is the desired product, then Splits 3–5 can also be used. Splits 3–5 control the separation of only 2 out of the 3 components, allowing the third component to distribute in both the extract and the raffinate ports. In Split 4, the middle component is the distributed product, and therefore, a third SMB is required for high yield. The SSWD equations for productivity and solvent efficiency can be found for each splitting option in Table 2.6. In the case study, the mixed product from the first SMB (Ring 1) is sent directly to the second SMB (Ring 2) without a concentration step.

Table 2.5 Description of Splitting Options: Ring 1 and Ring 2

Split	Ring 1 R/E	Ring 2 R/E	Ring 1 Standing Waves (p-q-r-s)	Ring 2 Standing Waves (p-q-r-s)
1	1/2,3	2/3	3-1-2-1	3-2-3-2
2	1,2/3	1/2	3-2-3-1	2-1-2-1
3	1,2/1,3	1/2	3-2-3-2	2-1-2-1
4a	1,2/2,3	1/2	3-1-3-1	2-1-2-1
4b	1,2/2,3	2/3	3-1-3-1	3-2-3-2
5	1,3/2,3	2/3	2-1-2-1	3-2-3-2

Table 2.6 Case Specific Productivity and Solvent Efficiency Equations for Ternary Case Study

Split Option	Diffusion Controlled Productivity	Diffusion Controlled Solvent Efficiency
Split 1 (3-1-2-1)	$\frac{1}{N_{DL,3}^*} \left[\left(\frac{\alpha_2}{\alpha_3} - \frac{\alpha_1}{\alpha_3} \right) - \frac{\eta_3}{15N_{DL,3}^* \alpha_3^2} \left(\frac{\beta_2^{III} \alpha_2^2}{f^{III} \eta_2} + \frac{\beta_1^{II} \alpha_1^2}{f^{II} \eta_1} \right) \right]$	$\frac{\left(\frac{\alpha_2}{\alpha_3} - \frac{\alpha_1}{\alpha_3} \right) - \frac{\eta_3}{15N_{DL,3}^* \alpha_3^2} \left(\frac{\beta_2^{III} \alpha_2^2}{f^{III} \eta_2} + \frac{\beta_1^{II} \alpha_1^2}{f^{II} \eta_1} \right)}{\left(1 - \frac{\alpha_1}{\alpha_3} \right) + \frac{\eta_3}{15N_{DL,3}^* \alpha_3^2} \left(\frac{\beta_3^I \alpha_3^2}{f^I \eta_3} + \frac{\beta_1^{IV} \alpha_1^2}{f^{IV} \eta_1} \right)}$
Split 2 (3-2-3-1)	$\frac{1}{N_{DL,3}^*} \left[\left(1 - \frac{\alpha_2}{\alpha_3} \right) - \frac{\eta_3}{15N_{DL,3}^* \alpha_3^2} \left(\frac{\beta_3^{III} \alpha_3^2}{f^{III} \eta_3} + \frac{\beta_2^{II} \alpha_2^2}{f^{II} \eta_2} \right) \right]$	$\frac{\left(1 - \frac{\alpha_2}{\alpha_3} \right) - \frac{\eta_3}{15N_{DL,3}^* \alpha_3^2} \left(\frac{\beta_3^{III} \alpha_3^2}{f^{III} \eta_3} + \frac{\beta_2^{II} \alpha_2^2}{f^{II} \eta_2} \right)}{\left(1 - \frac{\alpha_1}{\alpha_3} \right) + \frac{\eta_3}{15N_{DL,3}^* \alpha_3^2} \left(\frac{\beta_3^I \alpha_3^2}{f^I \eta_3} + \frac{\beta_1^{IV} \alpha_1^2}{f^{IV} \eta_1} \right)}$
Split 3 (3-2-3-2)	$\frac{1}{N_{DL,3}^*} \left[\left(1 - \frac{\alpha_2}{\alpha_3} \right) - \frac{\eta_3}{15N_{DL,3}^* \alpha_3^2} \left(\frac{\beta_3^{III} \alpha_3^2}{f^{III} \eta_3} + \frac{\beta_2^{II} \alpha_2^2}{f^{II} \eta_2} \right) \right]$	$\frac{\left(1 - \frac{\alpha_2}{\alpha_3} \right) - \frac{\eta_3}{15N_{DL,3}^* \alpha_3^2} \left(\frac{\beta_3^{III} \alpha_3^2}{f^{III} \eta_3} + \frac{\beta_2^{II} \alpha_2^2}{f^{II} \eta_2} \right)}{\left(1 - \frac{\alpha_2}{\alpha_3} \right) + \frac{\eta_3}{15N_{DL,3}^* \alpha_3^2} \left(\frac{\beta_3^I \alpha_3^2}{f^I \eta_3} + \frac{\beta_2^{IV} \alpha_2^2}{f^{IV} \eta_2} \right)}$
Split 4 (3-1-3-1)	$\frac{1}{N_{DL,3}^*} \left[\left(1 - \frac{\alpha_1}{\alpha_3} \right) - \frac{\eta_3}{15N_{DL,3}^* \alpha_3^2} \left(\frac{\beta_3^{III} \alpha_3^2}{f^{III} \eta_3} + \frac{\beta_1^{II} \alpha_1^2}{f^{II} \eta_1} \right) \right]$	$\frac{\left(1 - \frac{\alpha_1}{\alpha_3} \right) - \frac{\eta_3}{15N_{DL,3}^* \alpha_3^2} \left(\frac{\beta_3^{III} \alpha_3^2}{f^{III} \eta_3} + \frac{\beta_1^{II} \alpha_1^2}{f^{II} \eta_1} \right)}{\left(1 - \frac{\alpha_1}{\alpha_3} \right) + \frac{\eta_3}{15N_{DL,3}^* \alpha_3^2} \left(\frac{\beta_3^I \alpha_3^2}{f^I \eta_3} + \frac{\beta_1^{IV} \alpha_1^2}{f^{IV} \eta_1} \right)}$
Split 5 (2-1-2-1)	$\frac{1}{N_{DL,3}^*} \left[\left(\frac{\alpha_2}{\alpha_3} - \frac{\alpha_1}{\alpha_3} \right) - \frac{\eta_3}{15N_{DL,3}^* \alpha_3^2} \left(\frac{\beta_2^{III} \alpha_2^2}{f^{III} \eta_2} + \frac{\beta_1^{II} \alpha_1^2}{f^{II} \eta_1} \right) \right]$	$\frac{\left(\frac{\alpha_2}{\alpha_3} - \frac{\alpha_1}{\alpha_3} \right) - \frac{\eta_3}{15N_{DL,3}^* \alpha_3^2} \left(\frac{\beta_2^{III} \alpha_2^2}{f^{III} \eta_2} + \frac{\beta_1^{II} \alpha_1^2}{f^{II} \eta_1} \right)}{\left(\frac{\alpha_2}{\alpha_3} - \frac{\alpha_1}{\alpha_3} \right) + \frac{\eta_3}{15N_{DL,3}^* \alpha_3^2} \left(\frac{\beta_2^I \alpha_2^2}{f^I \eta_2} + \frac{\beta_1^{IV} \alpha_1^2}{f^{IV} \eta_1} \right)}$

2.4 Results and Discussion

Rate model simulations were done as specified in Section 3 for each potential splitting option for the ternary separation example. The simulated column profiles verify that the splits were controlled using the SSWD. A summary of the results of the simulations for Ring 1 can be found in Table 2.7. The case study compares several possible splitting strategies for the separation of three components. The effects of retention factor on productivity and solvent efficiency are demonstrated in the case study. The effect of column configuration on productivity is also demonstrated. The results of this case study are paired with the SSWD equations to develop general guidelines for ternary SMB separations.

Table 2.7 Summary of Ring 1 Rate Model Simulation Results

Split Option	Standing Waves (p-q-r-s)	$C_{Phe} / C_{i,feed}$	$C_{His} / C_{i,feed}$	$C_{Trp} / C_{i,feed}$	P_R^*	F/D	Y_{target}	Y_{Phe}	Y_{His}	Y_{Trp}
1	3-1-2-1	0.036	0.65	0.036	0.06	0.04	0.99	0.99	0.99	0.99
2	3-2-3-1	0.70	0.70	0.30	0.11	0.27	0.99	1.00	1.00	0.99
3	3-2-3-2	0.88	0.72	0.31	0.12	0.30	0.99	0.99	1.00	0.99
4	3-1-3-1	0.69	0.97	0.29	0.17	0.29	0.99	1.00	1.00	0.99
5	2-1-2-1	0.37	0.72	0.26	0.06	0.32	0.99	0.99	0.98	0.98

2.4.1 Verification of SSWD yields and effectiveness of splitting using rate model simulations

Given target yields (99%), material properties, and equipment parameters (see Table 2.4), the SSWD method was used to find the operating parameters to achieve maximum productivity for each of the splitting options (See Appendix C). The operating parameters were used in rate model simulations to obtain column profiles and effluent histories. The yields were calculated from the VERSE simulated effluent history and compared with the target yields from the SSWD. The results in Table 2.7 verify that the simulated yields agree within 1% with the target yields specified in SSWD for all five splits.

Simulated column profiles at the beginning of a step for Ring 1 at cyclic steady state for all five splitting strategies are shown in Fig. 2.3. The profiles indicate that the SSWD splitting strategies were successful. As expected, all the specified standing waves in the SSWD were confined to their respective zones. In Fig. 2.3a the desorption wave of Phe is pinched in the boundary between zone I and zone II. The adsorption wave of Trp is pinched at the boundary between zone II and zone III. In Fig. 2.3b, the pinched waves also occur. The desorption wave of His is pinched at the boundary between zone II and zone III, and the adsorption wave of Phe is pinched at the boundary between zone III and zone IV. Fig. 2.3c and 2.3e show the wrap of His and Trp respectively across all four zones. In Fig. 2.3d, Phe is distributed between the extract and the raffinate, but because both the desorption and adsorption waves are pinched, Phe does not wrap the same way as seen in Fig. 2.3c or 2.3e.

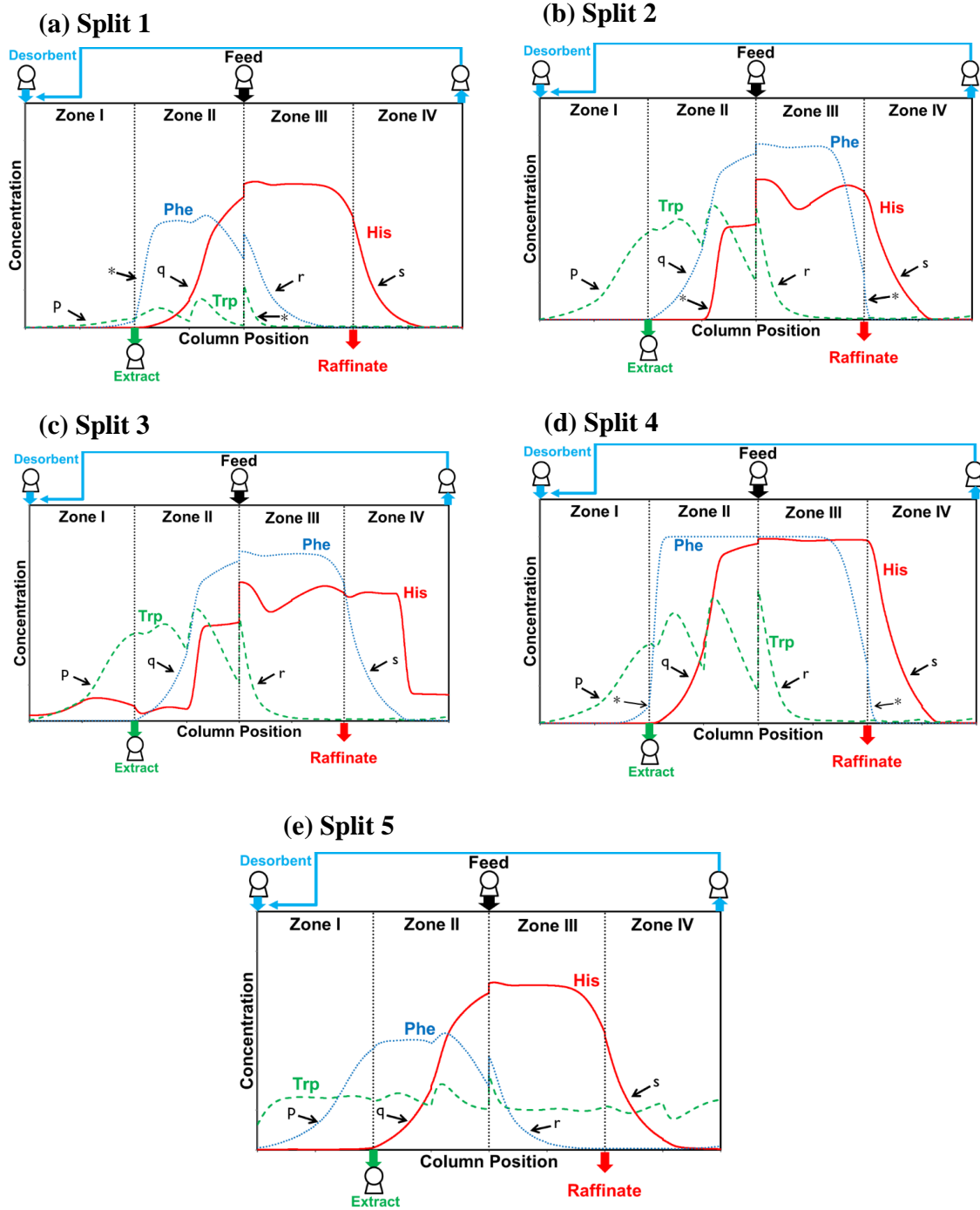


Figure 2.3 Column profile at the beginning of a step for Ring 1 (a) Split 1, (b) Split 2, (c) Split 3, (d) Split 4, and (e) Split 5. Standing waves in each zone are labeled. *Denotes a pinched wave.

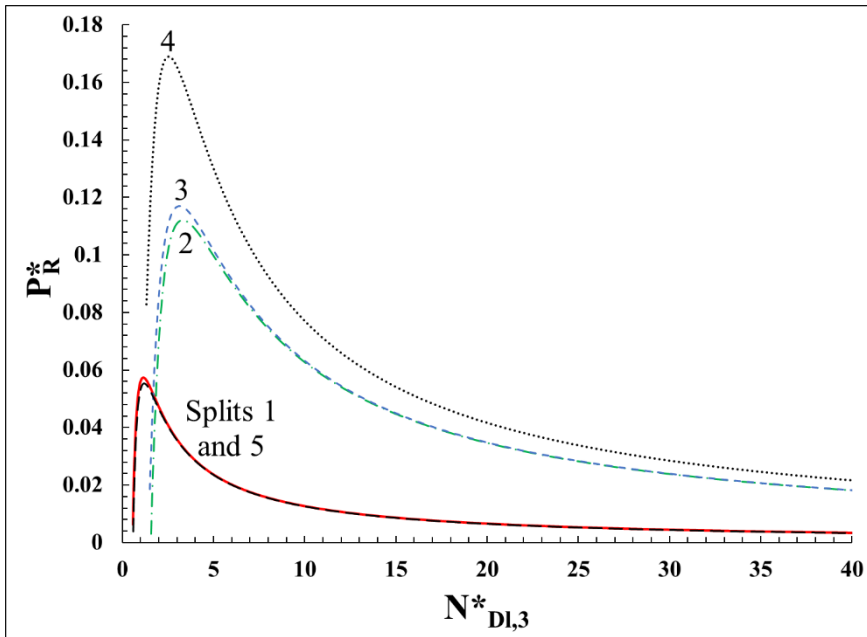
2.4.2 Effect of Retention Factors on Productivity

As expected from the SSWD equations, productivity is dependent on the retention factors of only the heavy key and light key components. This is easily seen in the ideal case, Eq. (26), but is also true when considering mass transfer effects. This is demonstrated when comparing Splits 1 and 5, or Splits 2 and 3 (see Table 2.7). Splits 1 and 5 have the same heavy key and light key components and thus have the same maximum productivity within the slight differences caused by differences in $N_{Dl,n}$ due to small differences in port velocity between the different cases. This is true in Splits 2 and 3 as well. These cases have the same heavy and light key components but differ in components standing in zones I and IV.

Figure 2.4a shows dimensionless productivity as a function of $N_{Dl,3}^*$ for all the splits. A maximum productivity is shown for every split as expected from Eq. (30). At small values of $N_{Dl,3}^*$, the effect of the diffusion term is large because it is proportional to $(1/N_{Dl,3}^*)^2$, but as $N_{Dl,3}^*$ increases, the first term (proportional to $1/N_{Dl,3}^*$) dominates. The net result of these two terms is a peak, showing the maximum productivity at a specific value of $N_{Dl,3}^*$ for each split.

As expected from Eq. (30), the peak productivity for the splits with larger differences in heavy key and light key retention factors is larger. While Split 4 has the highest dimensionless productivity, it would require an additional SMB to obtain pure products. It is shown in Fig. 2.4a that the productivity curves of Split 1 and Split 5 are nearly identical and Splits 2 and 3 are very similar as well. As predicted from the SSWD equations (see Table 2.7), only the retention factors of the heavy and light key components affect the productivity of the system.

(a)



(b)

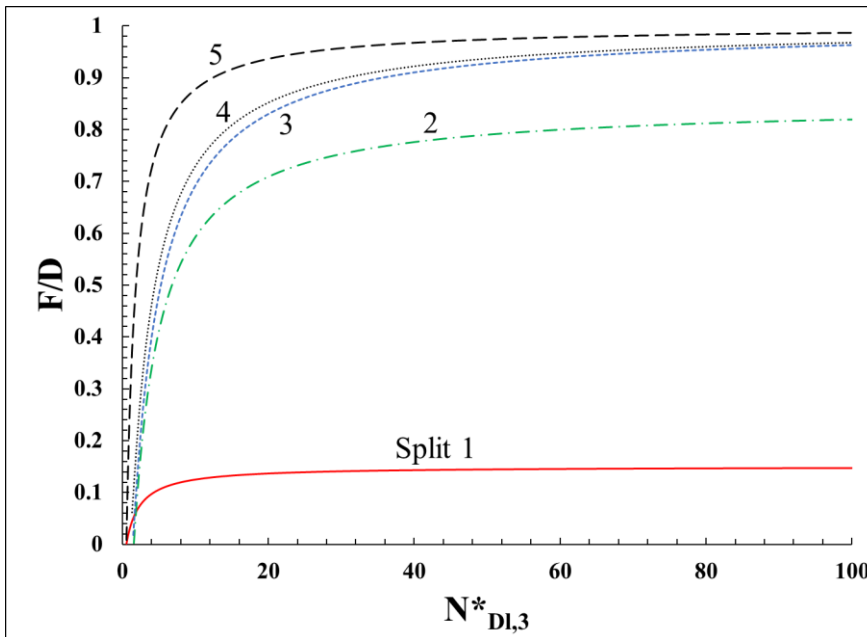


Figure 2.4 (a) Dimensionless productivity as a function of $N_{DL,3}^*$ from case study. Solution curves for different splitting options. (b) Solvent efficiency as a function of $N_{DL,3}^*$ from case study

The effect of the heavy key retention factor was investigated by examining the maximum productivity over a range of retention factor values when the material and equipment properties from the case study are fixed. The results can be seen in Fig. 2.5. This was done for two cases: (1) when the heavy key component is not the most retained component in the system, similar to Split 1 in the case study (see Fig. 2.5a), and (2) when the heavy key component is the most retained component in the system, similar to Split 2 in the case study (see Fig. 2.5b). These cases were selected because they are the only splits that control the waves of three different components. In both cases, the maximum productivity increases with increasing retention factors, then levels off at higher retention factors. This is because at higher retention factors, the diffusion terms become larger, reducing the benefits of a larger difference in light key and heavy key retention factors. Therefore, the general rule can be deduced that for a fixed range of retention factors, maximizing the difference in heavy key and light key retention gives a higher productivity.

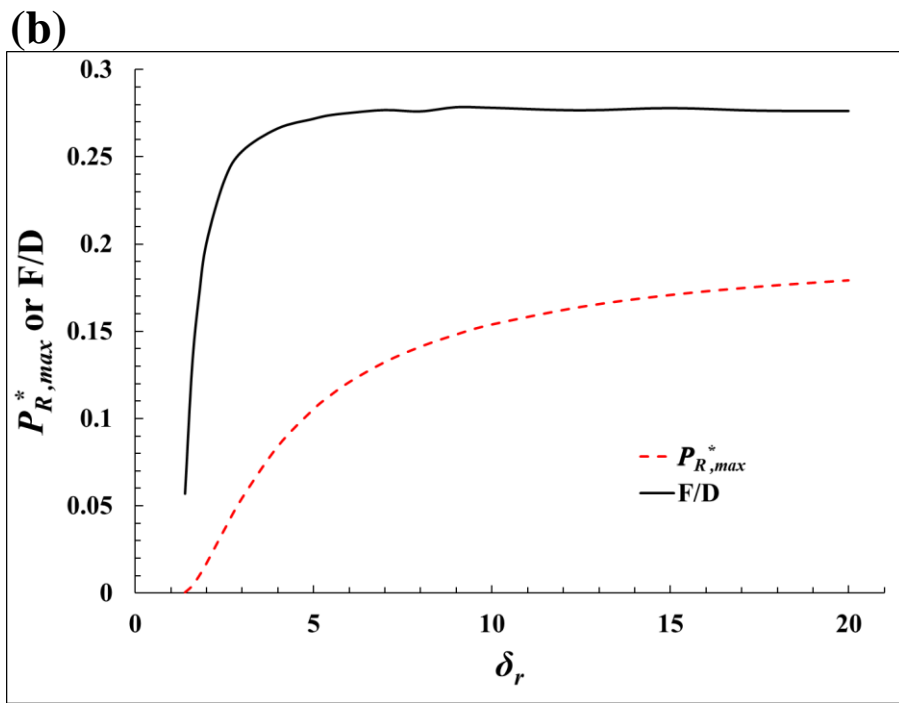
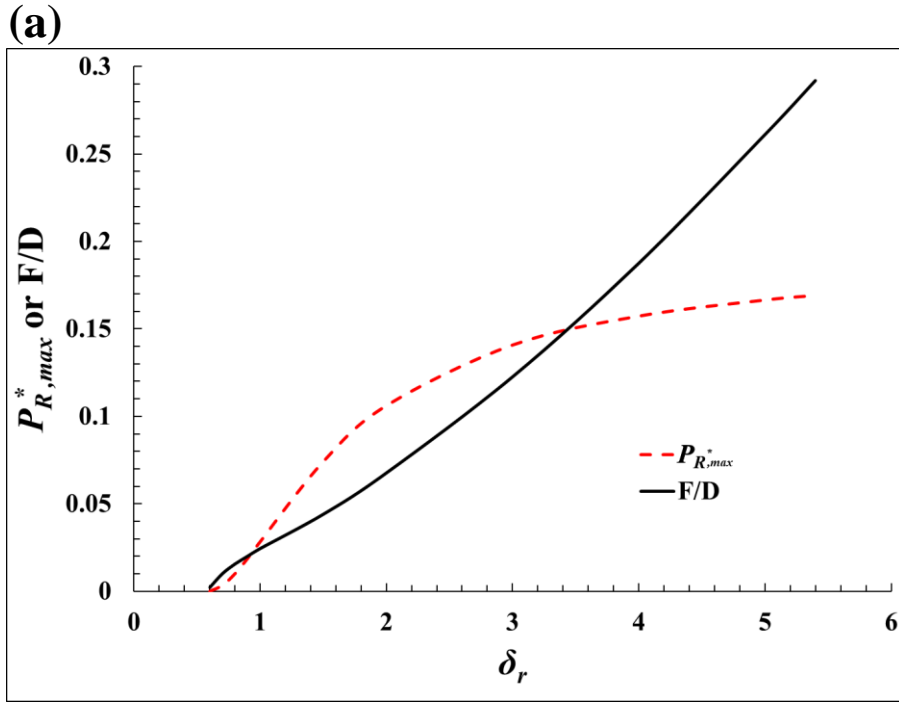


Figure 2.5 (a) Effect of Heavy Key Retention Factor when the Heavy Key is not the most Retained (Split 1). (b) Effect of Heavy Key Retention Factor when the Heavy Key is Most Retained (Split 2)

2.4.3 Effect of Retention Factors on Solvent Efficiency

Equation (17) shows that the solvent efficiency is dependent on the retention factor of the heavy key, light key, and the key components in zones I and IV. A large difference between the heavy key and light key retention factors and a small difference in the retention factors of the key components in zone I and IV lead to a high solvent efficiency. This is illustrated when comparing Split 1 and Split 5 in Fig. 2.5b and Table 2.8. These two cases have the same heavy key and light key components but have different key components in zones I and IV. Because in Split 1, component 3 is zone I key instead of component 2, the solvent efficiency drops from 1 to 0.15 in the ideal case, and 0.32 to 0.04 for the non-ideal case (Table 2.8).

Table 2.8 Comparison of Solvent Efficiency with Ideal Cases for Ring 1

Split	Ideal F/D	Ideal F/D Value	F/D
1	$\frac{\delta_2 - \delta_1}{\delta_3 - \delta_1}$	0.15	0.04
2	$\frac{\delta_3 - \delta_2}{\delta_3 - \delta_1}$	0.85	0.27
3	$\frac{\delta_3 - \delta_2}{\delta_3 - \delta_2}$	1	0.30
4	$\frac{\delta_3 - \delta_1}{\delta_3 - \delta_1}$	1	0.29
5	$\frac{\delta_2 - \delta_1}{\delta_2 - \delta_1}$	1	0.32

Large retention factors can also lead to a decrease in solvent efficiency because the mass transfer correction terms are proportional to δ^2/η in each of the different zones. It should be noted that these terms are significant in the case study as the solvent efficiencies from the rate model simulations are roughly 1/3 of the ideal solvent efficiencies which can be seen in Table 2.8. Figure 4b. shows the solvent efficiency as a function of $N_{DL,3}^*$. As $N_{DL,3}^*$ increases, the solvent efficiency approaches the ideal solvent efficiency. When selecting a splitting strategy or solvent/sorbent, the ideal solvent efficiency can be used as a crude guide.

The effects of the heavy key retention factor on the solvent efficiency at maximum productivity were also investigated and the results are shown in Fig. 2.5. The difference between Split 1 (Fig. 2.5a), where the heavy key component is not the most retained component, and Split 2, where the heavy key component is the most retained component are significant in this case. As shown in the figure, when the heavy key component is not the most retained component, increasing the heavy key retention factor results in a higher solvent efficiency. This is because the numerator of the solvent efficiency equation is larger while the denominator remains mostly unchanged except for minor diffusion effects. However, in Split 2, the solvent efficiency quickly increases in value and then levels off, because $\delta_r = \delta_n$. As δ_r in the numerator increases, δ_n in the denominator increases at the same rate. This means that at relatively high δ_r values, the solvent efficiency approaches a constant.

2.4.4 Ring 2 of the Case Study

A summary of the results of the Ring 2 of the case study is shown in Table 2.9. The column profiles for these rings can be seen in Fig. 2.6. Table 2.9 and Fig. 2.66 show that the target yields for the SSWD equations were reached within 1%. They also verify that the multi-component equations simplify down to the binary equations. The second ring of this case study would only be necessary if the desired product was the middle product (Phe) or if all three components were desired as products. Each of these SMB systems were designed for maximum productivity using the two component SSWD equations. The worst of the splitting options is Split 4 as it requires an additional SMB to purify all three products with high yield. This case should not be used under any normal circumstances as the equipment and solvent costs for an additional ring makes this solution impractical.

Table 2.9 Summary of Ring 2 Rate Model Simulation Results. *Note: Feed values are based on the initial feed concentrations from Ring 1 (8 g/L)

Split Option	Standing Waves (p-q-r-s)	$C_{Phe}/C_{i,feed}^*$	$C_{His}/C_{i,feed}^*$	$C_{Trp}/C_{i,feed}^*$	P_R^*	F/D	Y_{target}	Y_{Phe}	Y_{His}	Y_{Trp}
1	3-2-3-2	0.031	N/A	0.011	0.12	0.30	0.99	0.99	N/A	0.99
2	2-1-2-1	0.25	0.50	N/A	0.06	0.33	0.99	0.99	0.98	N/A
3	2-1-2-1	0.31	0.51	N/A	0.06	0.33	0.99	0.99	0.98	N/A
4a	2-1-2-1	0.25	0.69	N/A	0.06	0.33	0.99	0.99	0.98	N/A
4b	3-2-3-2	0.076	N/A	0.088	0.12	0.30	0.99	0.99	N/A	0.99
5	3-2-3-2	0.32	N/A	0.079	0.06	0.30	0.99	0.99	N/A	0.99

By comparing the results of Splits 1 and 2 it becomes clear which splitting strategy is the most beneficial for multicomponent separations. Split 1 does the more difficult split first (lower difference in heavy key and light key retention factors), and Split 2 does the easier split first (higher difference in heavy key and light key retention factors). Because Split 1 does the more difficult split first, the feed concentration of Phe into Ring 2 is nearly 1/20 that of Split 2 (See Table 2.8). If Phe is the product, the Ring 2 productivity for Split 1 is 6.8 kg Phe/(kg sorbent * day) while the productivity for Split 2 is 61.8 kg Phe/(kg sorbent day), making Split 2 nearly 10 times more productive. The concentration of Phe in the product stream in Ring 2 from Split 2 is eight times larger than that of Split 1 as well (see Table 2.9). Split 3 has even higher productivity and product concentration than those of Split 2, however Trp is wrapped between both product streams. This makes Split 2 the best case if all 3 components are desired products but Split 3 the best case if only the middle component is desired as a product. This means that the easiest split should be done first to give higher productivity, solvent efficiency, and extract product concentration. One can also change the sorbent, solvent, temperature, etc. for Ring 2 to give even higher productivity. Therefore, it may be possible to do the more difficult separation even more effectively in Split 2 or Split 3.

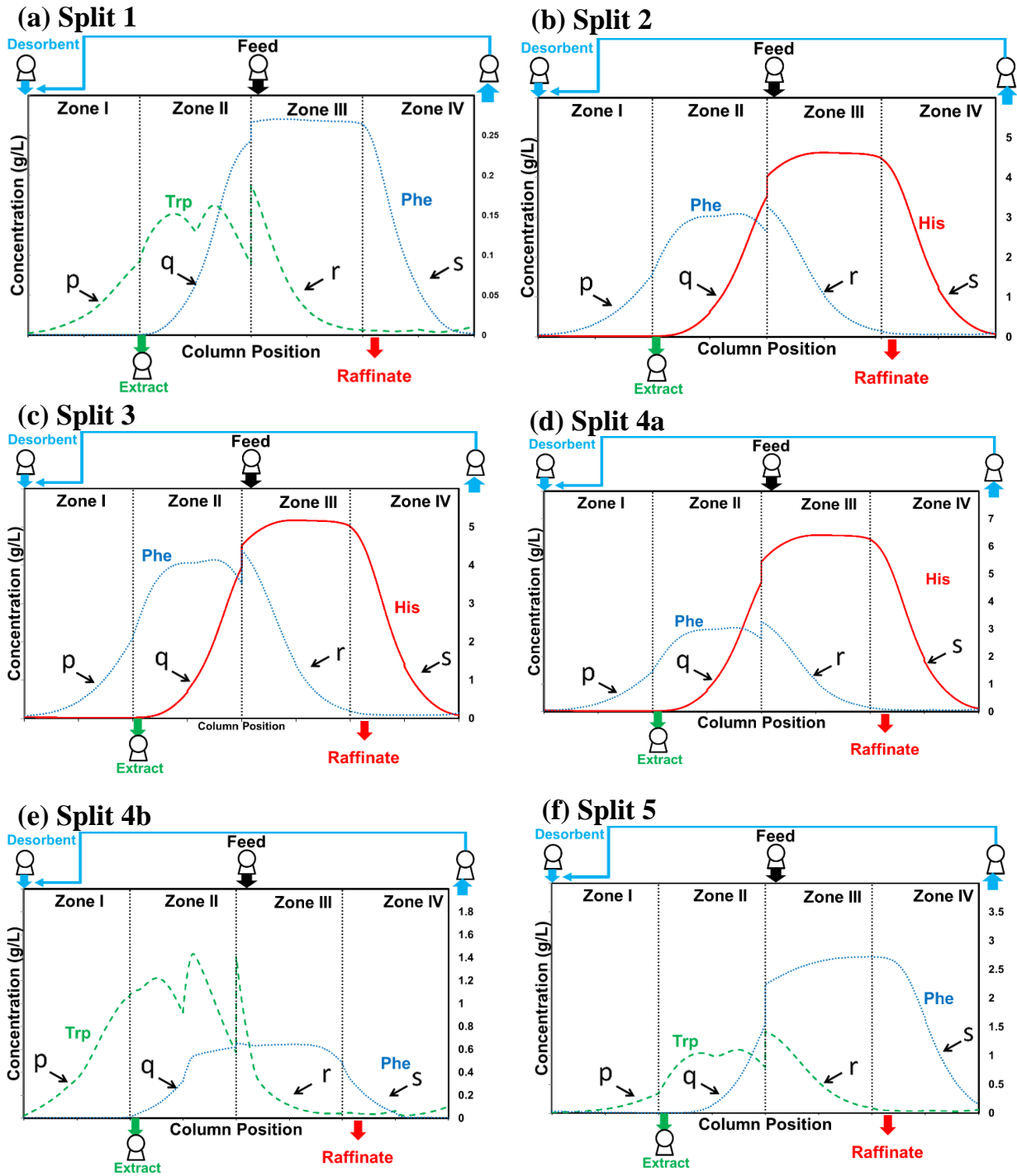


Figure 2.6 Column profiles at the end of a step for Ring 2 at cyclic steady state. (a) Split 1, (b) Split 2, (c) Split 3, (d) Split 4a, (e) Split 4b, and (f) Split 5. Standing waves in each zone are labeled.

2.4.5 Effect of Column Configuration on Productivity and Solvent Efficiency

Split 2 was the most productive splitting method if all three components are desired products. The material properties and splitting strategy from Split 2 were used to test the effect of column configuration on productivity and solvent efficiency (similar trends were observed when examining Split 1). The SSWD equations are derived from the true moving bed solution. For systems with significant diffusion effects (small $N_{Dl,n}^*$) more than one column is needed in each zone so that the separation in SMB approaches that in the true moving bed. For this reason, to test the effect of column configuration on productivity, several configurations were tested that utilized 12 columns with at least two columns per zone. The most productive of these column configurations was found using Eq. (35a-35d). It was assumed that the ratio of decay factors was approximately 1. This maximum productivity configuration, along with several other configurations were compared to the 3-3-3-3 configuration used in the case study. The results are shown in Fig. 2.7a. The configuration predicted by Eq. (35) was the configuration with the highest productivity of the tested configuration. The relationship between column configuration and solvent efficiency is not as clear because all the zone fractions affect the solvent efficiency. In this case, the effects are not as significant in terms of solvent efficiency as shown in Fig. 2.7b. Of the tested configurations, the 3-3-3-3 configuration had slightly higher solvent efficiency than the other options in this case.

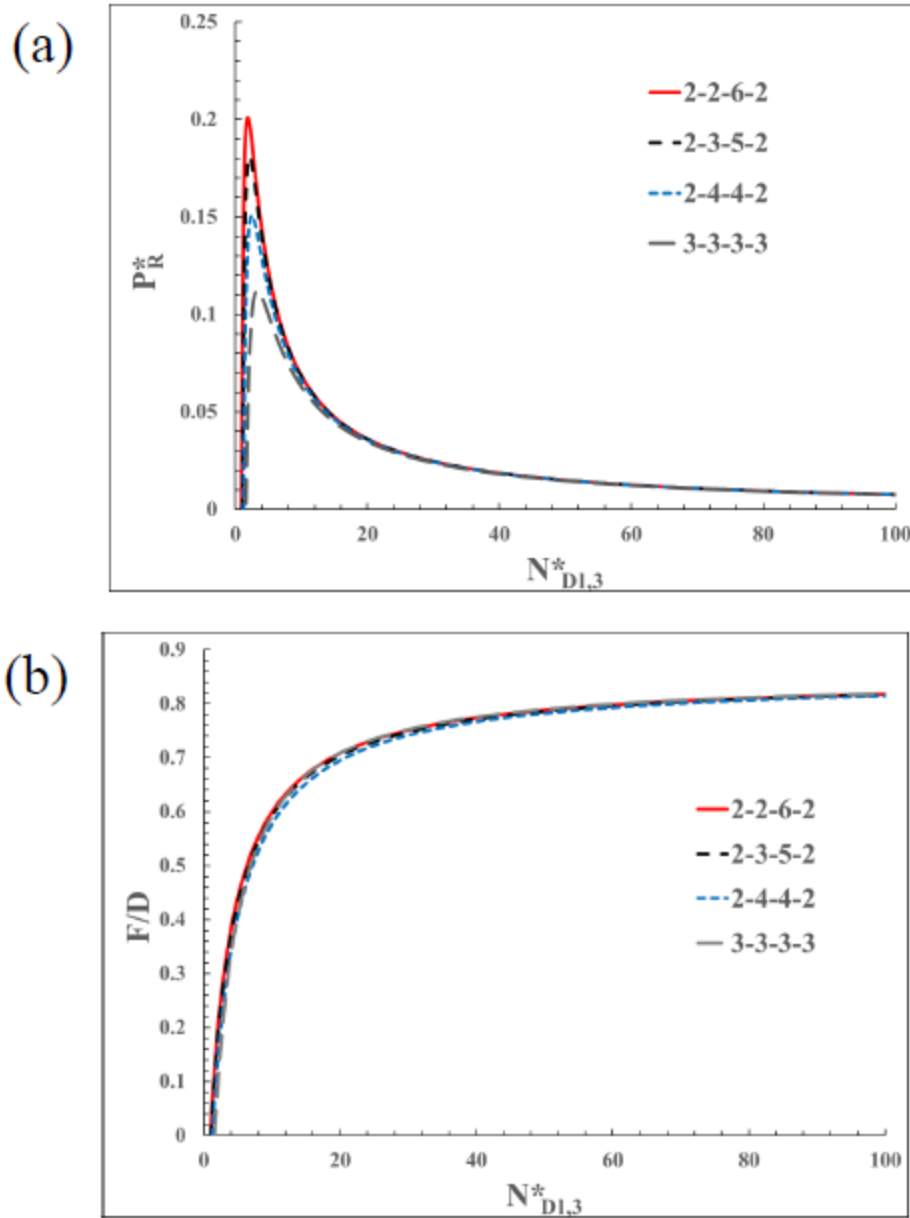


Figure 2.7 (a) Productivity as a function of $N_{D1,3}^*$ for different column configurations with 12 columns for Split 2. (b) Solvent efficiency as a function of $N_{D1,3}^*$ for different column configurations with 12 columns for Split 2. Similar Trends were observed in Split 1

2.4.6 Design Rules Derived from SSWD Equations

A summary of the differences between binary and ternary SMBs can be found in Table 2.10. Binary cases have only one splitting strategy. In ternary cases, it is important to choose the correct splitting strategy for the separation goal. It is desirable for the target component to be

separated in one SMB when possible. Therefore, one should pick a solvent/sorbent/temperature combination that will make the target component the most retained or the least retained component in the series. If the target compound is the least retained, Split 1 is preferred. If the target compound is the most retained component, Split 2 is preferred.

Table 2.10 Differences Between Binary and Ternary Systems

Binary Systems	Ternary Systems
1 possible splitting strategy	5 possible splitting strategies
All waves are standing	Some waves standing, some waves pinched
Ideal F/D is always 1	Ideal F/D not 1 unless a pseudo binary case (wrapped component)
Productivity and solvent efficiency dependent on retention and diffusivity of both components	Productivity dependent on retention and diffusivity of heavy key and light key components Solvent efficiency dependent on retention and diffusivity of all standing components
Optimal column configuration for productivity dependent on retention and diffusivity of both components	Optimal column configuration for productivity dependent on retention and diffusivity of only heavy key and light key components

The key design strategy is to pick a solvent sorbent system with the largest difference in heavy key and light key retention factors. This will increase both productivity and solvent efficiency. Additionally, this system should be designed to minimize the range of retention factors, as this will increase the solvent efficiency and thus reduce extract product dilution. Additionally, δ^2/η is the weighting factor for the diffusion terms in both the productivity and solvent efficiency equations. This means that for a given difference in heavy key and light key retention factors, the absolute values of the retention factors should be minimized to reduce the loss of productivity or solvent efficiency due to diffusion.

If it is impossible to make the target product the most or least retained component, the easiest split should be done in Ring 1. The impurity that is closest in retention factor to the target

can be wrapped to reduce the separation burden for Ring 2. If two or all three components are targeted products, the easiest split should be performed first as a larger difference in heavy key and light key retention factors raises productivity, solvent efficiency, and product concentration. Other sorbent or solvent options should be considered for Ring 2 to see if the range of retention factors can be minimized. Solvent efficiency in the first ring can affect productivity in the second ring.

In cases where the sorbent is very costly, the separation cost can become dominated by the productivity. In this case, it is beneficial to optimize operating conditions and the column configuration for maximum productivity. The column configuration which gives the maximum productivity was found to be a function of the retention factors and diffusivities of the heavy and light key components.

2.5 Conclusions

While SMB systems have higher sorbent productivity and solvent efficiency than batch chromatography, their applications for large scale production have been limited, especially for multi-component separations. A major barrier is the difficulty in designing an efficient process for multi-component separations. For ternary systems, there are 27 design parameters, which include yields, equipment parameters, material properties, and operating parameters, that must be specified to achieve efficient separation with high product purity and high yield. Furthermore, SMB can only split a mixture into two products. When the middle component of a ternary mixture is a desired product, several splitting strategies exist. Previously there were no simple methods from the literature for determining which splitting strategy gives the best productivity or solvent efficiency.

Through the development of dimensionless groups, SSWD equations were developed for linear multicomponent adsorption systems. The SSWD equations relate the productivity and solvent efficiency to a key dimensionless design parameter, making it possible to explain the effects of design parameters and splitting strategies on the separation. Rate model simulations verified that the SSWD equations can guarantee target yields at high purity in a ternary example system. Productivity, solvent efficiency, and product concentration are improved by having a larger difference in heavy key and light key retention factors. If only one component in the mixture is the desired product, the sorbent, solvent, pH, or other conditions affecting adsorption, should be

selected such that the desired product is the most or least retained so that it can be separated with one SMB. If a middle component, or if more than one component are desired products, more than one SMB is required. In this case the easiest split should be done first to increase the overall productivity, solvent efficiency, and product concentration. Low solvent efficiency in the first ring can significantly reduce the productivity of the second ring. Impurities that have similar retention factors to the target component can be distributed in both products in the first ring to reduce the separation burden of the second ring. This study provides the fundamental equations, general design rules, and splitting strategies which have wide applications for the design and development of multicomponent SMB systems.

3. STANDING-WAVE DESIGN OF THREE-ZONE, OPEN-LOOP NON-ISOCRATIC SMB FOR PURIFICATION

Results in this chapter are reprinted from BMC Chem. Eng Vol. 1, 17 Standing-wave Design of Three-Zone, open-loop non-isocratic SMB for purification, Copyright (2019), with permission from BMC.

3.1 Introduction and Background for Non-Isocratic SMB

Stepwise elution is implemented in batch chromatography to reduce cycle time, save solvent, or obtain concentrated products [41–44]. For example, a step change in pH was used in the purification of Immunoglobulin G (IgG), where the protein adsorbed at pH 7.4 and eluted at pH 3 [41]. A step change in solvent strength or ionic strength can also be utilized for biochemical separations [42,45]. However, if the feed contains strongly competitive impurities, a long column (or a low loading) is needed for the separation of the target product from the impurities, resulting in low column utilization and a diluted product [46]. If the sorbent selectivity is high, column utilization is limited by wave spreading due to mass transfer effects. High column utilization is usually achieved at the cost of a low productivity by using a low flow rate to minimize wave spreading. These limitations of batch chromatography can be mitigated using continuous chromatography as explained below.

If the adsorbent has a perfect selectivity for the target product and all the impurities do not adsorb, one can use a periodic counter current system with three columns for capturing a target product to achieve both high productivity and high column utilization, as shown in Fig. 3.1 [47,48]. In the absence of an absorbing impurity, only one column is needed for washing, elution, and regeneration. Moreover, two columns can be used in the loading zone to achieve nearly 100% utilization of the adsorbent capacity if appropriate flow rates are used. The leading column in the loading zone is used for full capacity utilization, and the second column in the loading zone is used to confine the adsorption wave of the target product, as shown in Fig. 3.1. Once the first column is completely loaded, it can be stripped, and the process is repeated using the second and the third column. Periodic counter current systems can also be used in cases without perfect selectivity. However, the yield, purity, or productivity will be reduced compared to systems with perfect

selectivity because longer columns, lower flowrates, or reduced purity or yield are required in this case.

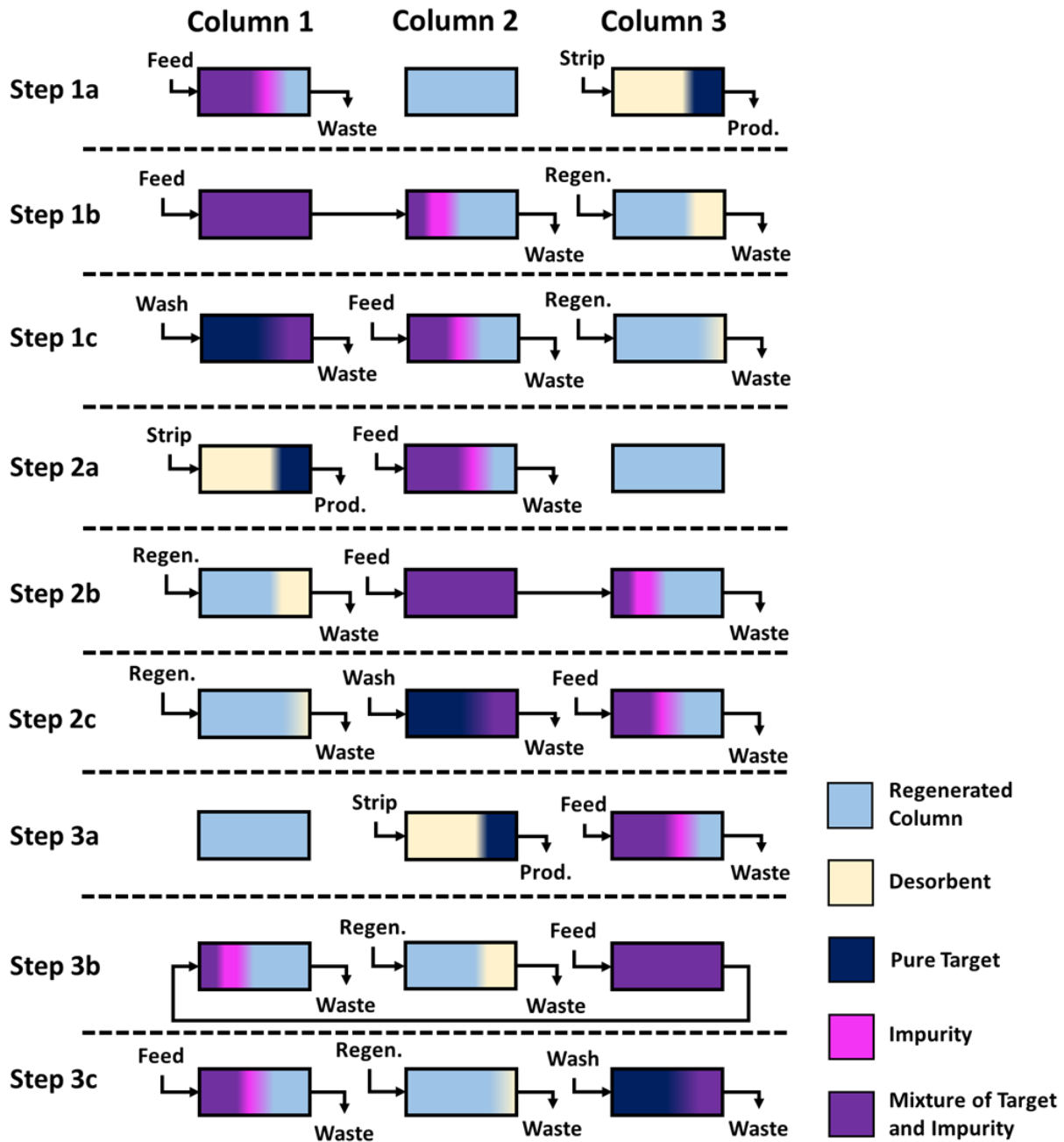


Figure 3.1 Example of 3 column periodic counter current separation. In Zone III, the feed is loaded into the column. Zone II assures that the less retained component is contained so that it does not leak into the extract product. In Zone I, the desorbent is fed into the column to collect the more retained product as extract. The colors in this figure are the same as Fig. 3.1.

Periodic counter current systems are used in a variety of commercial processes; however, they are most useful in biological applications where sorbents are designed to have very high selectivity for the target component [47–50]. The design and optimization of periodic counter current systems is usually done by systematic search using experiments or rate model simulations, which require solving partial differential equations [46,49,51–54]. Similar systems with two columns can be used to reduce equipment complexity but sacrifice some column utilization, compared to three column systems [55,56]. Other techniques such as sequential multi-column chromatography, which adds an additional step to aid in regeneration, and multicolumn countercurrent solvent gradient purification (MCSGP), which is a hybrid of batch and continuous chromatography, can also be used to achieve more efficient separations than batch chromatography [57–59]. By utilizing more effective configurations, sorbent productivity is increased. A detailed discussion of these and other alternative techniques can be found in Steinebach et al. [59].

If the feed contains a competitive impurity, then a periodic counter current system must sacrifice some productivity to produce high-purity product with high yield. For such a system, a 3-zone, non-isocratic, open-loop simulated moving bed can produce a concentrated high-purity product with high yield and high productivity. In a simulated moving bed, products are separated into either a lower affinity raffinate product or a higher affinity extract product. A four-column system is shown in Fig. 3.2 as an example. Each of the three zones in this configuration has a distinct purpose. The purpose of Zone I is to desorb the target component or the higher affinity component for collection in the extract product. The affinity of the target component is lower at a lower pH value, for example. In this case, a lower pH solution acts as a desorbent and is fed into Zone I. Because the solvent or the buffer for the target is a non-adsorbing component, the solvent wave or the pH wave will travel quickly through Zone I, allowing for the target component to be desorbed and released into the extract stream. If necessary, Zone I can also be used for regeneration or re-equilibration. Zone II acts as a washing and separation zone. Makeup solvent or buffer at the feed pH is fed into Zone II to elute the remaining weakly adsorbing or non-adsorbing impurity component back into Zone III for collection in the raffinate. Zone II is used to confine the desorption wave of the less adsorbed components and to ensure that they are not collected in the extract product. Zone III is the feed zone. In this zone, the less adsorbed component or any non-adsorbing components are eluted through the column into the raffinate. The adsorption wave of

the higher affinity component (in this study, the target) is confined in this zone to prevent its leakage into the raffinate.

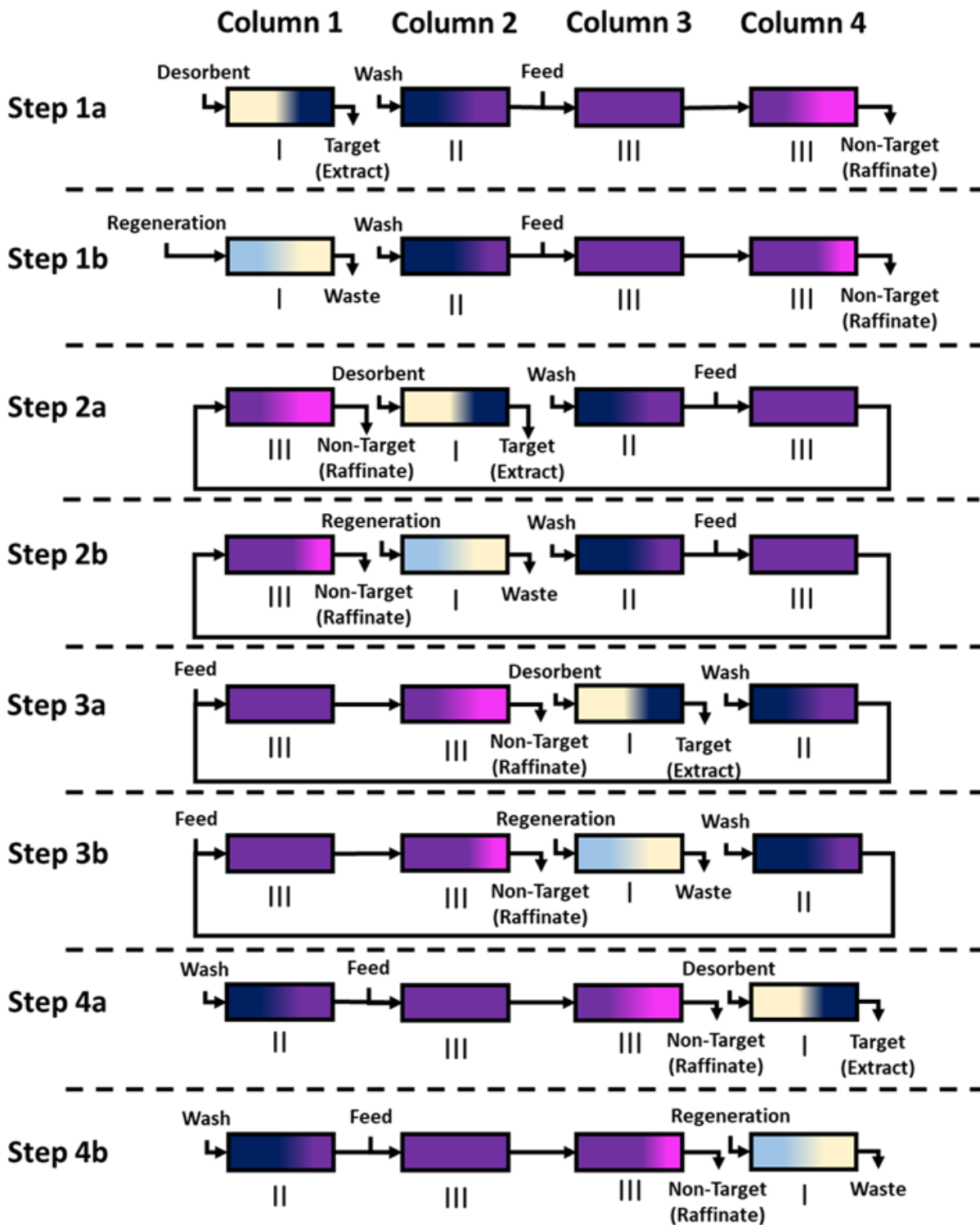


Figure 3.2 3-zone open-loop simulated moving bed

A strong desorbent is used in Zone I to facilitate desorption of the target product, resulting in a higher product concentration, shorter processing time, higher solvent efficiency, and higher sorbent productivity. Since the extract only collects the target product (TP) that is free of the competing impurity (IMP), high product purity can be achieved. High loading is also achieved, because all three zones contain the target and only partial separation of the target band from the impurity bands is needed to recover high-purity product. Furthermore, since elution, separation, and loading occur simultaneously in different zones, overall cycle time is reduced. For these reasons, the 3-zone, open-loop SMB can have much higher product purity, yield, solvent efficiency, and sorbent productivity than conventional batch step-wise elution chromatography. These advantages are especially important for applications involving costly sorbents, high-value products, or fragile products which can degrade during a long processing time. For such applications, it is not important to recycle solvent using a closed-loop system to reduce the overall separation costs.

In previous literature studies, non-isocratic SMB systems have been designed in both closed loop configurations in which a recycle is present and in open-loop configurations without recycle [28,60–62]. This study will use a 3-zone, open-loop configuration. The open-loop is advantageous because it prevents the mixing of pH, which could also be ionic strength or solvent strength, across different zones. Additionally, recycle is unnecessary in this case because in most protein separations, high product yield is more important than low solvent usage [63]. Without solvent or buffer recycle, a fourth zone is not needed for confining the non-adsorbing or weakly adsorbing components, which can be collected directly in the raffinate. Furthermore, by avoiding mixing the recycle stream with the desorbent stream, the desorbent composition is better-controlled in the open-loop system.

Several challenges exist in the design of 3-zone, non-isocratic non-ideal SMB systems. The well-known Triangle Theory was derived for ideal systems, which have no diffusion or dispersion effects. It can be used to quickly determine the operating parameters for complete separation for ideal systems [64]. However, since the Triangle Theory does not take into account any mass transfer effects in non-ideal systems, the triangle region for ideal systems cannot guarantee purity or yield for non-ideal systems. To ensure product purity and yield for non-ideal systems, grid search using rate model simulations are required within the triangle region [65]. For non-isocratic, non-ideal systems, a new triangle region must be searched for each modulator that is tested, further

increasing the number of searches. In contrast, the Standing-Wave Design directly solves the operating conditions that guarantee purity and yield for non-ideal systems. No grid search using rate model simulations is needed. SWD has been proposed for non-isothermal closed-loop systems, but the equations do not apply to non-isocratic open-loop systems [28,30].

To address these challenges, this study aims to develop a general design method for the 3-zone, open-loop, non-isocratic SMBs for non-ideal systems. Specifically, the objectives are to: (1) develop the Standing-Wave Design (SWD) equations and methods for non-isocratic, 3-zone, open-loop SMB systems with linear or Langmuir isotherms. (2) Verify the SWD using rate model simulations. (3) Compare the effectiveness (productivity, yield, purity, solvent efficiency) of the SWD method with conventional optimal batch stepwise elution systems, and (4) compare the effectiveness of the SWD design method with non-isocratic, non-ideal SMB systems designed based on the Triangle Theory.

The approach taken by this study is as follows. First, the general Standing-Wave Design equations for non-ideal systems are derived for 3-zone, open-loop SMBs. The general equations can be adapted for pH-SMBs with both linear and non-linear isotherms. Solvent strength could be substituted into the general isotherm equations with only minor alterations. Then, the material, feed, and equipment parameters from the literature are used in the new SWD method to obtain a new SMB design. The purity and yield specified in the design method are verified using Aspen Chromatography simulations. The results of the design in terms of productivity, purity, yield and solvent consumption are obtained from the rate model simulations and compared to the experimental literature results.

Some highlights of this study are as follows. The SWD eliminates the need for grid search using rate model simulations, which require solving partial differential equations when designing SMB separations for non-ideal systems. The processing time in the 3-zone SMB is much shorter than for batch step-wise elution, potentially reducing proteolytic degradation of target proteins. Because the SWD requires only solving algebraic equations, it can be used to quickly screen multiple designs or compare different resins to improve the SMB efficiency. Additionally, compared to batch step-wise elution systems, the 3-zone open-loop SMB could give an order of magnitude higher productivity in systems with weakly competing impurities and two orders of magnitude higher productivity in systems with strongly adsorbing impurities.

3.2 Methods

The SWD for non-ideal, isocratic, 4-zone SMB systems with linear isotherms was developed by Ma and Wang in 1997 [23]. This method accounted for mass transfer effects and did not require any rate model simulations to determine the operating parameters that can ensure high product purity and high yield. It was paired with optimization techniques to give the overall maximum productivity or minimum cost [24–26]. It was extended to non-linear isocratic systems [27,29] and systems with a pressure limit [31,32,40]. Recently, the SWD equations were solved in terms of dimensionless variables and dimensionless groups for binary and multi-component separations for isocratic systems with linear isotherms [1,2]. Sorbent productivity and solvent consumption were solved easily for isocratic SMB systems over a wide range of dimensionless operating parameters. The information could be paired with cost functions to find the optimal designs within minutes using a personal computer. The SWD has been extended to systems with different temperatures in different zones, which is the first extension of the SWD to non-isocratic SMBs [28,30]. These non-isothermal SWD methods only work for temperature swings in 2-zone or 4-zone close-loop SMBs and they do not apply to the 3-zone, open-loop SMBs.

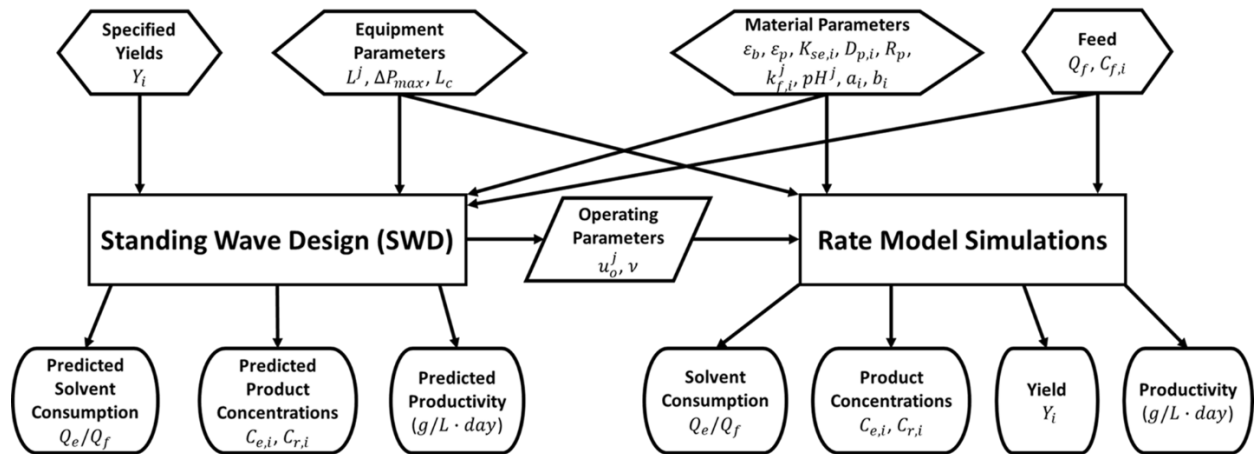


Figure 3.3 Overview of Standing Wave Design Inputs and Outputs. Complete list of variable definitions found in Table 3.1

An overview of the input and outputs of both the SWD and rate model simulations utilized in this paper are shown in Fig. 3.3. The specified yields and system parameters (equipment parameters, material parameters, and feed parameters) are used to solve the SWD equations for the operating parameters, and to predict solvent consumption, product concentrations, and productivity. This can be done without rate model simulations. The operating parameters along

with the equipment parameters, material parameters, isotherm parameters, and feed were input into the rate model simulations to verify the yields, solvent consumption, product concentrations, and productivities. A complete notation table is given in Table 3.1.

Below, the general Standing-Wave equations are derived for non-isocratic, 3-zone, open-loop SMBs. The procedure for solving the equations and other details of the design method are also explained. The isotherms for linear and non-linear non-isocratic systems are introduced first in Section 2.1. The Standing-Wave Design equations for non-isocratic ideal systems are derived in Section 2.2, and the equations for non-ideal systems are derived in Section 2.3. The methodology and the parameters for two examples are given in Section 2.4. A discussion of the rate model simulations can be found in Section 2.5. An overview of the implementation of the SWD method is given in Appendix D.

Table 3.1 Chapter Notation Table of All Variables

Notations	Description	Notations	Description
$a_i(pH)$	Equilibrium distribution coefficient as a function of pH value of component “i” in a linear system, or Langmuir “a” value as a function of pH value of component “i” in a non-linear system.	L_C	Column length
$a_{o,i}, x_i$	Adsorption equilibrium constant in Example 2 Eq. (20)	L^j	Length of Zone j
a, b, c	Coefficients in quadratic formula in Eq. (12)	n	pH dependent equilibrium order in Example 1 Eq. (18)
$b_i(pH)$	Langmuir “b” value as a function of pH value in a non-linear system.	P	Phase ratio, $P = \frac{1-\varepsilon_b}{\varepsilon_b}$
C_1^{II}	Concentration of component 1 in the make-up solvent in Zone II	pH^j	pH in Zone j
C_2^I	Concentration of component 2 in the desorbent in Zone I	pH_{ref}	Reference pH in Example 1 Eq. (18)
$C_{E,i}$	Average concentration of component “i” in the Extract	Q_f	Feed flow rate
$C_{R,i}$	Average concentration of component “i” in the Raffinate	Q_j	Flowrate in Zone j
$C_{f,i}$	Feed concentration of component “i”	Q_E	Extract flow rate
C_i	Bulk concentration of component “i” in the fluid	Q_R	Raffinate flow rate
$C_{p,1}$	Plateau concentration of component 1 (less retained component) in Zone III	q_i	Solid phase concentration on a solid volume basis of component “i”
$C_{p,2}$	Plateau concentration of component 2 (more retained component) in Zone II	q_{max}	Sorbent capacity
$C_{s,1}$	Plateau concentration of component 1 after feed port in Zone III	R_p	Particle radius
$C_{s,1}^*$	Plateau concentration of component 1 in Zone II before mixing with the feed port	S	Cross-sectional area of the column
$C_{s,2}$	Plateau concentration of component 2 after feed port in Zone III	t_s	Step time
$C_{s,2}^*$	Plateau concentration of component 2 in Zone II before mixing with the feed port	u_o^j	Zone velocity
$D_{p,i}$	Pore diffusivity of component “i”	$u_{w,i}^j$	Wave velocity of component “i” in Zone j
d_p	Particle diameter	Y_i	Yield of component “i”
$E_{b,i}^j$	Axial dispersion coefficient of component “i” in Zone j	β_i^j	Decay coefficient of component “i” in Zone j.
K_A	Association equilibrium constant in Example 1 Eq. (18)	δ_i^j	Retention factor of component “i” in Zone j
$K_{se,i}$	Size exclusion factor of component “i”	ε_b	Bed void fraction
$k_{e,i}^j$	Lumped overall mass transfer coefficient of component “i” in Zone j	ε_p	Particle porosity
$k_{f,i}^j$	Film mass transfer coefficient of component “i” in Zone j	v	Port velocity

3.2.1 Adsorption Isotherms

The Standing-Wave Design (SWD) equations are derived first for non-isocratic systems with linear isotherms. In non-isocratic systems, the isotherms are dependent on the composition of the mobile phase. Several factors can affect the adsorption characteristics of a solute, including pH, temperature, solvent strength, or ionic strength. Since the purification of proteins and antibody fragments used as examples were performed using a pH step change, the isotherms will be written as functions of pH. In systems where the solvent strength, ionic strength, or temperature is used to alter adsorption, the isotherms could also be expressed as a function of those variables. A linear isotherm is shown in Eq. (1) where q_i is the solid phase concentration on a solid volume basis of component “i”, $a_i(pH)$ is the equilibrium distribution coefficient of component “i” shown as a function of pH, and C_i is the concentration of component “i” in the mobile phase.

$$q_i = a_i(pH)C_i \quad (1)$$

For non-linear systems, which have a concentrated feed with two or more components, the multi-component Langmuir isotherm model can be used to express the competitive adsorption isotherms of multiple solutes. This model is based on competitive, mono-layer adsorption of multiple solutes. Each adsorption site can be considered as located in the center of a square in a lattice, and each solute is smaller than the square. In this model, solute size or shape does not affect the competitive adsorption [66]. A multi-component Langmuir isotherm is shown in Eq. (2).

$$q_i = \frac{a_i(pH)C_i}{1 + \sum_{j=1}^n b_j(pH) C_j} \quad (2)$$

Because the pH, solvent strength, ionic strength, or temperature can affect the affinity for the sorbent and/or the overall capacity, both the “a” and “b” values in Eq. (2) are functions of the modulating variable (in this case pH). It is evident from this equation that the maximum sorbent capacity is equal to a_i/b_i . If a system is run in the isocratic mode, the values of a_i and b_i are held constant. However, the functional form of a_i and b_i can be changed to fit a variety of modulators or solutes. In this study, two specific functions are used to account for the pH dependence of the isotherms of two different solutes in the two examples in Section 2.4.

3.2.2 Standing-Wave Design for Ideal, Linear, or Non-Linear Systems

The SWD method for SMB is based on the steady state solution for a true moving bed. For an ideal system, the wave velocity of a key component “i” in zone “j” ($u_{w,i}^j$) is set equal to the average port velocity (v), which is the column length divided by the step time (Eq. (3d)). If the wave velocity and the port velocity are the same, the wave appears to be “standing” relative to the port and a steady state can be achieved in a true moving bed. The component with the lower sorbent affinity will be labeled component 1 and the component with the higher sorbent affinity is labeled as component 2. For a 3-zone, open-loop binary separation, the wave velocities ($u_{w,i}^j$) of component “i” in zone “j” are matched with the port velocity (v) shown in Eq. (3).

$$u_{w,2}^I = v \quad (3a)$$

$$u_{w,1}^{II} = v \quad (3b)$$

$$u_{w,2}^{III} = v \quad (3c)$$

$$v = \frac{L_c}{t_s} \quad (3d)$$

L_c is the column length, and t_s is the step time. The wave velocity can be expressed in terms of the zone velocity (u_o^j), the phase ratio (P) which is equal to $(1 - \varepsilon_b)/\varepsilon_b$ where ε_b is the bed void fraction, and the retention factor (δ_i^j) which is defined in Eqs. (7) and (8).

$$u_{w,i}^j = \frac{u_o^j}{1 + P\delta_i^j} \quad (4)$$

Eq. (4) can be rearranged to give the following form:

$$u_o^I = (1 + P\delta_2^I)v \quad (5a)$$

$$u_o^{II} = (1 + P\delta_1^{II})v \quad (5b)$$

$$u_o^{III} = (1 + P\delta_2^{III})v \quad (5c)$$

The zone velocities and port velocity can be determined using Eq. (5) paired with the mass balance around the feed port (Eq. (6)). S is defined as the cross-sectional area of the column. Q_f is the feed flow rate.

$$v = \frac{Q_f}{S\varepsilon_b P(\delta_2^{III} - \delta_1^{II})} \quad (6)$$

The retention factor for a linear isotherm is shown in Eq. (7).

$$\delta_2^I = \varepsilon_p + (1 - \varepsilon_p)a_2^I(pH) \quad (7a)$$

$$\delta_1^{II} = \varepsilon_p + (1 - \varepsilon_p)a_1^{II}(pH) \quad (7b)$$

$$\delta_2^{III} = \varepsilon_p + (1 - \varepsilon_p)a_2^{III}(pH) \quad (7c)$$

For non-linear, isocratic systems with Langmuir isotherms, the retention factors have been derived previously [28,30–32]. The retention factors for non-isocratic, non-linear systems are similar to those for isocratic systems reported previously, except that a_i and b_i are functions of pH or other modulators, as shown in Eq. (8).

$$\delta_2^I = \varepsilon_p + (1 - \varepsilon_p)a_2^I(pH) \quad (8a)$$

$$\delta_1^{II} = \varepsilon_p + \frac{(1 - \varepsilon_p)a_1^{II}(pH)}{1 + b_2^{II}(pH)C_{p,2}} \quad (8b)$$

$$\delta_2^{III} = \varepsilon_p + \frac{(1 - \varepsilon_p)a_2^{III}(pH)}{1 + b_1^{III}(pH)C_{s,1} + b_2^{III}(pH)C_{s,2}} \quad (8c)$$

Eq. (8) allows for the retention factors to be determined using the plateau concentrations $C_{s,i}$ and $C_{p,i}$ (see Figure 3.4). The plateau concentrations are determined using the Hodograph solutions, shown in Appendix D [31]. The subscripts “ E ” and “ R ” refer to the average concentration in the extract and raffinate streams, respectively. The superscript Roman numerals refer to the concentration of a component entering that zone. The “*” refers to the concentration before mixing at the feed port.

3.2.3 Standing Wave Design for Non-Ideal Systems

In non-ideal systems, wave spreading occurs because of mass transfer effects. Wave spreading can cause leakage into the adjacent zones. For this reason, the zone velocities in non-ideal systems must be adjusted to confine the waves in the desired zones. A difference in wave velocity is used to counter wave spreading or “focus” the waves. The wave velocities in the first and second zones must be greater than the port velocity to focus the waves, whereas the wave velocity in the third zone must be smaller than the port velocity to prevent loss of the more retained component (component 2) in the raffinate. The adjusted zone velocities are shown in Eq. (9a-9c), where Δ_i^j is a mass transfer correction term [13]. After substituting in the value of the mass transfer correction term, the adjusted zone velocities are shown in Eq. (9e-g).

$$u_o^I = (1 + P\delta_2^I)v + \Delta_2^I \quad (9a)$$

$$u_o^{II} = (1 + P\delta_1^{II})v + \Delta_1^{II} \quad (9b)$$

$$u_o^{III} = (1 + P\delta_2^{III})v - \Delta_2^{III} \quad (9c)$$

$$\Delta_i^j = \frac{\beta_i^j}{L^j} \left(E_{b,i}^j + \frac{P\delta_i^{j2} v^2}{k_{e,i}^j} \right) \quad (9d)$$

$$u_o^I = (1 + P\delta_2^I)v + \frac{\beta_2^I}{L^I} \left(E_{b,2}^I + \frac{P\delta_2^{I2} v^2}{k_{e,2}^I} \right) \quad (9e)$$

$$u_o^{II} = (1 + P\delta_1^{II})v + \frac{\beta_1^{II}}{L^{II}} \left(E_{b,1}^{II} + \frac{P\delta_1^{II2} v^2}{k_{e,1}^{II}} \right) \quad (9f)$$

$$u_o^{III} = (1 + P\delta_2^{III})v - \frac{\beta_2^{III}}{L^{III}} \left(E_{b,2}^{III} + \frac{P\delta_2^{III2} v^2}{k_{e,2}^{III}} \right) \quad (9g)$$

In Eq. (9), β_i^j is the decay coefficient of component “*i*” in zone “*j*”, which is defined as the natural log of the ratio of the maximum concentration of component “*i*” to the minimum concentration of component “*i*” in zone “*j*”, L^j is the length of zone “*j*”, $E_{b,i}^j$ is the axial dispersion coefficient of component “*i*” in zone “*j*”, and $k_{e,i}^j$ is the lumped overall mass transfer coefficient of component “*i*” in zone “*j*”.

$$\frac{1}{k_{e,i}^j} = \frac{R_p^2}{15K_{se,i}\varepsilon_p D_{p,i}} + \frac{R_p}{3k_{f,i}^j} \quad (10)$$

R_p is the particle radius, $K_{se,i}$ is the size exclusion factor of component “*i*”, $D_{p,i}$ is the intraparticle diffusivity, and $k_{f,i}^j$ is the film mass transfer coefficient of component “*i*” in zone “*j*”. Eq. (9) can be paired with the mass balance around the feed port (Eq. (11)) to solve for the port velocity.

$$\frac{Q_f}{\varepsilon_b S} = u_o^{III} - u_o^{II} \quad (11)$$

When Eq. (9) is plugged into Eq. (11), the result can be manipulated to give the following quadratic equation form.

$$av^2 + bv + c = 0 \quad (12a)$$

where:

$$a = \frac{\beta_1^{II} P \delta_1^{II2}}{k_{e,1}^{II} L^{II}} + \frac{\beta_2^{III} P \delta_2^{III2}}{k_{e,2}^{III} L^{III}} \quad (12b)$$

$$b = -P(\delta_2^{III} - \delta_1^{II}) \quad (12c)$$

$$c = \frac{Q_f}{\varepsilon_b S} + \frac{\beta_1^{II} E_{b,1}^{II}}{L^{II}} + \frac{\beta_2^{III} E_{b,2}^{III}}{L^{III}} \quad (12d)$$

The quadratic formula can then be used to solve for the port velocity which can be used to solve for each of the zone velocities.

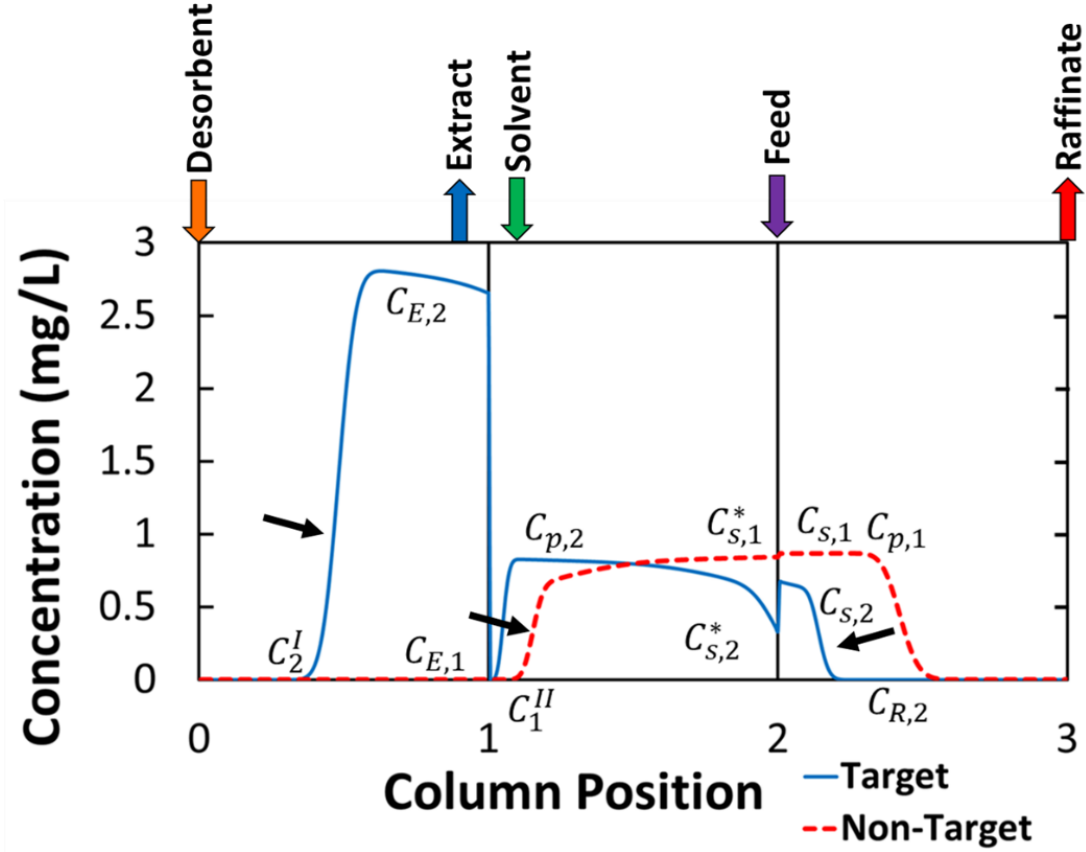


Figure 3.4 Example column profile from 3-zone open-loop SMB. The plateau concentrations are denoted with the p and s subscripts. The * denotes the concentration before the feed port. Subscript R and E denotes raffinate concentration and extract concentration respectively. The concentrations with a numeral superscript denote the concentration of the feed into that zone which in both cases listed here is zero. Concentrations shown in middle step. Profile from Example 1 Case 1.

The decay coefficients for nonlinear systems are defined below in terms of the maximum and minimum concentrations defined in Fig. 3.4. The final form is shown on the right in terms of yields, flowrates, known concentrations, and plateau concentrations.

$$\beta_2^I = \ln \left[\frac{C_{E,2}}{C_2^I} \right] = \ln \left[\frac{Y_2}{1 - Y_2} \right] \quad (13a)$$

$$\beta_1^{II} = \ln \left[\frac{C_{s,1}^*}{C_1^{II}} \right] = \ln \left[\frac{Q_{II}}{Q_f(1 - Y_1)} \right] \quad (13b)$$

$$\beta_2^{III} = \ln \left[\frac{C_{s,2}}{C_{R,2}} \right] = \ln \left[\frac{C_{s,2}Q_{III}}{Q_f C_{f,2}(1 - Y_2)} \right] \quad (13c)$$

where $C_{E,2}$ is the concentration of component 2 in the extract, $C_{R,2}$ is the concentration of the more retained component in the raffinate, C_2^I is the concentration of component 2 that can be leftover in the Zone I while still achieving the target yield. C_1^{II} is the concentration of the less retained component (component 1) that can remain Zone II and still achieve the target yield. $C_{s,1}^*$ is the concentration of component 1 right before the feed port in Zone II, and $C_{s,2}$ is the plateau concentration of component 2 after the feed port in Zone III. The values of these terms are adjusted for a 3-zone open-loop system. The β_i^j terms in Eq. (13) can be expressed in terms of zone velocities, known concentrations, and target yields. The concentrations of component 2 in the raffinate and extract are calculated based on the overall mass balance as follows:

$$C_{E,2} = \frac{Q_f Y_2 C_{f,2}}{Q_I} \quad (14)$$

$$C_{R,2} = \frac{Q_f(1 - Y_2)C_{f,2}}{Q_{III}} \quad (15)$$

Where Y_2 refers to the yield of component 2 which is specified in the design, $C_{f,2}$ is the feed concentration of component 2, Q_f is the feed flow rate, Q_I is the Zone I flow rate or the extract flow rate, and Q_{III} is the Zone III flow rate or the raffinate flow rate. The plateau concentration ($C_{s,2}$) is solved using an iterative process as explained in Appendix D.

C_2^I and C_1^{II} can be determined based on the overall mass balances of component 2 and component 1 respectively. The resulting expressions are shown below.

$$C_2^I = \frac{C_{F,2}Q_F(1 - Y_2)}{Q_I} \quad (16)$$

$$C_1^{II} = \frac{C_{F,1}Q_F(1 - Y_1)}{Q_{II}} \quad (17)$$

Based on the mass balance at the boundary between Zones II and III, $C_{s,1}^*$ can be approximated using $C_{f,1}$. This approximation is based on the assumption that $C_{s,1}$ is approximately equal to $C_{R,1}$.

Substituting Eq. (14-17) into the first from shown in Eq. (13) and making the stated approximations gives the final form of Eq. (13).

The four SWD equations, Eqs. (9), and (12-17), are solved to obtain the four operation parameters (three zone velocities and the port velocity). The value of the decay coefficients and the retention factors are not known when beginning the problem because they are dependent on the plateau concentrations. Therefore, an iterative method must be used to solve for port velocity and zone velocities from the four SWD equations (Eq. (9e-g) and Eq. (11)). An initial guess for the plateau concentrations and decay coefficients is required to solve for the port velocity and zone velocities. Convergence is achieved more quickly if the initial guess is close to the actual solution. For this reason, the solution for ideal systems is obtained first, and used as the initial guess for solving the SWD equations for non-ideal systems.

3.2.4 Example Systems

Example 1: Langmuir Isotherms with Counter-Ion Modulator

The first example to be discussed in this paper was introduced in Candy et al. 2012. In that study, an IgG sample was separated from a weakly adsorbing impurity using an optimized batch stepwise elution process. The parameters from this example were taken from the literature and they can be estimated using the methods described in Candy et al. [41]. The protein has a high solubility (>100 g/L) [67]. A silica-based adsorbent, AbSolute, ($d_p = 44 \mu\text{m}$) was used in a column, 5 mm in diameter and 8.5 cm in length. The optimal loading fraction, length and flowrate were found using a trusted-region simplex search [46]. In the process of Candy et al. 2012, a step change from pH 7.4 to pH 3 was used to elute the target protein. In this study, an open-loop, 3-zone SMB was designed using the same material and feed parameters for comparison with the optimal batch stepwise elution system; however, the pH of the desorbent was 5.4 instead of 3. The feed concentration used was 1 g/L for both the product and the impurity. This was done to assure that the assumption that the pH wave travels faster than the desorption wave is met. At a pH of 5.4, the target component adsorbs weakly (See Fig. 3.5). At a pH of 3 or lower, the target eventually becomes approximately non-adsorbing, and thus would move at the same velocity as the pH wave.

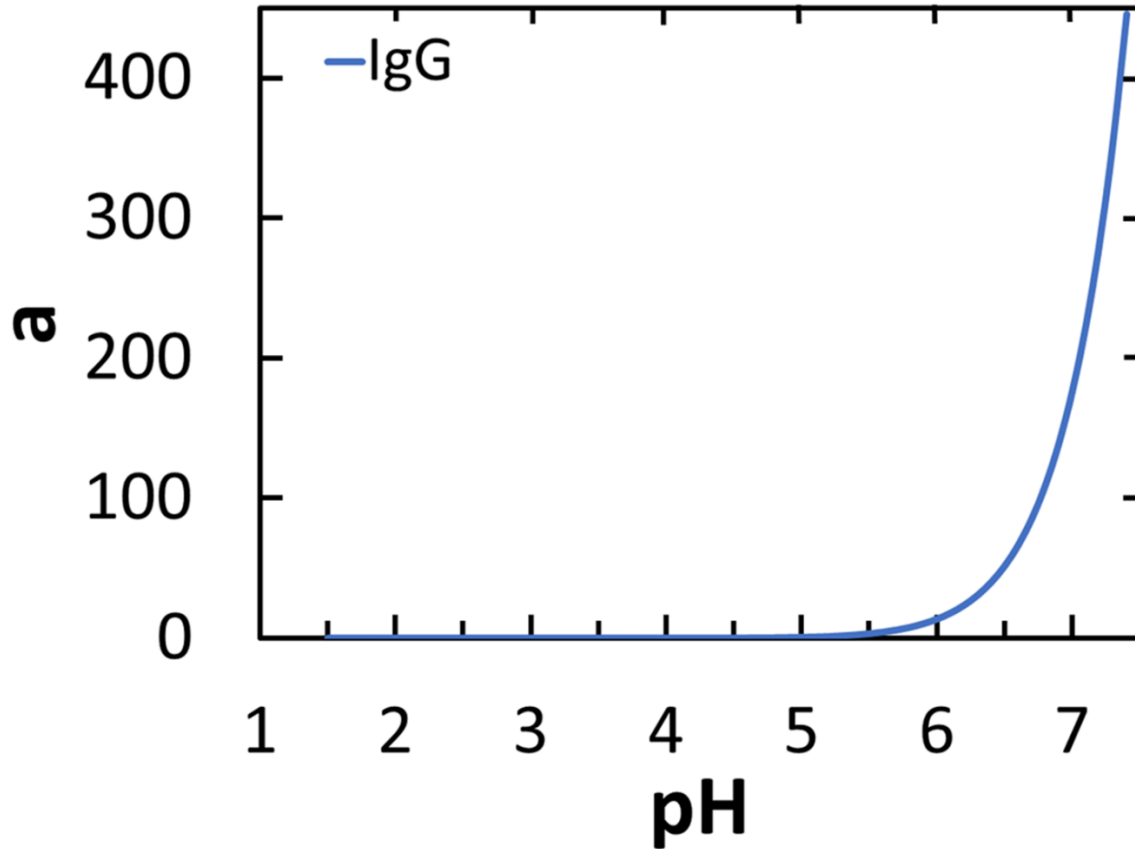


Figure 3.5 Langmuir “a” value for target protein for Example 1. The isotherm parameter for the impurity is not shown on this figure because it is a constant 1.6 and would not be easily visible on the scale shown in the figure. Adsorption done at pH 7.4 and desorption done at 5.4

The target component isotherm was modeled using a modulated Langmuir isotherm [41]. The modulator in this case is a function of the normalized pH. The Langmuir “a” and “b” values for the target component were:

$$a_i(pH^j) = q_{max}K_A \left(\frac{pH^j}{pH_{ref}} \right)^n \quad (18a)$$

$$b_i(pH^j) = K_A \left(\frac{pH^j}{pH_{ref}} \right)^n \quad (18b)$$

In this equation, q_{max} is the sorbent capacity, K_A is the association equilibrium constant, n is the pH dependent equilibrium order, pH_{ref} is a reference pH, and pH^j is the pH in zone “j”. The impurity in this example was modeled with a linear isotherm. When this modulated isotherm is matched with a linear isotherm for an impurity, the retention factors are as follows:

$$\delta_2^I = \varepsilon_p + (1 - \varepsilon_p)q_{max}K_2 \left(\frac{pH^I}{pH_{ref}} \right)^n \quad (19a)$$

$$\delta_1^{II} = \varepsilon_p + \frac{(1 - \varepsilon_p)a_1^{II}}{1 + K_2 \left(\frac{pH^{II}}{pH_{ref}} \right)^n} C_{p,2} \quad (19b)$$

$$\delta_2^{III} = \varepsilon_p + \frac{(1 - \varepsilon_p)q_{max}K_A \left(\frac{pH^{III}}{pH_{ref}} \right)^n}{1 + K_A \left(\frac{pH^{III}}{pH_{ref}} \right)^n} C_{s,2} \quad (19c)$$

The values of the constants from the literature are given in Table 3.2 and the effect of pH on the Langmuir “a” value of the target component is shown in Fig. 3.5. Because the impurity has a linear isotherm that is independent of pH, and the linear “a” value is very low in comparison to the Langmuir “a” value at high pH values, the impurity isotherm is not shown in Fig. 3.5. The selectivity for this separation is very large (>100). It is important to note that the Standing-Wave Design equations have been derived on a solid sorbent volume basis. The parameters in the literature and listed later in this paper were on a column volume basis and were converted to a solid volume basis using the bed void fraction and porosity before the SWD equations were solved.

Three columns were used in the design of this SMB because the mass transfer effects were small due to the small size of particles used in this separation. The full simulation parameters for this are given in Table 3.2. The target yield for this separation was set to 99% for both components.

Because the resin used in this example is a silica-based resin and is thus stable under high pressures (>690 kPa), a case study was done using this example in which three-zone open-loop pH-SMBs were designed at different pressure limits. The pressures in all cases were calculated using the Ergun equation [37]. In Case 1, the pressure limit used in the study Candy et al. 2012 (250 kPa) was used for the design. In Case 2, the pressure limit was increased to 690 kPa, which is a common limit for low pressure systems. In Case 3, no pressure limit was set, and the system was limited by the step time. The step time limit was ten seconds. Any value less than ten seconds was considered too short to control accurately. The zone flow rates and step times are given along with the results in Results Section 3.1.

Table 3.2 column and Simulation Parameters for Examples 1 and 2. All other parameters not shown in table can be found in Appendix E. Different Lumped resistance film modes were used based on the available data from the literature sources. Parameters taken from Candy et al. [1] and Cristancho and Seidel-Morgenstern [26].

System Parameters								
L_C (cm)	Number of columns	Column Diameter (cm)	d_p (μm)	ε_b	ε_p	Y	$E_{b,i}^j$	Film Mass Transfer Coefficient
2.5	3	Exp. 1: 0.5 Exp. 2: 0.7	Exp. 1: 44 Exp. 2: 34	0.35	0.69	0.99	Chung and Wen	Wilson and Geankoplis
Isotherm Parameters								
Example 1								
Target Compound				Impurity				
q_{max}	K_A	pH_{ref}	n	a_1				
73 g/L	6.1 L/g	7.4	16.6	1.6				
Example 2								
$a_{o,i}$		x_i		$a_{o,i}$			x_i	
0.79		2.01		0.79			1.43	
Simulation Settings and Numerical Parameters								
PDE Discretization Method	Number of Elements	Material Balance Assumption	Kinetic Model Assumption	Lumped Resistance Film Mode				
QDS	Exp. 1: 181 Exp. 2: 150	Convection with Estimated Dispersion	Linear Lumped Resistance	Exp. 1: Fluid Exp. 2: Solid				
Mass Transfer/Film Coefficient	Loading Basis		Step Size	Integration Method				
Constant	Volume Basis		0.000005-0.005	Fixed Step Implicit Euler				

Example 2: SMB Purification of Antibody Fragments [65]

The second example discussed in this paper is based on a system introduced in Cristancho and Seidel-Morgenstern. In their study, single chain antibody fragments were separated using a simulated moving bed system designed based on the Triangle Theory, without using a search algorithm and rate model simulations to take into account of any mass transfer effects. The material, feed, and equipment parameters were taken from the literature study unless noted otherwise [65]. The columns used in this system were 2.5 cm \times 0.7 cm i.d. HisTrap HP columns by GE Healthcare Bio-Sciences. Adsorption and separation occurred at pH 7 whereas desorption occurred at pH 3.8.

In this system, both the impurity and the target protein were modeled using a modulated linear isotherm [65]. The form of the isotherms was:

$$q_i = a_{o,i}pH^{x_i}C_i \quad (20)$$

where $a_{o,i}$ and x_i are constants. In this example, the impurity competes with the target protein for adsorption. The parameters are listed in Table 3.2, and the linear isotherm value as a function of pH is shown in Fig. 3.6. Based on the parameters in Table 3.2 the selectivity for this system is 3.1 at a pH of 7. The selectivity is reduced to 2.2 at pH 3.8. The selectivity in Example 2 is lower than in Example 1.

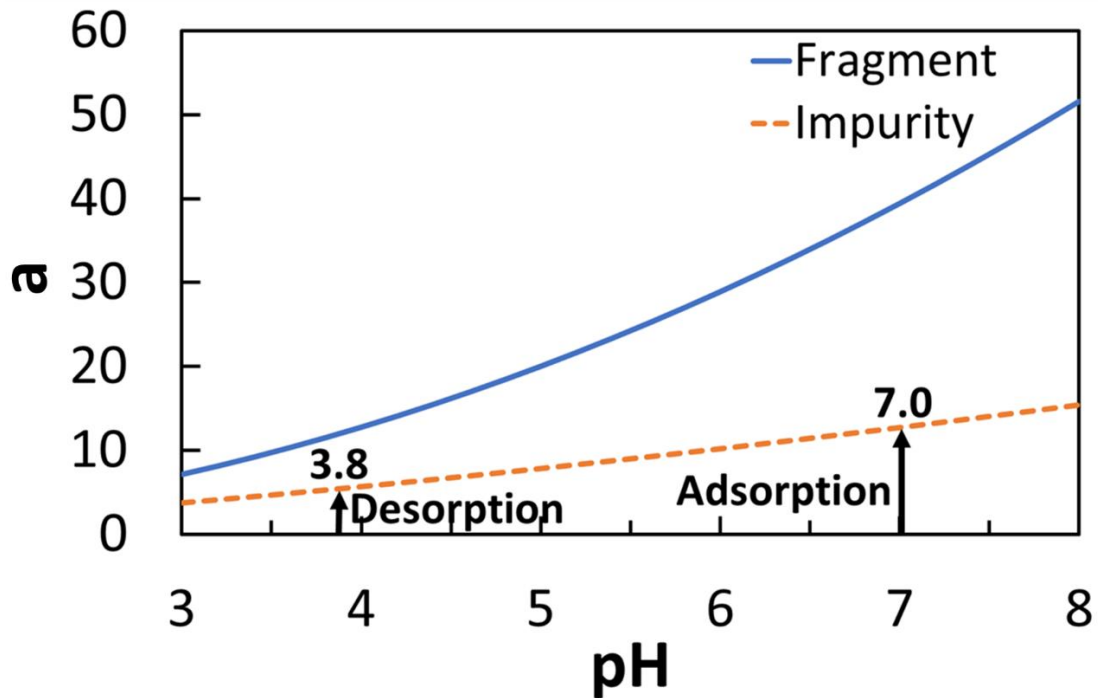


Figure 3.6 Isotherm parameters for the fragment and impurity for Example 2. Adsorption will take place at a pH value of 7.0 and desorption will take place at a pH value of 3.8. The selectivity is greater at pH 7.0

For this example, a 3-zone pH SMB was designed with three columns. The small particles in this example also allowed for sharp waves and high product purities with only one column in each zone. The pH-SMB designed using the SWD had the same column length and diameter as the literature example [65]. The target yield of both components was set at 99%. A summary of the simulation and column parameters is given in Table 3.2, and a summary of the flow rates and step times can be found in Results 3.2. Two case studies were performed in this example to

examine the effects of larger particles (80 μm , Case 2) and shorter column length (1 cm, Case 3). The other physical parameters and numerical parameters in all three cases were the same.

3.2.5 Rate Model Simulations

The simulations of all cases in this study were performed using Aspen Chromatography. The mass balance equation for the Aspen Chromatography model can be found in Appendix E. The SMB template was modified for the simulations. The isotherms for both examples were programmed into the workbook using the user defined isotherms option. In all simulations, the pH was programmed as an adsorbing component with an equilibrium distribution coefficient of 10^{-5} and thus the pH was approximately non-adsorbing. In each case, the smallest step size in the range given in Table 3.2 was used to begin each simulation. After the initial step, the step size was increased to the larger value to improve the speed. This was done to prevent instability in Aspen Chromatography during the initial loading of the column. Any parameters that have been changed from the recommended default settings in Aspen Chromatography can be found in Table 3.2. All other parameters have been left at the default setting for the SMB template.

The SMB simulations in this study did not have dead volume, and the pH was approximated as a non-adsorbing component. Small particles also minimized wave spreading in the column. A combination of these effects allowed for skipping step 1b in Fig. 3.2. As Column 1 is moved to Zone III in Step 2a, the pH wave moved much faster through the column than the adsorption wave of the target protein. If large dead volume, mass transfer effects, or buffer interactions with the resin could cause the pH wave to spread, there may be a need to allow for equilibration and regeneration between Step 1b and Step 2a. One possible solution to this problem are to add an additional column to Zone III. By adding this additional column, the pH equilibration will happen before the higher affinity product reaches the second column in Zone III. Another possibility is to tune the decay coefficient of Zone I so that it is higher. By raising the velocity in Zone I, this will allow extra time within a step to re-equilibrate the first zone after the extract product is collected. Because dead volume is usually much smaller than column volume in industrial applications, this problem was not considered in this study.

3.3 Results

A summary of the results from Example 1 is given in Section 3.1. The results from Example 2 are given in Section 3.2. Because of space limitations, only select profiles are shown in this section. The dynamic profiles of all other cases were qualitatively similar to these two example cases.

3.3.1 Results for Example 1

A summary of the results from the three different pressure cases can be found in Table 3. The rate model simulations indicated that the SWD method successfully separated the two components with high-purity (99.9%) and yield (99%). In all three cases, the target yield of 99% was achieved. The product concentration was about 19 g/L in all three cases. The simulated productivity in each case was significantly higher than in batch operation. At the same pressure as the batch operation, the productivity from the SWD pH-SMB was 5 times higher than the batch operation with both a higher yield and a higher product purity (Case 1). The productivity was about 14 times greater than the optimal batch system at the operating limit of low-pressure pumps and columns (Case 2). Solvent consumption is one-eighth of that of the optimal batch system. Examples of column profiles from Case 1 are shown in Fig. 3.7. The concentration of the target product is shown in Zone I.

Table 3.3 Results for Example 1: Comparison with Optimal Batch. No pressure limit was set in Case 3. The pressure was calculated in Cases 1 and 2 using the Ergun Equation [42].

Parameter	Separation of Target IgG from a Weakly Adsorbing Impurity			
	Case 1	Case 2	Case 3	Optimal Batch
Column length (cm)	2.5	2.5	2.5	8.5
Pressure limit (kPa)	250	690	2,580*	250
Number of columns	3	3	3	1
Flow rates (mL/min)	0.78/0.25/15.3 (I/II/III)	2.1/0.68/41.7 (I/II/III)	9.2/2.9/178 (I/II/III)	6.5
Step time (s), pH-SMB	121	44	10	
Cycle time (s)	362	132	30	450
Product conc. (g/L)	19	19	19	4.64
Solvent Consumption (L extract/L feed)	0.05	0.05	0.05	0.4
Purity	99.9	99.9	99.9	98.1
Yield	99.4	99.2	99.4	97.7
Productivity (kg/L/day)	15	40	171	2.9
Normalized Productivity	5.2	13.8	59.0	1

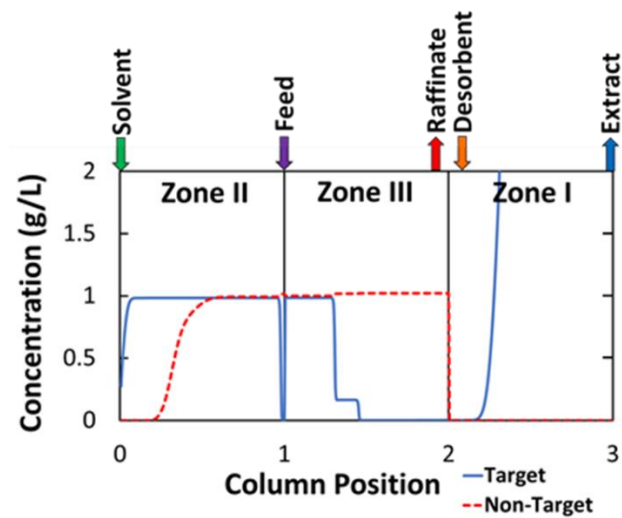
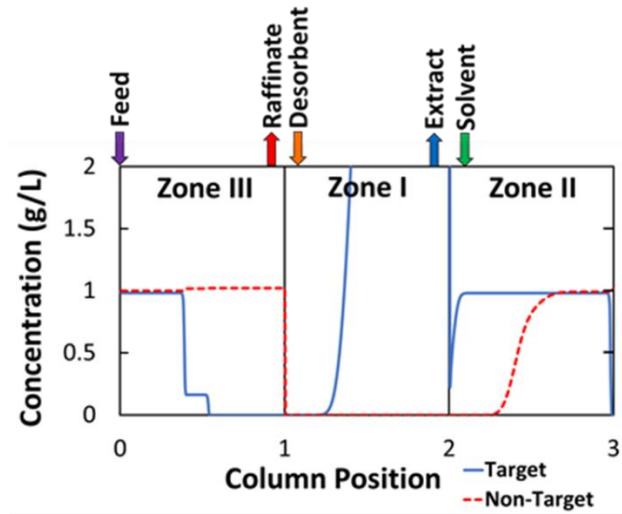
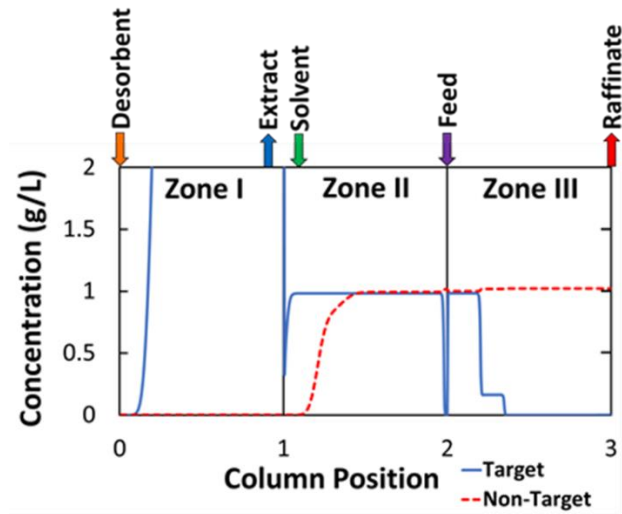


Figure 3.7 Example profiles for SMB designed for Case 1 of Example 1 using SWD

3.3.2 Results for Example 2

The results for three cases for Example 2 are summarized in Table 3.4. Case 1 used the same particle size (34 μm) and column length (2.5 cm) as the literature case. Case 2 used a larger particle size (80 μm), whereas Case 3 used a shorter column length (1 cm). For all the three cases, the SMBs were designed using the SWD and operated at a maximum pressure of 500 kPa, which is the pressure limit of the resin. The rate model simulations indicated that the SMB designed using the Standing-Wave Design achieved for all three cases the target yield of 99% with a product purity of 99%, which is higher than the best experimental literature case, which gave a purity of 66% and a yield of 91.4%. All three cases had an order of magnitude or higher productivity than the literature case. The productivity in the system with a shorter column length (Case 3) showed higher productivity than both the literature example and the large particle example at the same pressure (Case 2). Examples of the column profile for Case 1 are shown in Fig. 3.8.

Table 3.4 Results for Example 2: Comparison with Literature pH-SMB for the Separation of Target antibody fragments from a competitive adsorbing impurity. *Length of 2.5 cm was selected due to commercial availability of this column size. The inner diameter of the columns in both cases was 0.7 cm.

Parameter	Case 1	Case 2	Case 3	Literature pH-SMB
Column length (cm)*	2.5	2.5	1	2.5
Resin Pressure Limit (kPa)	500	500	500	500
Particle Size (μm)	34	80	34	34
Number of columns	3	3	3	4
Flow rates (mL/min)	12.0/13.1/36.1 (I/II/III)	86.7/84.1/161.1 (I/II/III)	27.9/30.8/60.8 (I/II/III)	1.03/1.02/2.3 (I/II/III)
Step time (s), pH-SMB	61	10	11	282-324
Cycle time (s)	182	30	33	1,128-1,269
Product conc. (mg/L)	1.7	0.78	0.95	1.1
Solvent consumption (L Extract/L Feed)	0.52	1.12	0.93	0.44
Purity	99	99	99	57-66
Yield	99	99	99	27.4-91.4
Productivity (g/L/day)	10	34	37	0.17-0.58
Normalized Productivity	17-59	58-199	64-220	1

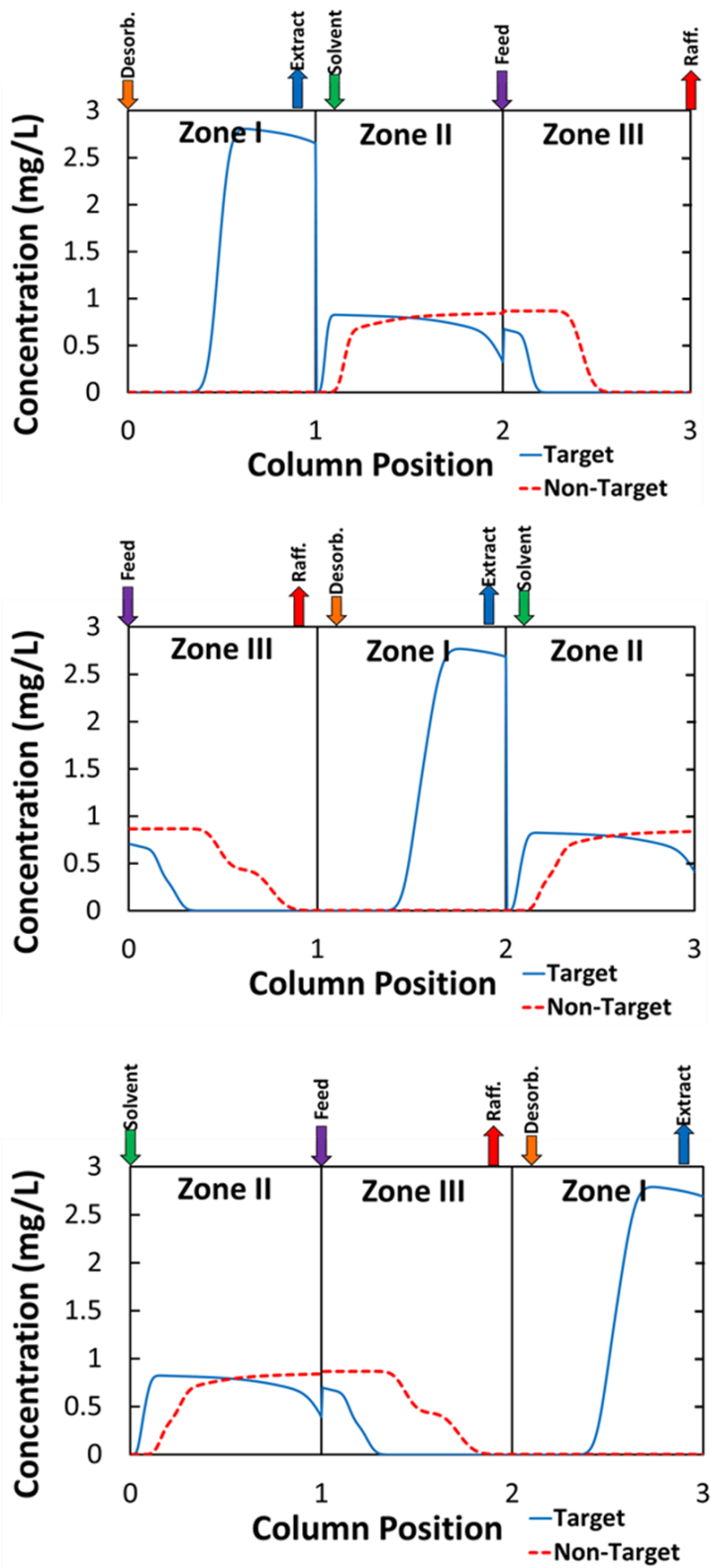


Figure 3.8 Example profiles for SMB designed for Case 1 of Example 2 using SWD. Profiles shown at the middle of a step

3.4 Discussion

A full comparison of a simulated moving bed design using the SWD method with an optimized batch system will be discussed in Section 4.1. Additionally, the implications of the effects of pressure will be discussed as well. In Section 4.2, an SMB designed using SWD will be compared to an SMB designed using the Triangle Theory. The benefits of the Standing-Wave Design method over other design methods will also be discussed.

3.4.1 Discussion of Example 1: Comparison with Optimal Batch Stepwise Elution

In the example batch system, productivity was optimized by adjusting the step change in pH, column length, loading volume, and elution volumes, while the flowrate was set at the pressure limit (250 kPa). A minimum product purity of 98% was required, meaning that based on the mass balance for a binary mixture of similar concentrations, the target yield was also 98%. In batch stepwise elution separation, a small band overlap was required to achieve 98% purity. Wave spreading due to mass transfer effects limited the productivity of the batch system. To achieve higher than 98% purity, say 99%, in this batch system, the productivity in Table 3 would be reduced as a result of the lower flowrate needed to decrease the wave spreading to meet the purity requirement.

The targeted yield for the SWD was first set at 98% to match the literature study. However, it was found that the optimal flow rate in Zone III for 98% target purity and yield exceeded the pressure limit (250 kPa) and the step-time was lower than 10 seconds. To operate the Zone III flow rate at the same pressure limit as the batch system, Case 1, the SWD can achieve 99% purity and yield, which are higher than the purity and yield of the batch system, 98%. Rate model simulations were used to verify the SWD of Case 1, and the results listed in Table 3 showed that indeed the target yield of 99% in SWD was achieved.

To further prove that the productivity of Case 1 was limited by the low-pressure requirement (250 kPa), the pressure limit was increased to 690 kPa in Case 2. Again, the rate model simulations of the SWD met the target yield and purity requirement (99%). The productivity was more than doubled compared to Case 1 and an order of magnitude higher than the Optimal Batch case. If the column packed with AbSolute were rated for 690 kPa, then the productivity could be greatly increased without a major increase in the equipment cost.

If high pressure equipment is available (Case 3), the productivity can be further increased for the same purity and yield (99%) with a similar product concentration. In the high-pressure case (Case 3) the pressure was estimated using the Ergun equation to be 2,580 kPa. The SWD results showed that the productivity was limited by the step time of 10 seconds. Still, Case 3 gave a productivity about 12 times that of Case 1 and 59 times that of the Optimal Batch case. If the sorbent cost is the major purification cost for this separation, it may be financially beneficial to utilize high pressure equipment for commercial operation.

In all three cases, the rate model simulated yield and purity exceeded the target yield and the target purity in the SWD because the flow rate correction terms in the SWD, Eq. (9) to counter the wave spreading due to mass transfer effects were derived from linear-adsorption isotherm systems. The correction does not account for wave sharpening effects in non-linear isotherm systems. For this reason, the purities and yields achieved in the simulation were even higher than the target values of 99%.

The yield and productivity of SMB in Example 1 are less affected by the mass transfer limitations than those of the batch system because SMB only requires a partial band separation in Zones II and III to achieve high product purity and high yield. This also means that a larger fraction of the bed volume can be used for separation, and the sorbent is used more efficiently. Furthermore, desorption, separation, and loading occur in parallel in SMB; the overall cycle time is reduced compared to batch. If the component is subject to proteolytic degradation, this shorter cycle time can reduce protein degradation during capture and purification. Additionally, a larger fraction of the bed is loaded, leading to a more efficient desorption step because more product can be released. This results in a higher product concentration and a solvent consumption that is potentially 8 times lower than the batch system.

3.4.2 Discussion of Example 2: Comparison with Literature SMB

The rate model simulations indicated that the simulated moving bed designed using the Standing-Wave Design method could have a productivity that was an order of magnitude higher than one designed using the Triangle Theory. It was noted in Cristancho and Seidel-Morgenstern that their pH-SMB was not optimized. To determine the best zone flow rates to achieve desired product purity and yield in non-ideal systems, the Triangle Theory involves a systematic search using rate-model simulations which require solving partial differential equations. The Standing-

Wave Design method allows for a high productivity, high-purity, and high yield design without search using rate model simulations. While the results were verified using rate model simulations, the design solution was obtained in less than a second because the four Standing-Wave Design equations are algebraic equations, not partial differential equations.

The SMB system in the literature had a wide pH front, which may have, along with the design method, which was not optimized, contributed to the low purity and yield in the literature system. The dead volume in columns for commercial production should be reduced, causing the pH waves to sharpen and improving the product purity and yield.

It is also important to note that the pressure limited the productivity of this system. The sorbent pressure limit was 500 kPa. A more robust sorbent with similar adsorption properties would increase the sorbent productivity. If the pressure limits the zone flow rates, one cannot operate at the maximum flow rate allowable by the mass transfer parameters. This is evident in Example 2, Case 2. The system with 80-micron particles (Case 2) had an increased overall productivity because larger particles allowed for faster flow at the same column length. Because Case 1 was not limited by the mass transfer effects, larger particles could be used in Case 2 without a reduction in purity. For the same column length, larger particles can be used to increase the productivity for this system. Alternatively, a shorter column with 34 μm particles (Case 3) would allow a higher feed flowrate to increase the productivity. Larger particles or shorter columns may help increase the productivity in Example 1 as well because the productivity is similarly limited by the pressure and not by the mass transfer efficiency.

Example 2 also indicates that the SMB gives even higher advantages over batch systems when there is a competitive impurity. The rate model simulations of the SMB designed using the SWD gave productivities that were an order of magnitude better than the SMB designed using the Triangle Theory, which was already an order of magnitude more productive than a batch system for the same separation [65]. That means that it is possible for an SMB designed using SWD is two orders of magnitude more productive than the reported optimal batch systems. The benefits compared to batch systems are greater for Example 2, because the feed contains a more competitive impurity. While the rate model simulations indicate that a two order of magnitude increase is possible in batch systems with a competitive impurity, experimental verification is needed in future studies.

3.5 Conclusions

Although the pH-SMB has shown potential for higher sorbent productivities and higher purity and yield separations than batch chromatography for non-isocratic systems, the use of pH-SMB systems has been limited. One reason for this limited use is the increased complexity compared to batch systems. The large number of system parameters make the design of effective non-isocratic SMBs challenging. To overcome this barrier, we developed a new design method that can find the operating parameters to achieve high product purity and high yield. The design method was verified using rate model simulations.

This study documents the theoretical foundation, equations, and algorithm of the Standing-Wave Design method for non-isocratic systems. The general equations for the Standing-Wave Design of non-isocratic and non-ideal systems were developed for both linear and non-linear isotherms. The Standing-Wave Design method allows for fast and efficient design of SMB systems without extensive search in the four-parameter space. In Example 1, rate model simulations indicated that the 3-zone, open-loop SMB achieved higher purity and yields and potential productivities between 5 and 14 times higher than that of an optimal batch stepwise elution system with low pressure equipment. In Example 2, the SMB system designed using the new SWD method showed an order of magnitude higher potential productivity compared to the pH-SMB designed using the Triangle Theory method. The SMB designed using the SWD method also produced products with higher purity and higher yield. In both examples, the pressure drop was the limiting factor for the feed flow rate in the system. Therefore, using larger particles or shorter columns could achieve a higher productivity because they allowed for higher flow rates. Higher pressure columns and equipment allow for higher productivity. Furthermore, the advantages of a 3-zone, non-isocratic SMB are most significant if the feed has a strongly competitive impurity. The ability to design efficient systems quickly without any trial-and-error experiments or simulations helps remove a major barrier for the application of the three-zone, open-loop SMB. Compared to batch stepwise elution systems, the 3-zone, open-loop SMB could potentially give an order of magnitude higher productivity in systems with weakly competing impurities and two orders of magnitude higher productivity in systems with strongly adsorbing impurities.

4. CONTINUOUS LIGAND-ASSISTED DISPLACEMENT FOR THE SEPARATION OF TWO OR THREE RARE EARTH ELEMENTS

4.1 Introduction and Background

The Rare Earth Elements (REEs) are key components of modern technology. They are used in magnets, computers, screens, and other electronics [68]. The supply of REEs in the US is at risk because there is no production of REEs in the United States, as all of the mined materials were exported to China for purification [69]. This is partially due to the costly, and environmentally damaging process used in the purification of REEs [70,71]. Industrially, a liquid-liquid extraction process is used for the separation of REEs from each other [71]. Because the REEs have similar physical properties, hundreds to thousands of mixer-settler units for liquid-liquid extraction are needed to purify the 17 REEs [72]. Very few resins have the selectivity to separate REEs using traditional chromatographic methods [73–75]. The resins that currently have significant selectivity are expensive and lack stability for multiple runs [76].

To address the issues with traditional chromatographic separations, Ligand-Assisted Displacement Chromatography (LAD) was developed in the 1940s and 1950s by Spedding et al. [3,77–82]. LAD utilizes the selectivity of chelating agents (ligands) to separate the REEs on a strong acid cation exchange resin. In LAD, a presaturant that is most preferred by the ligand is used to ensure that sharp bands form at the boundaries between REE bands. These REE bands resemble a displacement train that is formed in traditional displacement chromatography. The presaturant has the lowest effective sorbent affinity, creating a cascade in which lower affinity solutes are displaced by higher affinity solutes [74,75].

The separation mechanisms in LAD differ from those of ligand-assisted elution (LAE) [73]. In LAE, the presaturant has the lowest affinity for the ligand. The solute with the highest affinity for the ligand elutes first. The adsorption wave of each REE band is sharp, whereas the desorption wave is diffuse, because the effective sorbent affinities of REEs against the presaturant are greater than 1. The shape of the eluted REE bands are similar to that in conventional elution chromatography. Our previous studies showed that the ligand efficiency and REE product concentrations of LAE are an order of magnitude lower than those of LAD. For this reason, this study is focused on LAD.

The feasibility of LAD for the separation of REE mixtures was demonstrated by Lindstrom et al. in the 1950s and 1960s [83,84]. This was an attractive process because EDTA, the ligand used in these studies, is recyclable and generally regarded as safe. However, the LAD processes in these cases were not economically viable, because the productivity was too low and there were no simple, reliable methods for optimization or scale up.

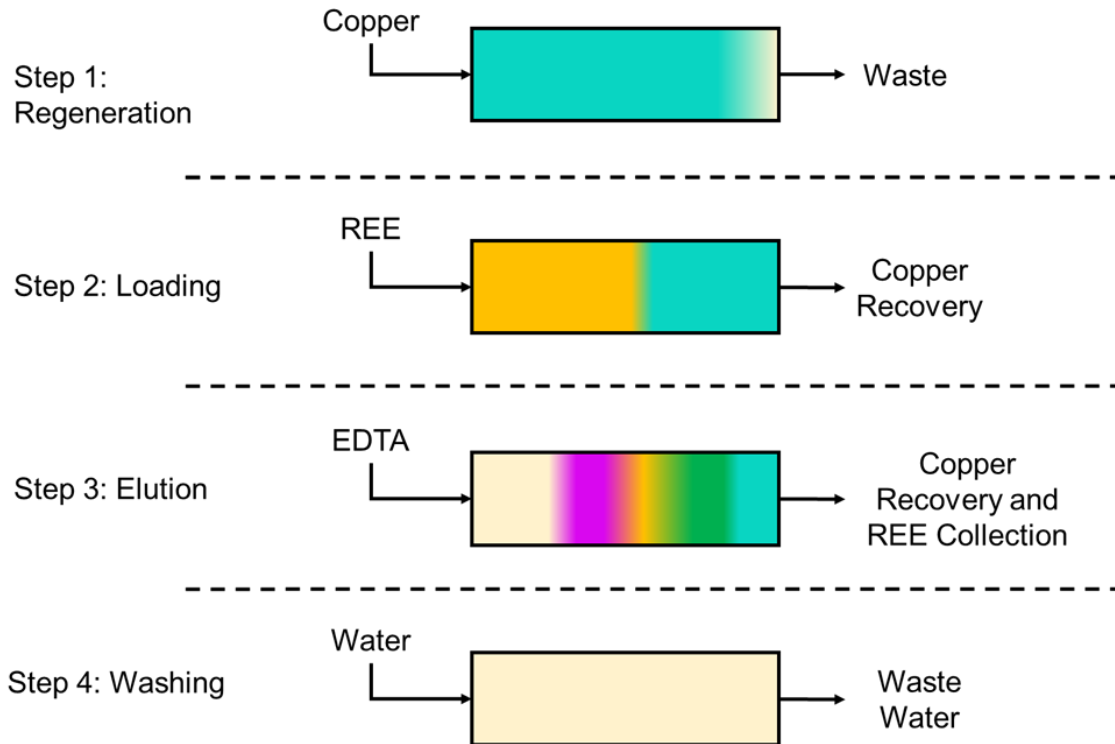


Figure 4.1 Example of batch LAD Process Cycle. After Step 4, the cycle is repeated

In the 1970s Helfferich and James developed a design method to determine the minimum column length required to separate REEs in ideal systems, which have no diffusion or dispersion effects [85]. LAD was also extended to separate heavy REEs by Moore et al in 1995 [86]. However, for commercial viability non-ideal systems are required as higher flowrates are needed for more competitive productivities. Recently, Choi et al. developed the Constant Pattern Design Method for the design of LAD [74,75]. This method determines the minimum column length required to separate REEs for non-ideal systems. This method was applied and tested for both binary, and multicomponent separations of equimolar mixtures of REEs for batch processing. An example of a batch LAD process is shown in Fig. 4.1. With this design method, competitive processes for the separation of REEs can be done at low cost with high productivity.

However, the industrial use of LAD has been limited by a few barriers. First, the productivity and yield of batch systems are limited by several factors. Regeneration, washing, loading, and separation occur in a single column. For low selectivity systems, the overall sorbent productivity is limited by the relatively long column length and low flowrate required for separating the individual bands. Furthermore, the regeneration and washing times also increase the cycle time significantly, reducing the average sorbent productivity.

A second limitation of batch chromatography is that to achieve high yields of REEs in complex mixtures, productivity must be sacrificed. In some feeds, minor and trace components with more than an order of magnitude lower concentrations than the major components make it difficult to separate all components with high purity and high yield. To collect these minor components with high yield, a very low velocity must be used to shorten the length of the mass transfer zones. Because of the low velocity, the overall productivity of these systems is extremely small.

Another barrier to the use of LAD industrially is the variability of the feed composition in real REE mixtures. Ores, magnets, and other common rare earth sources can have different compositions in each new batch. To determine the operating parameters for each batch, measurements must be taken of the composition of the feed. The experimental methods used to determine feed concentration have experimental errors. Limited work has been done to test the robustness of the constant pattern design method to variations or error in the feed composition.

To overcome these limitations, this study introduces a multi-zone continuous configuration that reduces the cycle times significantly by increasing the sorbent utilization and allows for the purification of all components with high purity, high yield, and high productivity. A concise splitting strategy based on the selectivity weighted composition factor (γ_i) is developed to reduce the separation load in each zone to further increase the productivity. This study demonstrates that it is possible to recycle the mixed bands from a LAD process without any further processing to increase the overall productivity and yield. While previous studies have suggested that the mixed bands can be recycled onto a column, the mixed bands in those studies were recycled onto the middle of the column instead of the front of the column where the feed was loaded. By loading some REEs in the middle of the column instead of the top of the column where the rest of the feed was loaded, the overall effective column length for separation was reduced [86]. This study also uses rate model simulations to examine the robustness of the constant pattern design method by

varying the feed composition to examine the effects on the yield and purity when the operating parameters are held constant.

This study extends the previous Constant Pattern Design method to continuous systems. An example of a continuous LAD system with two columns is shown in Fig. 4.2.

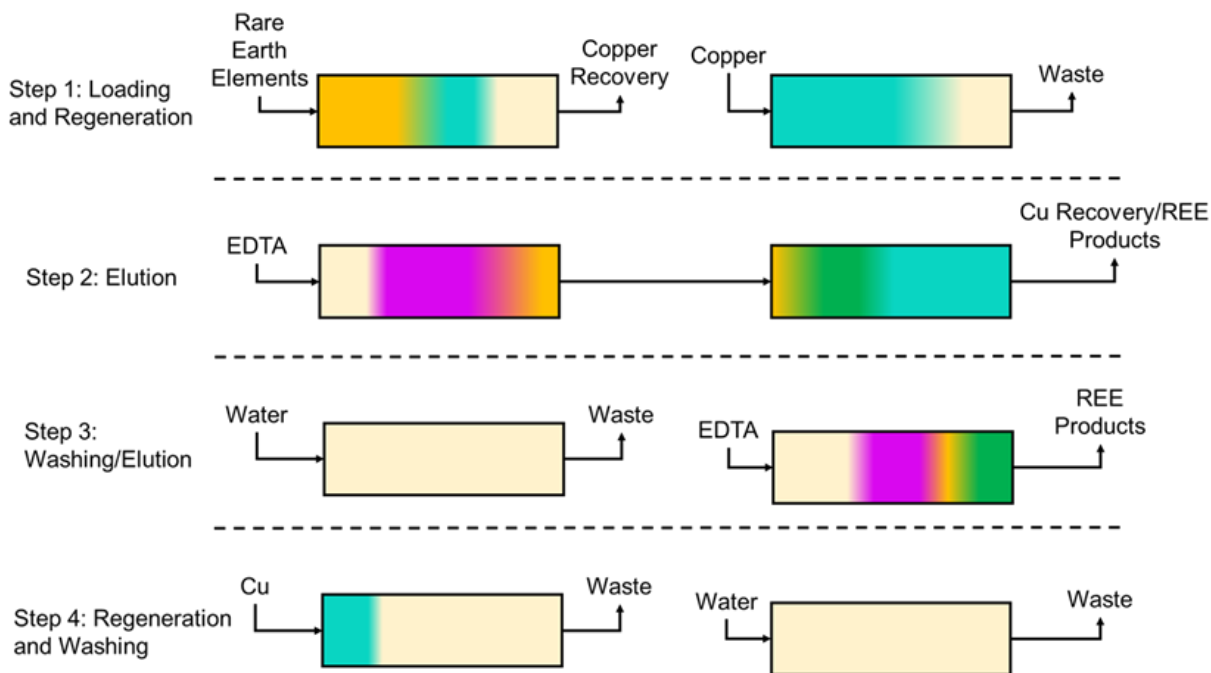


Figure 4.2 Example of a Continuous LAD Process with 2 columns; recycle of the mixed bands is not shown for simplicity

The objectives of this study are to (1) expand the Constant Pattern Design Method for batch LAD systems to continuous systems; (2) demonstrate the recycle of mixed bands to achieve high yield (>99%) at high productivities; (3) determine the optimal target yield based on the productivity and yield equations; (4) experimentally demonstrate continuous ligand-assisted displacement separations of equimolar binary and ternary mixtures as well as a complex mixture based on the composition of a magnet crude; and (5) test the robustness of the LAD method to variations in feed composition.

To achieve these objectives the following approach was taken: First the continuous configuration was demonstrated for the separation of binary and ternary equimolar mixtures. Next a complex mixture representative of a magnet crude was separated using two-zone continuous LAD. Finally, the robustness of this design method was tested using rate model simulations with

a variety of feed compositions. All other operating parameters were held constant in the rate model simulations.

The highlights of this study follow. The recycle of the mixed bands allows for >99% yield of REEs while maintaining high productivities. The productivity of a continuous LAD system is more than double that of a batch system without recycle for an equimolar mixture, and 60 times higher than conventional liquid-liquid extraction. The flexible configurations of continuous systems can accommodate a variety of feed mixtures. Less copper is required in continuous systems compared to batch leading to a reduction between 30-50%. For a complex mixture of Dy, Nd and Pr whose composition is representative of a magnet crude, the continuous multi-zone LAD system shows productivities two orders of magnitude higher than that of a single column batch system with similar yield (99%) and purity (>99%) and 70% higher than a batch continuous LAD. Variations within 10% of the measured feed composition did not show significant effect on the final product purity or yield.

4.2 Theory

The Constant Pattern Design Method for ligand-assisted chromatography was first developed in Choi et al. [74,75]. It can be used to determine the minimum column length needed to reach a constant pattern isotachic train for non-ideal systems. That method used a strategic combination of multiple dimensionless parameters to simplify the multi-dimensional design space into a two-dimensional space, or a map, Fig. 4.3. The map divides the space into two regions: a constant-pattern region and a transient pattern region. The boundary between the two regions can be correlated using a simple function, which can be used to calculate the minimum column length needed to reach the constant-pattern state. In this study, an improved map is developed. The previous map of Choi et al. was developed based on the simulation results obtained from a constant-separation factor isotherm model. In the actual system, when free ions are fed into the column, the adsorbent has negligible selectivity, therefore no REE separation occurs during loading. Separation occurs only after the ligand is introduced into the column. A new correlation (Fig. 4.3) was obtained using simulations based on the improved isotherm model, which more closely simulates the actual system. The improved maps, the yield equation derived based on shock layer theory for displacement chromatography, and the productivity equation used to solve for the maximum productivity for a continuous LAD system are discussed in the following sections.

When ligands are present in the feed, the constant separation factor model can be used to design the systems, however the previous map calculated the ideal loading length using Helfferich's solution for when there is no separation in the feed mixture. When the solution for separation during the feed solution is used, another similar correlation results and is shown later in Eq. (9b).

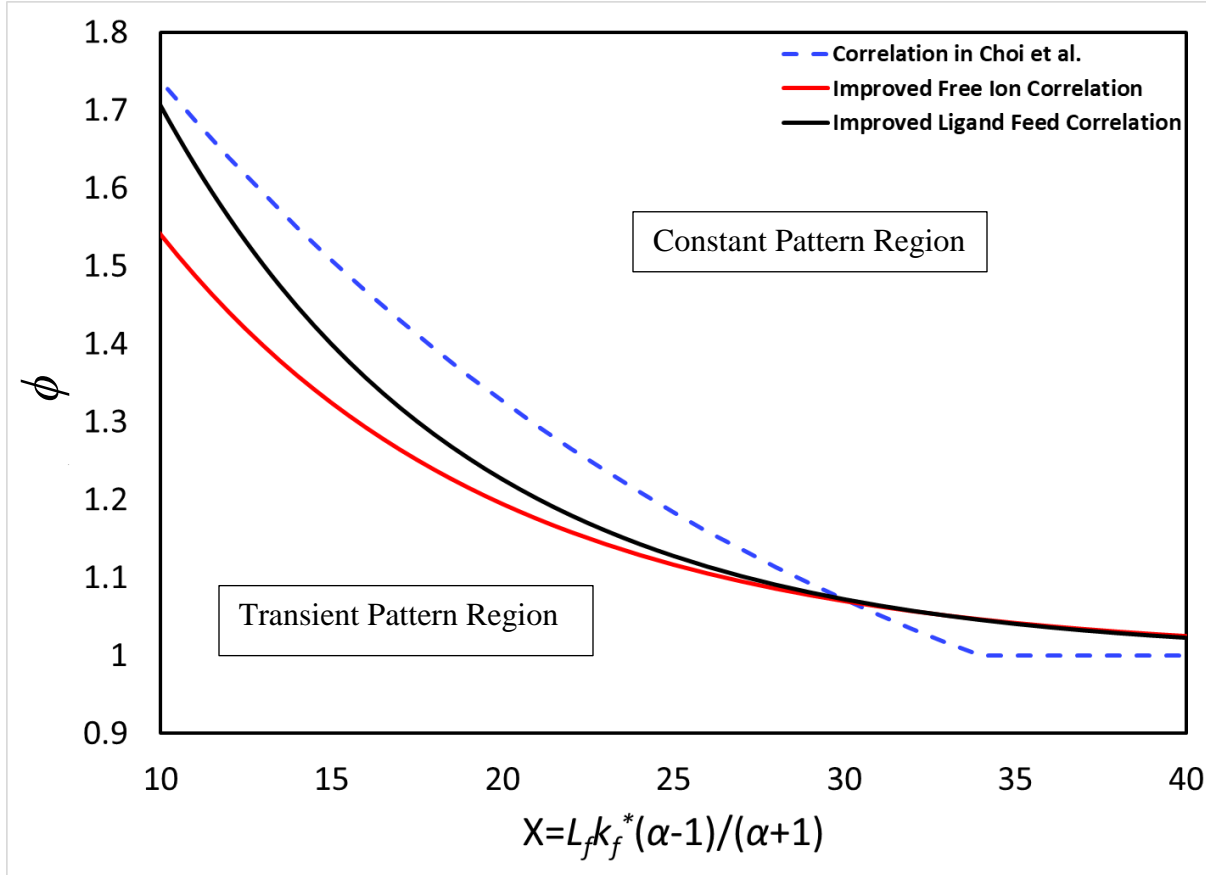


Figure 4.3 General Map for Non-Ideal LAD Design for the Constant Pattern Design Method

4.2.1 Constant Pattern Design of Ligand-Assisted Displacement

In ligand-assisted chromatography, the effective sorbent selectivity is a function of both the true sorbent selectivity and the ligand selectivity. This relationship is shown in Eq. (1). This allows for sorbents with low selectivity to be used for separation of REEs if a ligand with sufficient selectivity is used.

$$\alpha_{i,j}^e = \frac{\alpha_{i,j}^{sorbent}}{\alpha_{i,j}^{ligand}} \quad (1)$$

Where $\alpha_{i,j}^e$ is the effective sorbent selectivity. While the effective sorbent selectivity has been measured experimentally in this study, it can be estimated from the ligand selectivity, which is equal the ratio of the stability constants (K_C) as seen Eq. (2).

$$\alpha_{i,j}^{ligand} = \frac{K_{C,i}}{K_{C,j}} \quad (2)$$

In the previous literature about ligand-assisted displacement chromatography, the constant separation factor model was used as an isotherm which can be seen in Eq. (3).

$$q_i = \frac{q_{max} \alpha_{i,ref}^e C_{p,i}}{\sum_{j=1}^N \alpha_{j,ref}^e C_{p,j}} \quad (3)$$

Where q_i is the solid phase concentration of component “i”, q_{max} is the total column capacity, and $C_{p,i}$ is the concentration of component “i” in the pore phase. This isotherm provided a reasonable approximation; however, it was limited because the effective sorbent selectivity was a constant that was active in the loading phase, meaning that separation was occurring during loading in the model that was not taking place in the experimental system. The map developed for this isotherm was adjusted to account for these differences, however it is possible to create a model that more accurately reflects the experimental system by allowing the selectivity to “turn on” and “turn off” at different parts of the process.

This improvement was achieved using a modified Langmuir isotherm, which can be seen in Eq. (4).

$$q_i = \frac{a_{0,i} e^{-S_{a_1} C_{p,1}} C_{p,i}}{1 + \sum b_{0,j} e^{-S_{b_j} C_{p,1}} C_{p,j}} \quad (4)$$

In which $a_{0,i}$ is the Langmuir “a” value for component “i”, S_{a_1} is a modulator value for the “a” value, and $b_{0,j}$ is the Langmuir “b” value for component “j”. In this isotherm, the values are controlled by the concentration of the modulator component. By making the modulator component non-adsorbing, it can be used to “turn on and off” the selectivity. The modified Langmuir isotherm is otherwise equivalent to the constant separation factor isotherm when the Langmuir “a” and “b” values are much larger than 1. To calculate the equivalent selectivity, Eq. (5) can be used.

$$\alpha_{i,j}^e = \frac{a_{0,i} e^{-S_{a_i}}}{a_{0,j} e^{-S_{a_j}}} = \frac{a_{0,i}}{a_{0,j}} e^{S_{a_j} - S_{a_i}} \quad (5)$$

Similarly, to the previous work in Choi et al, the maximum loading fraction to reach an isotachic train in ideal systems can be calculated using wave interference theory (Helfferich et. al).

In binary systems, the maximum loading fraction for free ions is shown in Eq. (6a) and for feeds with ligand present in Eq. (6b).

$$L_f = \frac{\alpha_{12}^e - 1}{\alpha_{12}^e} \quad (6a)$$

$$L_f = \left(\frac{1}{\alpha_{12}^e - 1} + x_1 \right)^{-1} \quad (6b)$$

Where L_f is the loading fraction. In multicomponent systems, the maximum loading fraction is dependent on the effective sorbent selectivity and composition. In ternary systems without ligand in the feed, the maximum loading fraction is the smallest of the following set in Eq. (7a), when there is ligand in the feed it is the smallest of set Eq. (7b) [85]:

$$\left\{ \frac{\alpha_{13}^e - 1}{\alpha_{13}^e}, \frac{h_2^o(\alpha_{12}^e - 1)(\alpha_{13}^e - 1)}{\alpha_{12}^e \alpha_{13}^e (h_2^o - 1)}, \left(1 + \frac{\alpha_{13}^e(\alpha_{13}^e - h_1^o)}{h_1^o(\alpha_{13}^e - 1)(\alpha_{13}^e - \alpha_{12}^e)} \right)^{-1} \right\} \quad (7a)$$

$$\left\{ \frac{\alpha_{13}^e - 1}{\alpha_{13}^e x_1 + \alpha_{12}^e x_2 + x_3}, \frac{(\alpha_{12}^e - 1)(\alpha_{13}^e - 1)}{h_1^o(h_2^o - 1)}, \frac{(\alpha_{13}^e - 1)(\alpha_{13}^e - \alpha_{12}^e)}{h_2^o(\alpha_{13}^e - h_1^o)} \right\} \quad (7b)$$

Where h_i^o is the h-value for component “i”.

Using the loading fraction calculations, and the new isotherm, a revised map was produced. The improved correlation can be seen in Fig. 4.3. The correlation gives the minimum dimensionless column length required to form a constant pattern isotachic train Eq. (8a). Similar calculations can be done when there is separation in the loading phase using Helfferich’s solution for the ideal loading fraction. The resulting correlation is shown in Eq. (8b)

$$\phi = 1 + 1.5e^{\frac{-X}{9.8}} \quad (8a)$$

$$\phi = 1 + 2.2e^{\frac{-X}{8.8}} \quad (8b)$$

Where:

$$\phi = \frac{L_C}{L_{iso-id}} \quad (9)$$

In this case, L_C is the column length, and L_{iso-id} is the length needed to form an isotachic train in ideal systems.

The length of the mass transfer zone expression in terms of dimensionless groups from Choi et al. holds true with the new model. This expression is shown below:

$$\frac{L_{MTZ,CP}}{L_{feed}} = \frac{1}{k_f^* L_f} \left(\frac{\alpha^e + 1}{\alpha^e - 1} \right) \beta \quad (10)$$

Where:

$$\beta = \ln \left| \frac{1 - \theta}{\theta} \right| \quad (11)$$

$$\frac{1}{k_f^*} = \frac{1}{Pe_b} + \frac{1}{15N_D} + \frac{1}{N_f} \quad (12)$$

$$Pe_b = \frac{L_C}{10\varepsilon_b R_p} \quad (13)$$

$$N_D = \frac{K_{se}(1 - \varepsilon_b)\varepsilon_p D_p L_C}{\varepsilon_b u_o R_p^2} \quad (14)$$

$$N_f = \frac{3L_C(1 - \varepsilon_b)k_f}{\varepsilon_b u_o R_p} \quad (15)$$

L_{feed} is the length of column saturated after feed. θ is the breakthrough cut, ε_b is the bed void fraction, R_p is the particle radius, K_{se} is the size exclusion coefficient, ε_p is the particle void fraction, D_p is the axial dispersion coefficient, u_o is the linear velocity, and k_f is the film mass transfer coefficient. k_f^* is the dimensionless mass transfer coefficient, Pe_b is the Peclet number in the axial direction, N_D is the ration of the dispersion compared to the convection rate, and N_f is the film flow rate compared to the convection rate.

By rearranging the mass transfer zone length equation, it is possible to find the yield. The yield is expressed in terms of dimensionless groups. Paired with the general map, a design that reaches a constant pattern and meets the minimum yield requirement can be determined.

$$Y_i = 1 - \frac{\beta}{2\gamma_i L_f k_f^*} \quad (16)$$

Where:

$$\gamma_i = x_i \left(\frac{\alpha_{i-1,i}^e + 1}{\alpha_{i-1,i}^e - 1} + \frac{\alpha_{i+1,i}^e + 1}{\alpha_{i+1,i}^e - 1} \right)^{-1} \quad (17)$$

4.2.2 Optimal Productivity

In continuous operation, the mixed bands can be recycled. This can make the effective yield of the system 100% regardless of the nominal yield. For this reason, the design yield should be targeted to optimize the productivity. The productivity can be determined based on the yield and map.

$$P_{R,i} = \frac{\varepsilon_b x_i C_d u_o L_f}{L_c} \left(1 - \frac{\beta}{2\gamma_i L_f k_f^*} \right) \quad (18)$$

By using a simple loop, all possible yields can be tested to determine the highest productivity. The largest productivity can then be used to determine the possible operating parameters. The productivity equation shown assumes that the cycle time is equal to elution time. This is a more accurate assumption in continuous systems, where the regeneration and loading can take place simultaneously with the elution. A similar result can be achieved by cycling through a range of different flowrates and calculating the corresponding yields and productivities of a product with a specified purity.

4.2.3 Continuous Chromatography Configuration

Examples of continuous separation for the separation of REEs are given in Fig. 4.4-4.5 for 2 component and 3 component examples respectively. In continuous operation the column is divided up into 2 or more smaller columns. By segmenting the system, it is possible for different operations to be taking place at different places in the column. For example, it is possible to be loading the beginning of the column and eluting the end of the column at the same time. Alternatively, it is possible for multiple regeneration steps to happen simultaneously, or even multiple elution steps at the same time. This gives the loading and yield advantages of a longer column while reducing the cycle time to that of a smaller column. This could also be used to allow for longer column lengths without approaching the pressure limit. Finally, it also allows for a reduction in presaturant use because continuous operation does not require REE to be loaded onto a copper presaturated column if there is a “loading column” that is going to be completely saturated with REE.

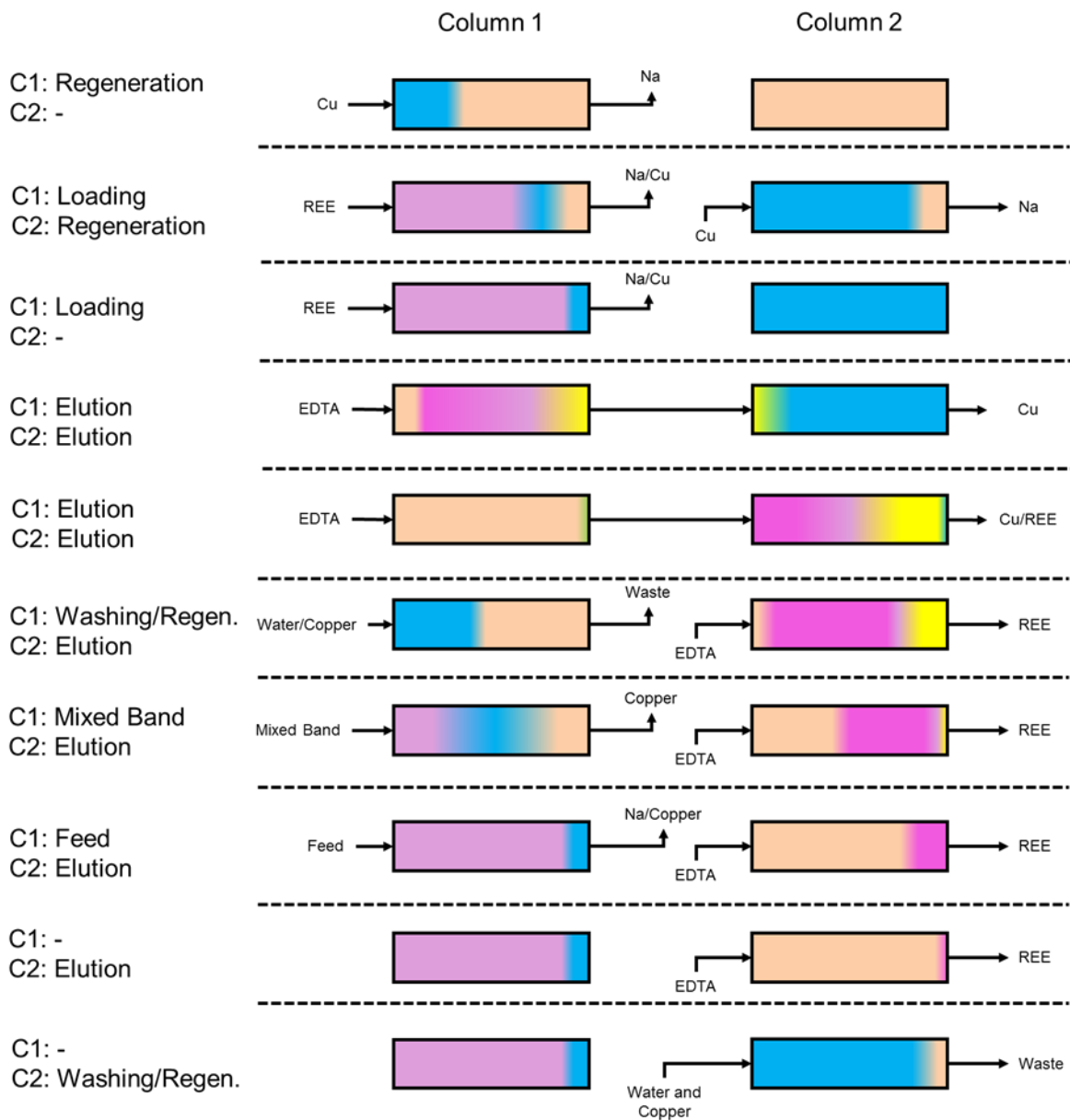


Figure 4.4 Detailed overview of 2 component continuous Ligand-Assisted Displacement Chromatography

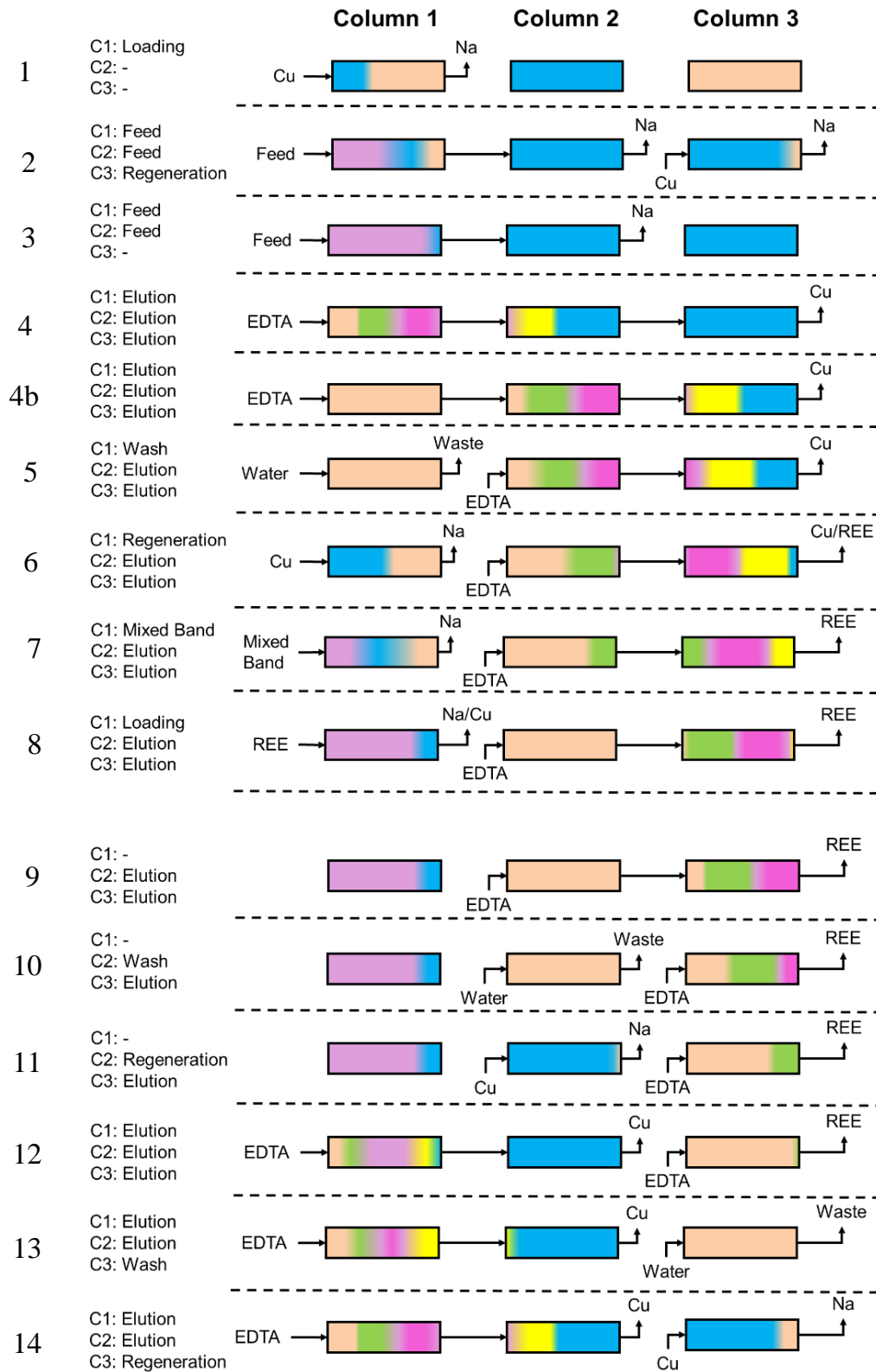


Figure 4.5 Detailed overview of 3 component continuous Ligand-Assisted Displacement Chromatography

4.2.4 Multizone Design for Separation of Complex Mixtures

Many feeds of REEs contain a wide range of compositions. Sometimes there even an order of magnitude difference in the amounts of different REEs. In cases where there is a wide range of compositions, it is very difficult to recover all components with a high purity and high yield in a single column. In a recently published paper by Ding et. al. a design method based on the selectivity weighted composition factor and splitting strategy was developed for batch systems [87]. Components with a low mole fraction or low selectivity correspond to low γ values (Eq. (17)). When the γ value is low for a component Eq. (16) suggests that the corresponding yield will also be low. In order to maintain a high yield, the value of k_f^* must be increased, meaning lower flowrates when the column length and particle size are held constant. As the mole fraction is decreased for a target component, the band width of collectable product is also decreased. To maintain the yield, the mass transfer zone must then be reduced. When a high yield and purity are required of a minority component, the flowrate required to achieve a high yield can be reduced by orders of magnitude compared to the equimolar case.

One solution to this problem of reduced productivity is to reduce the separation burden in the column by splitting the system into several different separation zones. In the first zone, the component with the highest selectivity weighted composition factor (γ) can be targeted and removed at a high yield. By performing the easiest separation first, the other components are then purified in subsequent zones. By separating the component with the highest γ value, the mole fraction of the remaining components is increased, thus increasing the γ value of each remaining component. This allows for the productivity to be high in both zones, and thus all of the components can be produced with high purity, high yield, and high productivity. While previously this zone splitting was done in batch systems, this study extends this approach to continuous systems. This study is also the first to utilize the new map when designing systems with ligand in the feed mixture. By using a more accurate map, there is not a need for as large of a safety factor, meaning that the productivity in the second zone can be greatly improved in this continuous system. Continuous systems can also significantly reduce the storage requirements for REEs as well by processing intermediate products as they are produced.

4.3 Materials and Methods

4.3.1 Materials

Reagent grade cupric sulfate pentahydrate ($CuSO_4 \cdot 5H_2O$), ethylenediaminetetraacetic acid (EDTA), neodymium (III) nitrate hexahydrate ($Nd(NO_3)_3 \cdot 6H_2O$), samarium (III) nitrate hexahydrate ($Sm(NO_3)_3 \cdot 6H_2O$), and praseodymium (III) nitrate hexahydrate ($Pr(NO_3)_3 \cdot 6H_2O$) were purchased from Sigma-Aldrich. Distilled deionized water (DDW) was produced using a Millipore filtration system. Solid sodium hydroxide and 36.5-38% hydrochloric acid were purchased from Mallinckrodt Baker. AG-MP50 resin (100-200 mesh) was purchased from Bio-Rad. Three 50" Millipore glass columns were used for these experiments. Experiments were performed using a SEMBA Octave using a diode array detector (Agilent 1260 infinity II) to monitor the effluent absorbance wavelengths at 401, 404, 444, 575, 600, and 700 nm.

4.3.2 Column Loading and Preparation

Resin for packing was soaked in DDW and sonicated for one hour to eliminate air bubbles and remove fine impurities. The resin was then put into a column for pretreatment first with 5 CV of 1 M NaOH, next with 2 CV of DDW, and then 5 CV of 1 M HCl. Next the resin was unpacked from the column. The resin was then put into water to form a 50% (v/v) slurry. The columns were then packed with the pretreated resin. A detailed summary of the packing method can be found in Choi et al. The column lengths packed were 38.4 cm, 42 cm, and 36 cm. The bed void and the particle void were calculated using a blue dextran pulse and a copper sulfate pulse test.

4.3.3 Experiment 1 Separation of 2 Rare Earth Elements Using Continuous LAD

To demonstrate the continuous operation of ligand-assisted displacement chromatography for the separation of REEs, a separation of Nd and Sm was performed. For this separation, two packed columns were used to form a total column length of 80.4 cm. The optimal design was obtained through the process described earlier in the optimization section of this paper. The target yield before the recycle to give the optimal productivity in this separation is 73%. The design k_f^* and L_f can be found in Table 4.1 along with the simulation parameters that were used to simulate

the experiment. An overview of the inputs, and outputs of each column during each run and cycle is given in Table 4.2.

Table 4.1 Simulation and Experimental Parameters

System Parameters									
L (cm)	ID (cm)	R (μm)	ε_b	ε_p	$C_{f,i}$ (N)	Experiment	k_f^*	L_f	Q_f (mL/min)
80.4	1.16	56	0.35	0.34	0.58	1	51.57	0.57	10.35
116.4						2	206.92	0.38	4.49
Isotherm Parameters (Modulated Langmuir Isotherm)									
Component		a	b	Sa	Sb				
1	Cu	1,600	1,000	0	0				
2	Sm	8,000	5,000	0	0				
3	Nd	8,000	5,000	-1.163	-1.163				
4	Pr	8,000	5,000	-1.751	-1.751				
5	EDTA-Na	230,400	144,000	0	0				
Mass Transfer Parameters									
Component	Brownian Diffusivity D_b (cm^2/min)	Pore Diffusivity D_p (cm^2/min)	Axial dispersion coefficient, E_b (cm^2/min)	Film mass transfer coefficient, K_f (cm/min)					
All species	4×10^{-4}	9×10^{-5}	Chung and Wen (1968)	Wilson Geankoplis (1966)					
Numerical Parameters (unit: N)									
Axial Element	Step size (L/u_0)	Collocation Points		Tolerance					
		Axial	Particle	Absolute	Relative				
100	0.01	4	2	10^{-4}	10^{-4}				

An example of the operation can be seen in both Figure 4.1 and Fig. 4.4. In this case, Column 1 was loaded with both copper and rare earth while Column 2 was regenerated using copper. After loading and regeneration was complete, EDTA was input into Column 1 and the eluent from Column 1 was used as the inlet for Column 2. This gave the effect of a single long column. Operation in this mode continued until the rare earth desorption wave was completely moved into the second column. When this occurred, the inlet of EDTA was moved from Column 1 to Column 2. At the same time, water was flushed into Column 1. While the REE band was still eluting from Column 2, Column 1 was regenerated with copper and then the mixed bands from the previous run were recycled onto the column, exchanging with copper. The remainder of the column loading was then completed with fresh feed. When the REE had completely eluted from Column 2, Column 2 was regenerated, and the process was repeated.

To avoid fluctuations in mixed band concentration, a mixed band synthetic solution was mixed ahead of time to be “recycled”. If a recycle is to be used, it is suggested that a large reservoir of solution be used to avoid fluctuations from run to run. The amount of copper needed for the remainder of the loading column was calculated based on the column capacity and a 1.5 times safety factor was used to make sure that the entire column was pre-equilibrated with copper.

Table 4.2 Summary of Inlets, Outlets and Cycle Times for 2 Component LAD Separation of Sm and Nd. Column 2 was preloaded with copper at the beginning of cycle 1.

Step #	Time of Step (sec)	Adjustment for cycle 2	Adjustment for cycle 3	Column 1		Column 2	
				Inlet	Outlet	Inlet	Outlet
1	120	-	-	Copper	Sodium	-	-
2	1314	-	-	REE	Sodium	-	-
3	2118	+248	-60	EDTA	Column 2	Column 1	Copper
4	276	-	+60	EDTA	Column 2	Column 1	Mixed Band
5	997	-240	-120	EDTA	Column 2	Column 1	Sm
6	358	-	-	Water	Waste	EDTA	Mixed Band
7	150	-	-	Copper	Sodium	EDTA	Nd
8	634	-	-	Mixed Band	Copper	EDTA	Nd
9	634	-200	-	Feed	Sodium	EDTA	Nd
10	352	+200	-	Feed	Sodium	Water	Waste
11	450	+180	-	-	-	Copper	Sodium
Repeat back to Step 3							

The first cycle was performed beginning from the loading stage. This means that the productivity of the first cycle is the same as that in a batch system. In the second cycle, the column was overloaded 10% over the nominal loading fraction to demonstrate the robustness of the method. In cycle 3, the operation was run according to the conditions consistent with the target cyclic steady state.

4.3.4 Experiment 2 Separation of 3 Rare Earth Elements Using Continuous LAD

Experiment 2 was performed to demonstrate the effectiveness of continuous LAD chromatography for separation of a three-component mixture. This was done by separating an equimolar mixture of Sm, Nd, and Pr using a continuous LAD system with three columns. The simulation parameters and column parameters can be found in Table 4.1. In this case, the total

length of the three columns was 116.4 cm. The target yield was optimized as previously described and determined to be 69% before a mixed band recycle.

Because of the larger dead volume and other operational variables, for Experiment 2 a safety factor of 10% was utilized in determining the design. To apply the safety factor, the X value was held constant by raising k_f^* by 10% and reducing L_f by 10%. This allowed for the design to shift up by 10% into the constant pattern region.

The operation of the continuous LAD was similar to the 2-column system, however the additional column allowed for more operations to be run simultaneously. An example of this setup can be seen in Fig. 4.5. An overview of the inlets and outlets during both cycles is given in Table 4.3. In this experiment, Column 1 was loaded with copper and REE, and Columns 2 and 3 were regenerated using copper sulfate. After regeneration and loading, EDTA was fed into Column 1 with the outlet of this column being used as the inlet to Column 2. Similarly, the outlet of Column 2 was used as the inlet for Column 3. As in the 2-component case, when the REE was eluted from Column 1, the EDTA port was moved forward to Column 2 and Column 1 was regenerated. Similarly, when the REE wave moved out of Column 2, the EDTA feed was changed to Column 3 and Column 2 was regenerated. After Column 2 was regenerated, EDTA was fed into Columns 1 and 3, and elution begun. This is possible because the original REE wave was eluted before the adsorption wave of REE reached the inlet to Column 3. Column 3 was then regenerated and then connected to Columns 1 and 2. From this point the cycle was repeated from the elution step.

In Experiment 2, only 2 cycles were performed. In Cycle 1, the productivity reflects the fact that the loading and regeneration were not performed simultaneously with the elution and thus is like that of a batch system. The second cycle reflects the advantages of the continuous processing once it has reached cyclic steady state.

Table 4.3 Summary of Inlets, Outlets, Flowrates, and cycle times for ternary separation of REEs. In Table Detect refers to the outlet going to the detector. All flowrates are in mL/min, and MB refers to the mixed band solution

Step	Time (s)	Adjustments Cycle 2	Column1 (C1)			Column 2 (C2)			Column 3 (C3)		
			Inlet	Outlet	Flowrate	Inlet	Outlet	Flowrate	Inlet	Outlet	Flowrate
1	420	-	Cu	Waste	10	-	-	-	-	-	-
2	600	-	Feed	C2	4.485	C1	Na/Cu	4.485	Cu	Na	10
3	1308	-	Feed	C2	4.485	C1	Na/Cu	4.485	-	-	-
4	9600	-	EDTA	C2	4.485	C1	C3	4.485	C2	Detect	4.485
5	300	-	Water	Waste	10	EDTA	C3	4.485	C2	Detect	4.485
6	600	-	Cu	Waste	10	EDTA	C3	4.485	C2	Detect	4.485
7	1920	-	MB	Waste	4.485	EDTA	C3	4.485	C2	Detect	4.485
8	1317	-	Feed	Cu/Na	4.485	EDTA	C3	4.485	C2	Detect	4.485
9	663	-	-	-	-	EDTA	C3	4.485	C2	Detect	4.485
10	300	-	-	-	-	Water	Waste	10	EDTA	Detect	4.485
11	600	-	-	-	-	Cu	Waste	10	EDTA	Detect	4.485
12	2700	+120	EDTA	C2	4.485	C1	Cu	4.485	EDTA	Detect	4.485
13	300	-	EDTA	C2	4.485	C1	Cu	4.485	Water	Detect	10
14	600	-	EDTA	C2	4.485	C1	Cu	4.485	Cu	Detect	10
15	6000	-	EDTA	C2	4.485	C1	C3	4.485	C2	Detect	4.485
Repeat back to step 5											

4.3.5 Experiment 3 Separation of REEs from magnet simulant

The purpose of experiment 3 was to demonstrate the continuous separation of REEs from a complex mixture of Dy, Nd, and Pr which simulates a crude magnet feed. In this experiment the separation was divided between 2 zones, Zone I and Zone II. In Zone I, Nd was separated from Dy and Pr using a 3-column system with an overall column length of 116.4 cm. The feed was a mixture of 0.05 N Dy, 0.83 N Nd, and 0.12 N Pr. In this zone, a target yield of 77.5% was used for Neodymium in the design method. The ligand used in this experiment was EDTA at a concentration of 0.09 M at pH 9. The corresponding effective capacity for this ligand condition is 1.4 meq. /mL. The experiment was also simulated using the VERSE simulation software. The full simulation parameters for this system can be found in Table 4.4. The switching schedule can be found in Table 4.5. Two cycles with these parameters were performed. When designing this system, a 5% safety factor was used. This was applied by reducing the value of k_f^* by 5% and as a result the flowrate was reduced by roughly 5% as well from 8.1 mL/min down to 7.8 mL/min. While Dy is detectable in the UV/Vis range, because of interference, Dy was measured using flame atomic adsorption in Zone I and was measured using the PDA detector in Zone IIa.

Table 4.4 Simulation parameters for Zone I of separation of REEs from magnet simulant

System Parameters								
L (cm)	ID (cm)	R (μm)	ε_b	ε_p	Experiment	k_f^*	L_f	Q_f (mL/min)
117.1	1.16	56	0.35	0.34	3	125	0.3775	7.8
Isotherm Parameters (Modulated Langmuir Isotherm)								
Component		a	b	Sa	Sb			
1	Cu	1,380	1,000	0	0			
2	Dy	6,750	5,000	0	0			
3	Nd	6,750	5,000	-1.61	-1.61			
4	Pr	6,750	5,000	-2.20	-2.20			
5	EDTA-Na	6,750	5,000	-3.81	-3.81			
Mass Transfer Parameters								
Component	Brownian Diffusivity D_b (cm^2/min)	Pore Diffusivity D_p (cm^2/min)	Axial dispersion coefficient, E_b (cm^2/min)		Film mass transfer coefficient, K_f (cm/min)			
All species	4×10^{-4}	9×10^{-5}	Chung and Wen (1968)		Wilson Geankoplis (1966)			
Numerical Parameters (unit: N)								
Axial Element	Step size (L/u_0)	Collocation Points		Tolerance				
		Axial	Particle	Absolute	Relative			
151	0.001	4	2	10^{-4}	10^{-4}			

Table 4.5 Summary of Inlets, Outlets, Flowrates, and cycle times for separation of REEs from crude magnet feed. In Table Detect refers to the outlet going to the detector. All flowrates are in mL/min.

Step	Time (s)	Column1 (C1)			Column 2 (C2)			Column 3 (C3)		
		Inlet	Outlet	Flowrate	Inlet	Outlet	Flowrate	Inlet	Outlet	Flowrate
1	390	Feed	C2	7.8	C1	C3	7.8	C2	Detect	7.8
2	2820	EDTA	C2	7.8	C1	C3	7.8	C2	Detect	7.8
3	300	Water	Waste	10	EDTA	C3	7.8	C2	Detect	7.8
4	660	Cu	Waste	10	EDTA	C3	7.8	C2	Detect	7.8
5	390	Feed	Waste	7.8	EDTA	C3	7.8	C2	Detect	7.8
6	750	-	-	-	EDTA	C3	7.8	C2	Detect	7.8
7	300	-	-	-	Water	Waste	10	EDTA	Detect	7.8
8	660	-	-	-	Cu	Waste	10	EDTA	Detect	7.8
9	780	EDTA	C2	7.8	C2	Waste	7.8	EDTA	Detect	7.8
10	300	EDTA	C2	7.8	C2	Detect	7.8	Water	Waste	10
11	660	EDTA	C2	7.8	C1	Detect	7.8	Cu	Waste	10
12	1380	EDTA	C2	7.8	C2	C3	7.8	C2	Detect	7.8
Repeat Back up to step 3										

Zone IIa Separation of Dy and Nd

In a two-zone continuous process the mixed bands are sent to Zone II for further separation. In Zone IIa, the mixed band containing Copper, Dysprosium, and Neodymium is separated. One of the key differences between Zone II and Zone I is that the REEs loaded into Zone II are already bound with EDTA. This means that during the loading process, there will be separation occurring. For this reason, the design of this zone was done using the ideal solution and map for ligand bound REEs. Because the rare earth is loaded onto a copper saturated column, the EDTA-Cu complex in the mixed band was ignored in the design because it will be inert in the process. For this binary process a two-column system with a total column length of 78.5 cm was utilized. A target yield of 77% for Dy was used. Because it would require >10 runs of Zone I to produce sufficient quantity of mixed band to demonstrate Zone IIa, a synthetic mixed band solution was made by loading free Dy and Nd onto a column and then eluting with 0.09 M EDTA at pH 9. The resulting feed concentration were 0.1 N Dy and 0.155 M Nd which is proportional to the concentrations in the mixed band resulting from Zone I. A 2-column continuous configuration was used in this separation. The full simulation parameters and schedule can be found in Tables 4.6 and 4.7 respectively. Two cycles were performed. The 10% safety factor was applied to the flowrate.

Table 4.6 Simulation parameters for Zone IIa of the separation of REEs from magnet simulant

System Parameters									
L (cm)	ID (cm)	R (μm)	ϵ_b	ϵ_p	$C_{f,i}$ (N)	Experiment	k_f^*	L_f	Q_f (mL/min)
78.5	1.16	56	0.35	0.34	0.58	3	95	0.58	7.54
Isotherm Parameters (Constant Separation Factor)									
Component						Selectivity Relative to Cu			
1	Cu					1			
3	Dy					5			
4	Nd					25			
5	EDTA-Na					125			
Mass Transfer Parameters									
Component	Brownian Diffusivity D_b (cm^2/min)		Pore Diffusivity D_p (cm^2/min)		Axial dispersion coefficient, E_b (cm^2/min)		Film mass transfer coefficient, K_f (cm/min)		
All species	4×10^{-4}		9×10^{-5}		Chung and Wen (1968)		Wilson Geankoplis (1966)		
Numerical Parameters (unit: N)									
Axial Element	Step size (L/u_0)	Collocation Points				Tolerance			
		Axial		Particle		Absolute		Relative	
151	0.01	4		2		10^{-4}		10^{-4}	

Table 4.7 Summary of Inlets, Outlets, Flowrates, and cycle times for separation of REEs from crude magnet feed in Zone IIa. Water washing and Copper regeneration steps done at 20 mL/min. All other flowrates set to 7.54 mL/min

Step #	Time of Step (sec)	Column 1		Column 2	
		Inlet	Outlet	Inlet	Outlet
1	2082	Feed	C2	C1	Detector
2	2118	EDTA	C2	C1	Detector
3	300	Water	Waste	EDTA	Detector
4	300	Cu	Waste	EDTA	Detector
5	300	Water	Waste	EDTA	Detector
6	1920	-	-	EDTA	Detector
7	300	-	-	Water	Detector
8	300	Feed	Waste	Cu	Detector
9	300	Feed	Waste	Water	Detector
10	1482	Feed	C2	C1	Detector
Repeat back to Step 2					

Zone IIb Separation of Nd and Pr

Similarly, in Zone IIb the mixed band of Nd and Pr was sent to a separate column to finish the separation. The REEs in this mixed band solution are also bound to EDTA and thus the ideal loading fraction and map for ligand bound REEs were used. This separation was also performed using a 78.5 cm two column system. A synthetic mixture was also used as a feed in this experiment. The feed was produced by saturating a column with a mixture of Nd and Pr and then eluting with 0.09 M EDTA at pH 9 to give a final concentration of 0.177 N Nd and 0.115 N Pr which was proportional to the mixture resulting from Zone I. The full simulation parameter table and operation schedule can be found in Tables 4.8 and 4.9 respectively. Several technical considerations prevented two cycles of this run from being performed.

The mixture of Nd and Pr with EDTA is not stable at the low pH values that elute from the column causing EDTA to precipitate after several hours. The particles in this feed can cause clogging and inconsistencies in the pump flow rates. Because the time to run 2 cycles was roughly 8 hours, it was not possible to run 2 cycles while the feed solution was still stable. Additionally, when base was added to raise the pH and prevent EDTA precipitation, Pr, was precipitated. It is suggested that in an industrial application of this system, the feed be loaded directly onto the column without storage in a tank to prevent precipitation issues due to this instability. Because of the instability in the feed solution, the concentrations loaded may have significant error which can make the simulation inaccurate. Additionally, the precipitation occurring meant that the detector

could not be connected to the outlet until it was visually confirmed that the rare earth was about to leave the column to reduce the chances of clogging from EDTA-Cu. It is possible that there was a lag time from when the detector was connected until it stabilized, and all air was removed from the detector. This means that the earlier data is less reliable than the later data in this case.

Table 4.8 Simulation parameters for Zone IIb of the separation of REEs from magnet simulant

System Parameters									
L (cm)	ID (cm)	R (μm)	ε_b	ε_p	$C_{f,i}$ (N)	Experiment	k_f^*	L_f	Q_f (mL/min)
78.5	1.16	56	0.35	0.34	0.58	3	175	0.54	3.9
Isotherm Parameters (Constant Separation Factor)									
Component					Selectivity Relative to Cu				
1	Cu				1				
3	Nd				5				
4	Pr				25				
5	EDTA-Na				125				
Mass Transfer Parameters									
Component	Brownian Diffusivity D_b (cm^2/min)	Pore Diffusivity D_p (cm^2/min)	Axial dispersion coefficient, E_b (cm^2/min)			Film mass transfer coefficient, K_f (cm/min)			
All species	4×10^{-4}	9×10^{-5}	Chung and Wen (1968)			Wilson Geankoplis (1966)			
Numerical Parameters (unit: N)									
Axial Element	Step size (L/ u_0)	Collocation Points			Tolerance				
		Axial	Particle		Absolute	Relative			
151	0.01	4	2		10^{-4}	10^{-4}			

Table 4.9 Summary of Inlets, Outlets, Flowrates, and cycle times for separation of REEs from crude magnet feed in Zone IIa. Water washing and Copper regeneration steps done at 20 mL/min. All other flowrates set to 3.9 mL/min

Step #	Time of Step (sec)	Column 1		Column 2	
		Inlet	Outlet	Inlet	Outlet
1	3306	Feed	C2	C1	Detector
2	5694	EDTA	C2	C1	Detector
3	300	Water	Waste	EDTA	Detector
4	300	Cu	Waste	EDTA	Detector
5	300	Water	Waste	EDTA	Detector
6	1800	-	-	EDTA	Detector
7	600	Feed	Waste	EDTA	Detector
8	300	Feed	Waste	Water	Detector
9	300	Feed	Waste	Cu	Detector
10	300	Feed	Waste	Water	Detector
11	1806	Feed	C2	C1	Detector
Repeat back to Step 2					

4.3.6 Robustness Study

Two separate robustness studies were done to test the effects of variation of the feed composition on the yield and purity of the target component. As a base case, the magnet crude feed was used. The simulation parameters were the same as those in Table 4.4. When variations occur or there are errors in the measurement of the feed concentration, the design cannot be adjusted to account for them because the error is unknown. Several variations in the feed composition were tested without adjusting the loading time or the flowrate in order to observe the effects of these changes on the resulting purity and yield. Two different types of safety factor were tested. In one case, the safety factor was achieved by reducing the velocity directly by 5 or 10%. In the other case, the separation was designed for a column 5 to 10% shorter than the simulated column. In both cases, a breakthrough cut of 0.05 was used. In all cases, a target yield of 78% for Nd was used and a dead volume of 2 mL. The column in all cases was simulated to be 117.1 cm with an inner diameter of 1.16 cm.

4.4 Results and Discussion

The results of Experiment 1 are discussed in section 4.4.1. The results of Experiment 2 are then discussed in 4.4.2. The effects of tightening the purity requirement are discussed in section 4.4.3. The separation and purification of Rare Earth Elements from a magnet crude is discussed in section 4.4.4. and the discussion of the robustness simulations is found in section 4.4.5. Next, the advantages of Continuous LAD compared to Batch LAD chromatography are discussed in section 4.4.6. Finally, the advantages of continuous LAD compared to the conventional liquid-liquid extraction process are discussed in section 4.4.7.

4.4.1 Experiment 1

A summary of the results for Experiment 1 is given in Table 4.4. The chromatographs for this system are given in Figures 4.6-4.8. In all three cycles the yields before recycling were within 1% of the minimum target yield and the steady state operation cycle achieved the target yield exactly. In all 3 experiments, a high purity 99% was achieved when using a 5% cut. The successful separation of REEs in Experiment 1 prove the viability of continuous LAD chromatography. The productivity in cycle 3, which is the cyclic steady state operation was overall 21% higher than the

productivity in cycle 1, which is representative of a batch system. This difference demonstrates the reduction in cycle time in continuous systems by operating the loading of Column 1 and elution of Column 2 simultaneously.

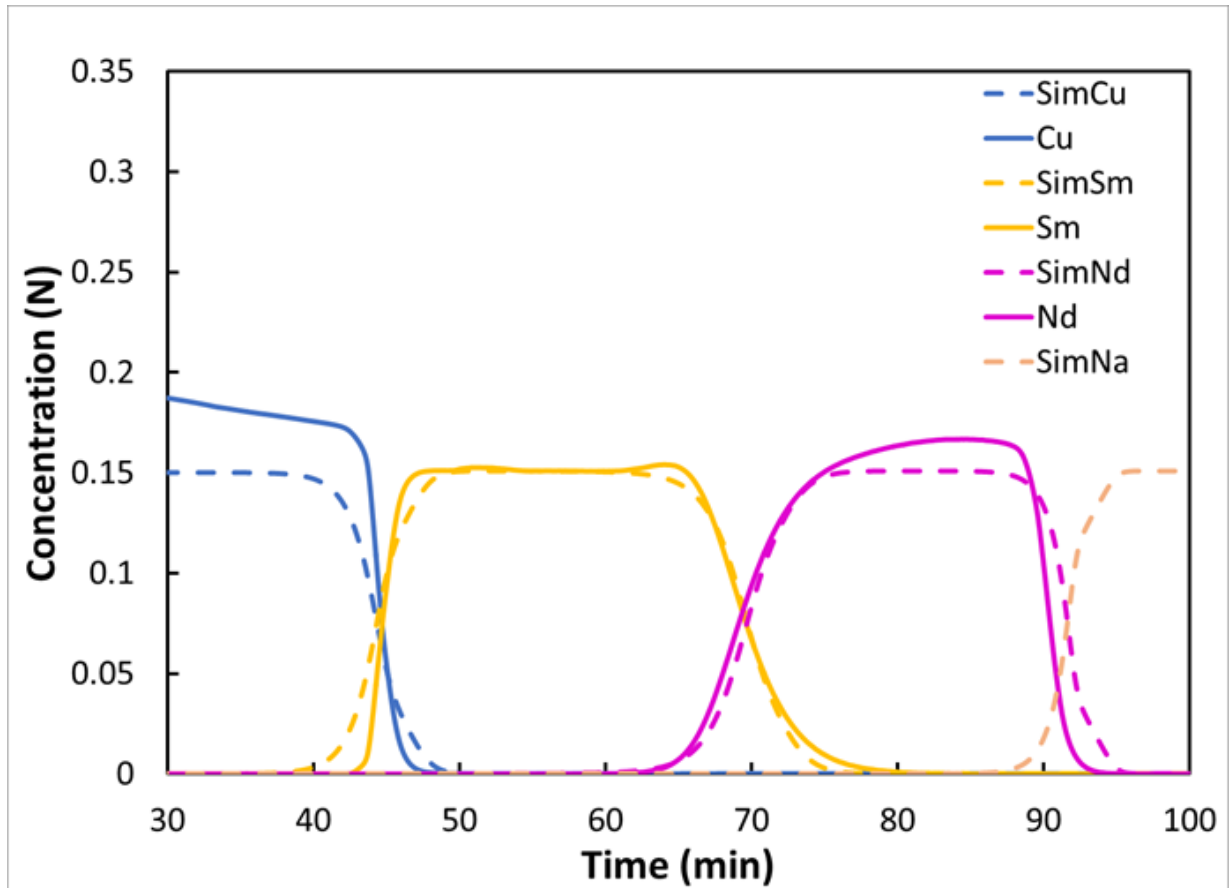


Figure 4.6 Cycle 1 of Experiment 1; Continuous Separation of Nd and Sm with VERSE simulations

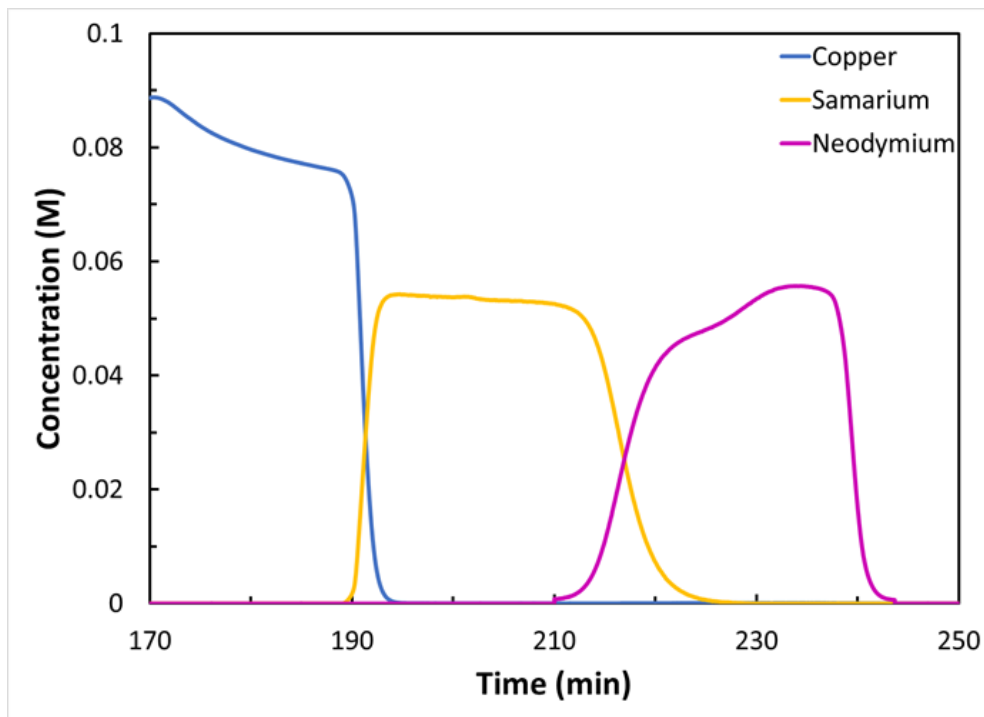


Figure 4.7 Cycle 2 of Experiment 1: Continuous Separation of Nd and Sm. Time is based on total run time

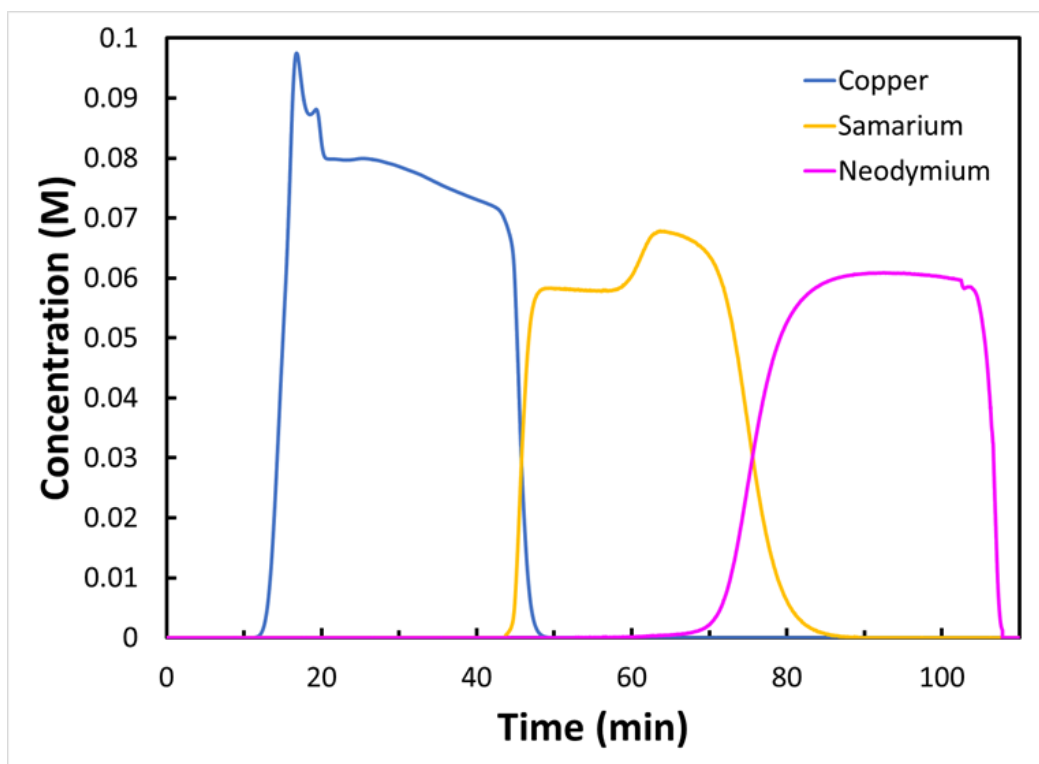


Figure 4.8 Cycle 3 of Experiment 1: continuous Separation of Nd and Sm. Time started at the elution stage

Table 4.10 Binary Continuous LAD Separation Results. Minimum Target Yield of 73%

		Sm	Nd
Cycle 1 (Start-up)	Yield (%)	78	72
	Purity (%)	99	99
	Productivity (kg/m ³ /day)	150	144
Cycle 2 (10% Overloaded)	Yield (%)	78	78
	Purity (%)	99	99
	Productivity (kg/m ³ /day)	254	206
Cycle 3 (Steady State Operation)	Yield (%)	73	80
	Purity (%)	99	99
	Productivity (kg/m ³ /day)	174	183

Cycle 2, which showed an overloaded column demonstrated the robustness to variations in this method. The yield, purity and productivity were all maintained and even increased in case of variation. While in this case, the yield was increased and the productivity and purity were maintained, the column was too overloaded to reach a constant pattern. This cycle was operated within a region in which the band width increased more than the mass transfer zone increased. As a result, the yield and productivity can be increased simultaneously. The issue with designing in this region of the design map, is that the limits of this region are unknown and thus it is currently impossible to create a scalable design based on this section of the map. Additionally, if the column is overloaded “too much” then there is a steep drop off in the yield and productivity. For these reasons, it is better in terms of robustness of design to operate in the constant pattern region instead of overloading the column.

4.4.2 Experiment 2

A summary of the results from experiment 2 can be found in Table 4.5. The chromatographs from this experiment are shown in Fig. 4.9-4.10. In cycle 1, the system was loaded for startup. For this reason, it is representative of the batch systems for this system. In cycle 2, the system was operated in a completely continuous manner. In both cases the yield before recycling was within 1% off the target yield, and in the cyclic steady state case the yield before recycling exceeded the minimum target yield. In all cases the purity with a cut of 0.05 exceeded 99% purity.

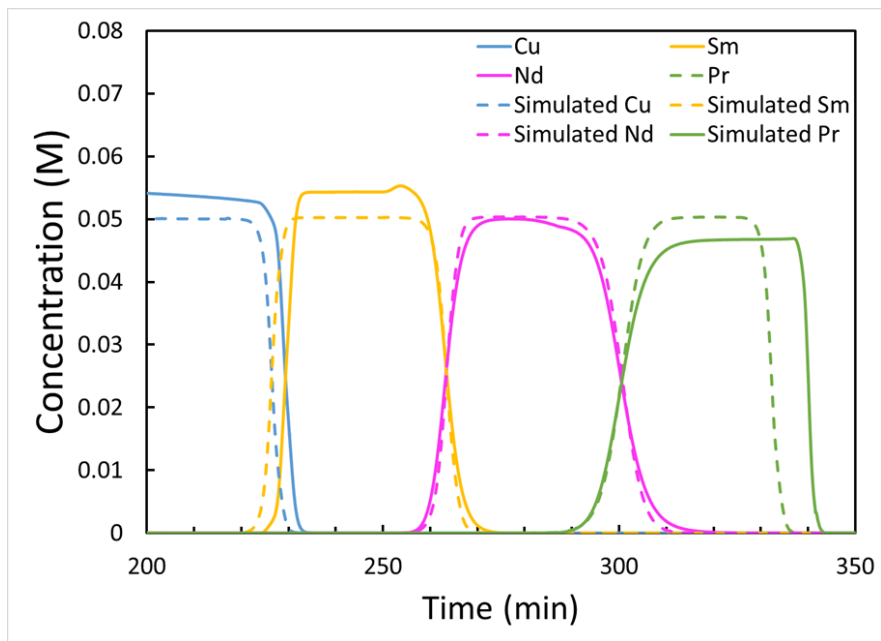


Figure 4.9 Cycle 1 of Experiment 2: Continuous Separation of Sm, Nd, and Pr. The difference in concentration for Pr between the simulated and experimental Pr is likely due to the pH difference shifting the ligand efficiency during the experiment. This can also be seen in Fig. 4.10

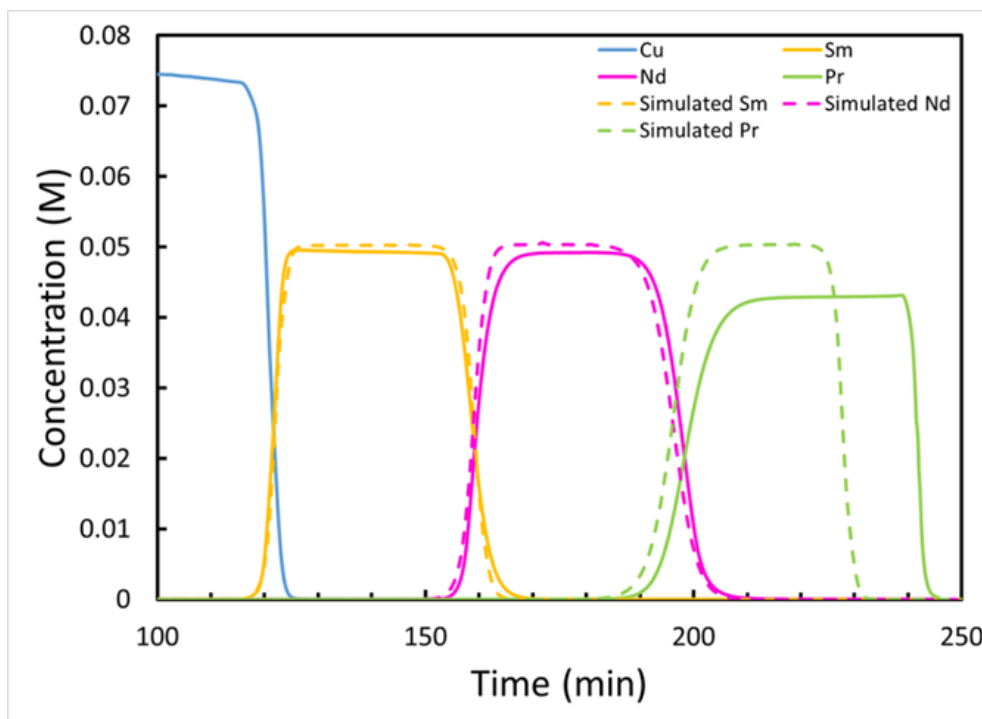


Figure 4.10 Cycle 2 of Experiment 2: Continuous separation of Sm, Nd, and Pr

Table 4.11 Ternary Continuous LAD Separation Results Minimum Target Yield 69%

		Sm	Nd	Pr
Cycle 1	Yield (%)	80	68	74
	Purity (%)	99.7	99.3	99.4
	Productivity (kg/m ³ /day)	32.8	26.8	28.5
Cycle 2 (Cyclic Steady State Cycle)	Yield (%)	87	75	87
	Purity (%)	99.7	99.3	99.6
	Productivity (kg/m ³ /day)	49.5	40.9	46.3

The total productivity in cycle 2 was 57% higher than in cycle 1. This shows an increase of nearly 60% in terms of productivity for continuous systems compared to batch when the number of components and columns is increased to 3 each. Compared to Experiment 1, this is a significant increase in the effect of continuous processing. This is because the additional column allows for not just loading and elution to be performed simultaneously, but also allow for elution of 2 different runs to occur simultaneously. This means that the time spent on regeneration is eliminated, and the time of elution is reduced as well. This principal can be carried even further as more columns are added to as system, further reducing the elution cycle time. Additionally, it allows for a long column length without waiting the entire elution time required for a separation with a long column. It is recommended that the individual column lengths be long enough to confine the loading zone to a single column for the simplicity of the design, however this is not a requirement. The productivity recorded in cycle 2 represents the highest recorded productivity for a ternary separation using Ligand-Assisted Chromatography as it is 52% higher than the ternary separation shown in Choi et al.

4.4.3 Stricter Purity Requirements

In each of these systems, the productivity and yield were optimized assuming a breakthrough cut of 0.05. A breakthrough cut of 0.05 guarantees purities >99% (Choi et al.). While this purity is sufficient for some applications, other applications require purities even higher. This can be achieved by either tightening the breakthrough cut in the design, or by tightening the actual collection experimentally by recycling more of the mixed band at the interface between two

components. Because the two strategies yield equivalent results, this study will employ the later strategy.

By lowering the yields before recycling of Sm, Nd, and Pr from 87%, 75%, and 87% to 81%, 48%, and 77% respectively, a purity of 99.9% can be achieved. This drop in the yield before the recycle results in a reduction of total productivity from 136.7 kg/m³day to 113.2 kg/m³day. However, with a recycle system, the effective yield for the process will still be >99% even when collecting product at purities >99.9%. Because this process is reproducible, after a few cycles the adjustments can be made to collect the higher purity product based on elution times without requiring extensive sampling.

4.4.4 Separation and Purification of REEs from a Simulated Crude Magnet Mixture using a Two Zone Continuous LAD

Zone I Separation of Nd from Simulated Magnet Crude Solution

This experiment shows the benefit of dividing the separation burden between multiple zones when there is a large difference in the concentration in a feed. Because Zone I is the largest fraction of the feed it has the highest effect on the overall productivity of the system. The chromatographs resulting from this experiment are shown in Fig. 4.11 and Fig. 4.12.

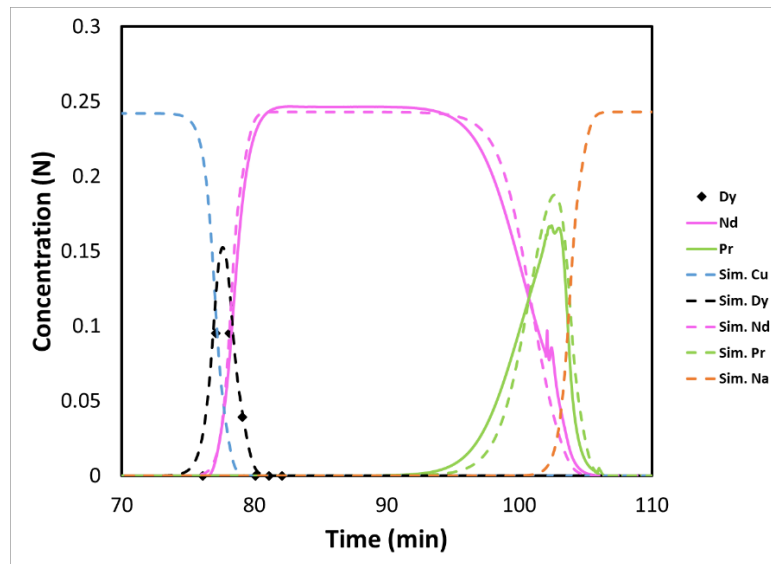


Figure 4.11 Chromatograph of Cycle 1 of Separation of Nd from Simulated Magnet Crude. The break at around 104 minutes is due to a temporary pause in the script due to instrument error. Dy fractions were collected every minute.

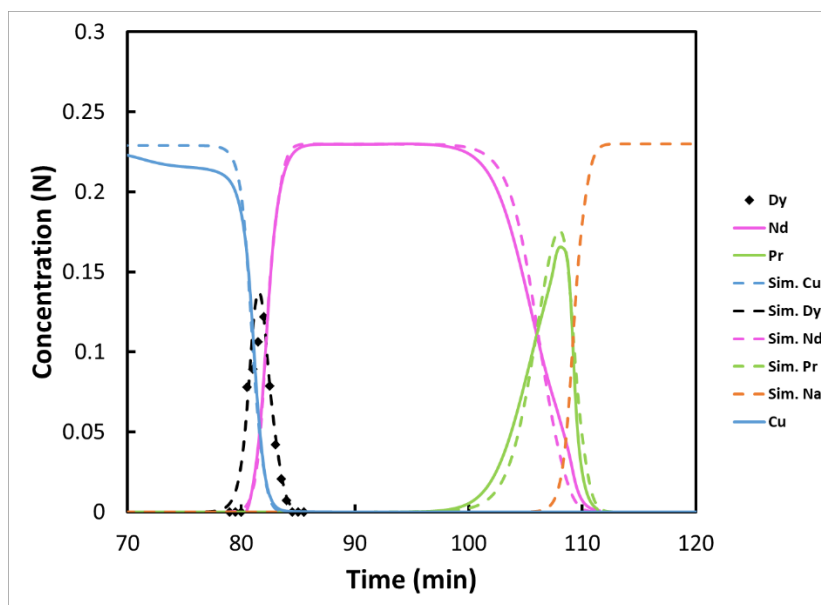


Figure 4.12 Chromatograph of Cycle 1 of Separation of Nd from Simulated Magnet Crude. Dy fractions were collected every thirty seconds.

The results of the experiment are shown in Table 4.12. In this experiment the design method achieved the target yield within a few percent. The purity was >99% and the productivity was 30% higher than that of a similar batch system. By reducing the cycle time by performing the loading, regeneration and elution simultaneously, a significant increase in productivity can be achieved. This also showed that the continuous configuration is viable for the separation of a complex mixture. The reason for the lower yield than the target can be explained by 2 different phenomena. The first is that in the continuous system, there is a large dead volume between the columns. This additional dead volume is a deviation from the simulated model and will increase the length of the mass transfer zone. However, even with the extra dead volume, the yield was achieved within 4%.

Table 4.12 Summary of Zone I Experimental Results

	Target Yield Nd (%)	Actual Yield Nd (%)	Purity Nd (%)	Productivity Nd (kg/m ³ day)
Cycle 1	77.5	73	99.5	141
Cycle 2	77.5	74	99.3	169

Zone IIa Separation of Dy and Nd

A summary of the results from Zone IIa are shown in Table 4.13. The chromatographs are shown in Fig. 4.13 and Fig 4.14.

Table 4.13 Summary of Cycles 1 and 2 from Continuous Zone IIa using 2 Columns

	Dy				Nd			
	Target Yield (%)	Actual Yield	Purity	Productivity (kg/m ³ day)	Target Yield	Actual Yield	Purity	Productivity (kg/m ³ day)
Cycle 1	77	79	99.6	159	-	91	99.8	251
Cycle 2	77	80	99.6	161	-	92	99.9	254

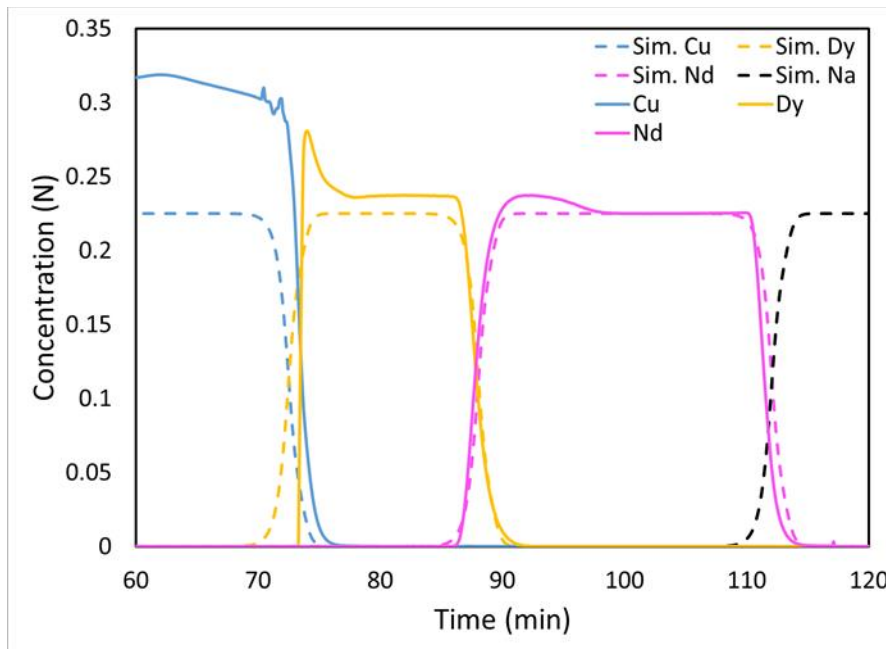


Figure 4.13 Chromatograph of Dy Nd separation simulation (dotted line) with experimental data (solid line) for Cycle 1. The Capacity used in the simulation was 1.4 meq./mL for a 78.5 cm column (1.16 cm ID). The elution ligand was 0.09 M EDTA at pH 9. The row up of Dy is an artifact due to the pH change that occurs between the elution of copper and dysprosium

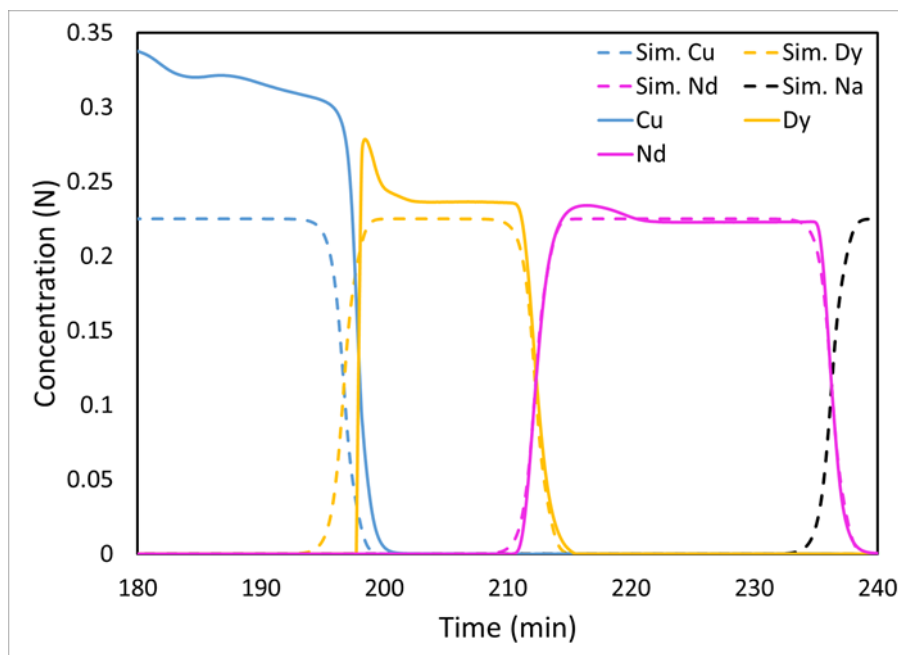


Figure 4.14 Chromatograph of Dy Nd separation simulation (dotted line) with experimental data (solid line) for Cycle 2. The Capacity used in the simulation was 1.4 meq./mL for a 78.5 cm column (1.16 cm ID). The elution ligand was 0.09 M EDTA at pH 9. The row up of Dy is an artifact due to the pH change that occurs between the elution of copper and dysprosium

In this case the target yield for Dy was exceeded by a few percent but matched within experimental error. The total productivity of this zone was $>400\text{kg/m}^3\text{day}$ which is more than 2 orders of magnitude higher than a liquid-liquid extraction system. By separating Dy and Nd in this separate zone it allowed for Nd to be collected at a high purity and yield in Zone I without sacrificing high productivity. Now, Dy can be collected with a high productivity in Zone II. Because Dy was measured using a PDA detector that is pH dependent, the row up in concentration shown in the experimental results is most likely an artifact based on the drop in pH that occurs when transitioning from copper to REE. This experiment also demonstrates the first continuous LAD system designed with a feed solution already bound to EDTA suggesting that the new map is accurate. These results paired with the results from Zone I demonstrate that a continuous multizone LAD separation is viable and beneficial.

Zone IIb Separation of Nd and Pr

The separation of Nd and Pr presented several unique challenges compared to the previous zones. The chief difficulty was due to the instability of the feed solution. EDTA-Pr is an extremely unstable solution that shows precipitation within minutes under agitation. Agitation was avoided to reduce the precipitation, however only a single cycle could be run before precipitation disrupted the pumps. Additionally, because of the low selectivity between Nd and Pr, the cycle time is much higher than the previous experiments. This can lead to precipitation of EDTA-Cu when flowing through the restriction of the detector. The summary of Zone IIb results are given in Table 4.14 and the chromatograph is shown in Figure 4.15.

Table 4.14 Summary of Cycle 1 from Continuous Zone IIb using 2 Columns

	Pr				Nd			
	Target Yield (%)	Actual Yield	Purity	Productivity (kg/m ³ day)	Target Yield	Actual Yield	Purity	Productivity (kg/m ³ day)
Cycle 1	77	74	99.4	68	-	60	99.0	87

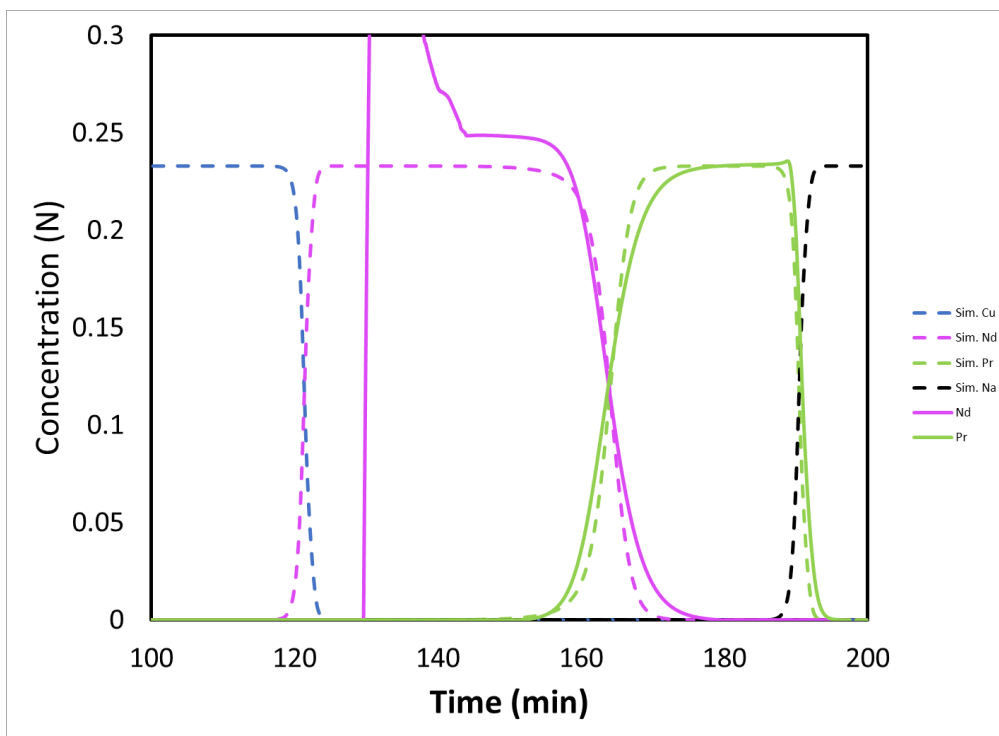


Figure 4.15 Chromatograph of Nd and Pr separation simulation (dotted line) with experimental data (solid line) for Cycle 1. The Capacity used in the simulation was 1.35 meq./mL for a 78.5 cm column (1.16 cm ID). The elution ligand was 0.09 M EDTA at pH 9. The row up of Nd is an artifact due to the pH change that occurs between the elution of copper and neodymium. It is also possible that the detector had not stabilized after being hooked up further exaggerating the row up. This is because copper is also visible on the same wavelength as Nd meaning that the copper signal must be removed to see the Nd signal.

Overall Productivity

By taking a weighted average of the productivity of each of these zones, the overall productivity of REEs is 190 kg/m³day which is 70% higher than the productivity reported in the most recent manuscript in a multizone batch system. Furthermore, this is more than two orders of magnitude higher productivity than a single column batch LAD process.

4.4.5 Robustness Analysis

The results of the robustness tests can be found in Table 4.15 and Table 4.16. In Table 4.15, the safety factor was achieved by reducing the flowrate by 5 and 10%. In this study it was identified that the yield and purity were most sensitive to changes in Nd concentration. For that reason, in the study shown in Table 4.16, only changes in Nd were examined when comparing the

effectiveness of a safety factor reducing design length or reducing velocity. Even with no safety factor the purity and yield were not extremely sensitive to changes in composition. This means that if there are small errors, the yield and purity will not be changes significantly, and using a 190% safety factor, these changes can be mitigated in all but the most extreme case.

Table 4.15 Summary of yield and purity of Nd with a variety of concentrations. Target yield 78% with a breakthrough cut of 0.05 and a dead volume of 2 mL was used in all cases. Loading was held constant and the safety factor was based on the flowrate. The highlighted concentrations (red) are the concentrations that have been changed compared to the base case.

Concentration (N)			No Safety Factor		5% Safety Factor		10% Safety Factor	
Dy	Nd	Pr	Yield Nd (%)	Purity Nd (%)	Yield Nd (%)	Purity Nd (%)	Yield Nd (%)	Purity Nd (%)
0.050	0.830	0.120	77.0	99.5	77.8	99.5	78.9	99.5
0.053	0.830	0.120	76.9	99.5	77.8	99.5	78.7	99.5
0.055	0.830	0.120	77.0	99.5	77.9	99.5	78.7	99.5
0.048	0.830	0.120	77.0	99.5	77.8	99.5	78.9	99.5
0.045	0.830	0.120	77.0	99.5	77.9	99.5	78.8	99.5
0.050	0.872	0.120	77.9	99.5	78.9	99.5	79.8	99.6
0.050	0.913	0.120	78.9	99.5	79.8	99.5	80.6	99.6
0.050	0.789	0.120	75.8	99.5	76.8	99.5	77.7	99.5
0.050	0.747	0.120	74.5	99.4	75.5	99.5	76.6	99.4
0.050	0.830	0.126	77.0	99.5	77.9	99.5	78.8	99.5
0.050	0.830	0.132	76.9	99.5	77.3	99.5	78.7	99.5
0.050	0.830	0.114	77.0	99.5	77.9	99.5	78.8	99.5
0.050	0.830	0.108	77.1	99.5	78.0	99.5	78.9	99.5
0.053	0.872	0.120	78.0	99.5	78.9	99.5	79.7	99.6
0.053	0.830	0.126	76.9	99.5	77.8	99.5	78.7	99.5
0.050	0.872	0.126	78.0	99.5	78.8	99.5	79.8	99.6
0.048	0.789	0.120	75.8	99.5	76.8	99.5	77.7	99.5
0.048	0.830	0.114	77.0	99.5	78.0	99.5	78.9	99.5
0.050	0.789	0.114	75.8	99.5	76.9	99.5	77.8	99.5

Table 4.16 Comparison of safety factors on the yield and purity of Nd with a variety of concentrations. Target yield 78% with a breakthrough cut of 0.05 and a dead volume of 2 mL. Loading was held constant. Safety factor was achieved by reducing the design column length.

Concentration (N)			No Safety Factor		10% Reduction in Design Column Length		10% Reduction in Velocity	
Dy	Nd	Pr	Yield Nd (%)	Purity Nd (%)	Yield Nd (%)	Purity Nd (%)	Yield Nd (%)	Purity Nd (%)
0.050	0.830	0.120	77.0	99.5	76.7	99.5	78.9	99.5
0.050	0.872	0.120	77.9	99.5	77.4	99.5	79.8	99.6
0.050	0.913	0.120	78.9	99.5	78.7	99.6	80.6	99.6
0.050	0.789	0.120	75.8	99.5	75.5	99.5	77.7	99.5
0.050	0.747	0.120	74.5	99.4	74.1	99.5	76.6	99.4

As evident in both studies, even with no safety factor, the purity is not sensitive to changes or errors in the feed concentration. The yield and purity were most sensitive to changes in the target component, but even in these cases a decrease in concentration by 10% only resulted in a decrease in yield by as much as 3%. In Table 4.16 it shows that a safety factor reducing the velocity was more effective than the safety factor reducing the design column length. A reduction in velocity represents moving the point on the “map” to the right into constant pattern region. Reducing the design length represents moving the point up into the constant pattern region. Based on this study, reducing the velocity is more effective as it shows high yield in all cases. The purity was more robust when reducing the column length so if purity is the key variable instead of yield, reducing the design length could be warranted.

4.4.6 Advantages of Continuous LAD compared to Batch LAD and Liquid-Liquid Extraction

There are several advantages of continuous LAD compared to batch LAD chromatography. First, the recycle of the mixed bands is naturally built into the cycle without sacrificing yield or productivity. For an equimolar ternary separation, to achieve the same purity and yield, a batch system with no recycle would require a column volume 2.3 times larger than a continuous system with a recycle based on the Constant Pattern design equations. This is even more pronounced if the system is not equimolar. Furthermore, less copper is required (30-50%) in the continuous systems compared to batch systems. As mentioned previously, the regeneration and loading can

be done simultaneously with elution. This reduces the cycle time to only the elution time. When 3 or more columns are used for a continuous separation, EDTA can be loaded into the column at two locations simultaneously. This forms a second elution train in the first two columns while the first elution train is still leaving the third (See Fig. 4.6 Step 12), further increasing the productivity. By utilizing multiple columns in the continuous configuration, there is an added flexibility to deal with a variety of feed mixtures.

The continuous LAD system developed in this study utilized an automated chromatography system. With operation parameters preset, the separation process achieved high yield, high purity, and high productivity with minimum human operation. This advancement in automation lays the foundation for process scaling-up and commercialization.

Compared to liquid-liquid extraction, the LAD separation of rare earth elements has the advantages of using only benign chemicals, higher productivity, more compact processing volume and almost zero waste. A brief comparison can be found in the table below.

Table 4.17 Comparison between conventional liquid-liquid extraction and Purdue technology

	Liquid-liquid extraction	Purdue	Advantages
Typical yield (%)	80-95%	>99%	No loss of REEs
Normalized productivity	1	100	100 times more productive
Normalized processing volume	100	1	100 times smaller
Extractant	Toxic	EDTA	Safe
Wastewater (tons/ton REO)	50 With 2.6 tons ammonium salts, pH=0.9	~0	Nearly zero waste

4.5 Conclusions

Although LAD was discovered in the 1950s, a general, scalable, and robust design method for LAD batch chromatography was only developed in 2018. The constant pattern design method allowed for the minimum column length required for a separation to be determined given a target yield and product purity. For a desired product purity, a higher yield can be achieved only by sacrificing productivity in batch chromatography.

In this study, the Constant Pattern Design Method was extended to continuous LAD systems. By recycling the mixed band regions, it was possible to achieve yields of >99% and product purity >99% without sacrificing productivity. Through the optimization of the productivity equation, it is possible to design LAD systems which maximize the productivity for a given column length. In this design, the minimum target yield is only a nominal yield, because the mixed band regions can be recycled directly back on to the column. This means that the mixed band region is not waste. The recycle of these mixed bands were demonstrated experimentally using a synthetic mixed band solution.

This study demonstrated the continuous separation of REEs using LAD experiments for both binary and ternary feed mixtures. In each case, nominal yields were achieved within experimental error. Additionally, the robustness of the Constant Pattern Design Method was demonstrated in a binary system by overloading the column by 10%. Even in this case the target yield was achieved without sacrificing productivity.

The REE concentrations in many feed mixtures can vary by an order of magnitude. Recovering a minority component with high purity and yield from such complex mixtures requires very slow flowrates, resulting in a very low sorbent productivity if a single column is used. A two-zone, continuous LAD system is designed and tested for complex mixtures. A systematic splitting strategy based on selectivity-weighted composition factors is derived theoretically and tested experimentally. The splitting strategy is incorporated into the constant-pattern design method and tested for the continuous two-zone LAD for the separation of complex mixtures of Dy, Nd, and Pr with a similar composition as the REE crudes derived from waste magnets. The results showed that for producing all three REEs with high purity (99%) and high yield (99%), a continuous two-zone LAD system has over 150 times higher sorbent productivity than a single-column LAD.

Because the two-zone LAD is continuous and the design method is based on intrinsic parameters, it can be easily scaled up for industrial production. Compared to liquid-liquid extraction, the continuous two-zone LAD requires only environmentally friendly chemicals and a few chromatography columns, which are 100 times smaller in processing volume. Most of the chemicals can be recycled, generating little waste and greatly reducing the environmental impact. The continuous LAD for the separation of complex feed mixtures is a key step toward the transformation of the commercial production of REEs from liquid-liquid extraction to continuous chromatography.

5. CONCLUSIONS AND RECOMMENDATIONS

5.1 Conclusions

This dissertation developed dimensionless design methods for a variety of different continuous chromatography techniques. Through the development of these design methods, significant improvements were made in the design and implementation of these different techniques.

In Chapter 2, the Speedy Standing Wave Design equations were developed for multicomponent separations with linear isotherms and a systematic splitting strategy was developed for the design of tandem SMBs. By performing the easiest split first, the overall productivity and solvent efficiency can be significantly improved. Rate model simulations were used to verify that the SSWD equations achieved target yields and purities. In systems where only one component is desired, the sorbent should be selected such that this component is the most or least retained so that it can be separated in a single SMB.

In Chapter 3, the Standing Wave Design Method was extended to non-isocratic three zone open loop SMBs. That standing wave design equations were derived and then verified using rate model simulations. In two example systems it was shown that non-isocratic SMBs designed using the standing wave design show an order of magnitude higher productivity than a comparable batch system when the impurities are weakly adsorbing. When the impurities are competitive, the SWD method produces SMB systems with 2 orders of magnitude higher productivity than comparable batch systems. Because the design is based on dimensionless groups, the resulting designs are easily scalable and no rate model simulations are required to design high yield, high purity, and high productivity SMBs.

In Chapter 4, the constant pattern design method was extended to continuous LAD systems. In this chapter, a continuous operation mode was developed that reduced the cycle time of LAD systems to further increase the productivity. In cases where the feed was equimolar, the continuous configuration increased the productivity between 20-50%. A multizone continuous LAD configuration was developed for the separation of a complex mixture of Dy, Nd, and Pr that simulated a crude magnet feed. The resulting overall productivity for this system was 190 kg/m³day which was two orders of magnitude higher than a single column batch system and 70%

higher than a multizone batch system. The robustness of the constant patten design method was demonstrated through a simulated case study and it was determined that adding a safety factor through the reduction of the flowrate was more effective than reducing the design length.

5.2 Recommendations

This dissertation developed the Speedy Standing Wave Design equations for multicomponent separations with linear isotherms. While this can be used as an approximation for the design of systems with non-linear isotherms, it is recommended that the equations be derived for common non-linear isotherms such as the Langmuir Isotherm. By extending to non-linear systems, it would allow for the design of a larger variety of SMB applications. The underlying standing wave design equations already exist, but non-dimensionalizing them would greatly improve the utility of the design.

In non-isocratic systems, the Standing Wave Design Equations were developed for three-zone open loop systems. In the future there are two improvements that are recommended for the design of these systems. Most importantly would be the development of the Speedy Standing Wave Design equations for both the linear and non-linear isotherms. Chapter 2 of this dissertation lays the groundwork for the development of the linear non-isocratic Speedy Standing Wave Design, but the development of the SSWD for systems with non-linear isotherms in non-isocratic systems would be dependent on first developing them for the isocratic cases. Another suggestion is the development of non-isocratic standing wave design equations for a closed system. While most non-isocratic variables are more easily controlled in an open loop system, there may be times when the solvent is very expensive and a recycle would be of benefit. This may also be more relevant in changes such as temperature swing which can be controlled more easily depending on scale.

For the separation of Rare Earth elements using LAD it is suggested that more ligands and resins be investigated for efficacy in this separation method. Currently the variable most limiting the productivity of these systems is the ligand concentration. Solubility issues cause precipitation and low product concentrations. By locating more soluble ligands, there is a possibility of further improvement in the productivity of LAD systems. Also, if resins are discovered that can work synergistically with the ligand effects in the mobile phase there is a possibility for significant improvement to LAD systems. It is also suggested that future studies should examine alternative rare earth feeds such as batteries or ores. This dissertation focused on the theoretical development

of the continuous operation mode and demonstrated it on one realistic feed solution, but there are several possible rare earth sources that have yet to be exploited. By demonstrating the flexibility of LAD on a variety of feeds, future studies can further bolster the competitiveness of LAD compared to other rare earth separation techniques.

APPENDIX A. STANDING WAVE EQUATIONS AND THE RELATION BETWEEN THE DECAY FACTOR β_i^j AND THE YIELD Y_i

Eq. (A.1)-(A.4) show the zone velocities of the four zones with the definition of the mass transfer correction term substituted into Eq. (3) in Chapter 2.

$$u_0^I = (1 + \phi\delta_p)v + \frac{\beta_p^I}{L^I} \left(E_{b,p}^I + \frac{\phi\delta_p^2 v^2}{K_p^I} \right) \quad (\text{A.1})$$

$$u_0^{II} = (1 + \phi\delta_q)v + \frac{\beta_q^{II}}{L^{II}} \left(E_{b,q}^{II} + \frac{\phi\delta_q^2 v^2}{K_q^{II}} \right) \quad (\text{A.2})$$

$$u_0^{III} = (1 + \phi\delta_r)v - \frac{\beta_r^{III}}{L^{III}} \left(E_{b,r}^{III} + \frac{\phi\delta_r^2 v^2}{K_r^{III}} \right) \quad (\text{A.3})$$

$$u_0^{IV} = (1 + \phi\delta_s)v + \frac{\beta_s^{IV}}{L^{IV}} \left(E_{b,s}^{IV} + \frac{\phi\delta_s^2 v^2}{K_s^{IV}} \right) \quad (\text{A.4})$$

The definition of the decay factor β_i^j was taken from the work of Hritzko et al., 2002 as follows [13].

$$\beta_p^I = \ln \left[\frac{Y_p \left(\frac{u_0^{III}}{u_0^{IV}} - 1 \right)}{(1 - Y_p) \left(1 - \frac{u_0^{II}}{u_0^I} \right)} \right] \quad (\text{A.5})$$

$$\beta_q^{II} = \ln \left\{ \frac{\left(\frac{u_0^I}{u_0^{II}} - 1 \right) \left[\frac{Y_q}{\left(1 - \frac{u_0^{IV}}{u_0^{III}} \right)} - 1 \right]}{(1 - Y_q) \left[\left(1 - \frac{u_0^{IV}}{u_0^{III}} \right) \right]} \right\} \quad (\text{A.6})$$

$$\beta_r^{III} = \ln \left\{ \frac{\left(1 - \frac{u_0^{IV}}{u_0^{III}} \right) \left[\frac{Y_r}{\left(\frac{u_0^I}{u_0^{II}} - 1 \right)} + 1 \right]}{(1 - Y_r) \left[\left(\frac{u_0^I}{u_0^{II}} - 1 \right) \right]} \right\} \quad (\text{A.7})$$

$$\beta_s^I = \ln \left[\frac{Y_s \left(1 - \frac{u_0^{II}}{u_0^I} \right)}{(1 - Y_s) \left(\frac{u_0^{III}}{u_0^{IV}} - 1 \right)} \right] \quad (\text{A.8})$$

APPENDIX B. IMPLEMENTATION OF SSWD

An example of the implementation of SSWD for the optimization of operating parameters of an SMB system is shown in Fig. B1. This example assumes fixed material parameters and column configuration. If the optimal column configuration is desired, the algorithm shown in Fig. B1. can be easily modified using a similar strategy as shown previously in Weeden and Wang for binary cases [2]. The target yield and material parameters ($\delta_1, \alpha_i, \eta_i, \phi, N^J$) are fixed for each design. The parameters should be used to select the splitting strategy for the system. Next, initial values for $N_{DL,n}^*$ and P_{ebl}^* are set based on guesses of minimum values. The β and Γ values are then guessed using the ideal solution where mass transfer effects are not considered. The zone velocities can then be calculated using Eq. (20a-d). From these new velocities, new values of β and Γ are calculated. If the new β values are the same as the guess of the β values within the tolerance, then the design is considered converged for the given $N_{DL,n}^*$ and P_{ebl}^* values. The column length, port velocity, and zone velocities can then be determined along with the pressure drop. If β is not the same within tolerance, the new calculated β is used as an initial guess and the procedure repeats. Once the pressure drop has been determined, it is evaluated if this design meets the pressure criteria for the SMB system. If it does, this design is stored. If it does not, then the design is not considered. This process is repeated for all combinations of $N_{DL,n}^*$ and P_{ebl}^* within the ranges being considered. Finally, after all combinations have been considered, the maximum productivity or minimum solvent consumption case is found from the stored values.

Table B.1. Final Form of SSWD Equations in Terms of Selectivity

General	Eq.	Diffusion Controlled	Eq.
$\frac{u_0^I}{v} = 1 + \phi\delta_p + \frac{\beta_p^I \phi \delta_n}{P_{ebl}^* f^I} + \frac{\phi \delta_n \beta_p^I \eta_n \alpha_p^2}{15N_{Dl,n}^* \alpha_n^2 \eta_p f^I}$	(B.1)	$\frac{u_0^I}{v} = 1 + \phi\delta_p + \frac{\phi \delta_n \beta_p^I \eta_n \alpha_p^2}{15N_{Dl,n}^* \alpha_n^2 \eta_p f^I}$	(B.7)
$\frac{u_0^{II}}{v} = 1 + \phi\delta_q + \frac{\beta_q^{II} \phi \delta_n \Gamma^{II}}{P_{ebl}^* f^{II}} + \frac{\phi \delta_n \beta_q^{II} \eta_n \alpha_q^2}{15N_{Dl,n}^* \alpha_n^2 \eta_q f^{II}}$	(B.2)	$\frac{u_0^{II}}{v} = 1 + \phi\delta_q + \frac{\phi \delta_n \beta_q^{II} \eta_n \alpha_q^2}{15N_{Dl,n}^* \alpha_n^2 \eta_q f^{II}}$	(B.8)
$\frac{u_0^{III}}{v} = 1 + \phi\delta_r - \frac{\beta_r^{III} \phi \delta_n \Gamma^{III}}{P_{ebl}^* f^{III}} - \frac{\phi \delta_n \beta_r^{III} \eta_n \alpha_r^2}{15N_{Dl,n}^* \alpha_n^2 \eta_r f^{III}}$	(B.3)	$\frac{u_0^{III}}{v} = 1 + \phi\delta_r - \frac{\phi \delta_n \beta_r^{III} \eta_n \alpha_r^2}{15N_{Dl,n}^* \alpha_n^2 \eta_r f^{III}}$	(B.9)
$\frac{u_0^{IV}}{v} = 1 + \phi\delta_s - \frac{\beta_s^{IV} \phi \delta_n \Gamma^{IV}}{P_{ebl}^* f^{IV}} - \frac{\phi \delta_n \beta_s^{IV} \eta_n \alpha_s^2}{15N_{Dl,n}^* \alpha_n^2 \eta_s f^{IV}}$	(B.4)	$\frac{u_0^{IV}}{v} = 1 + \phi\delta_s - \frac{\phi \delta_n \beta_s^{IV} \eta_n \alpha_s^2}{15N_{Dl,n}^* \alpha_n^2 \eta_s f^{IV}}$	(B.10)
$P_R^* = \frac{1}{N_{Dl,n}^*} \left[\left(\frac{\alpha_r}{\alpha_n} - \frac{\alpha_q}{\alpha_n} \right) - \frac{1}{P_{ebl}^*} \left(\frac{\beta_r^{III} \Gamma^{III}}{f^{III}} + \frac{\beta_q^{II} \Gamma^{II}}{f^{II}} \right) - \frac{\eta_n}{15N_{Dl,n}^* \alpha_n^2} \left(\frac{\beta_r^{III} \alpha_r^2}{f^{III} \eta_r} + \frac{\beta_q^{II} \alpha_q^2}{f^{II} \eta_q} \right) \right]$	(B.5)	$P_R^* = \frac{1}{N_{Dl,n}^*} \left[\left(\frac{\alpha_r}{\alpha_n} - \frac{\alpha_q}{\alpha_n} \right) - \frac{\eta_n}{15N_{Dl,n}^* \alpha_n^2} \left(\frac{\beta_r^{III} \alpha_r^2}{f^{III} \eta_r} + \frac{\beta_q^{II} \alpha_q^2}{f^{II} \eta_q} \right) \right]$	(B.11)
$\frac{F}{D} = \frac{\left(\frac{\alpha_r}{\alpha_n} - \frac{\alpha_q}{\alpha_n} \right) - \frac{1}{P_{ebl}^*} \left(\frac{\beta_r^{III} \Gamma^{III}}{f^{III}} + \frac{\beta_q^{II} \Gamma^{II}}{f^{II}} \right) - \frac{\eta_n}{15N_{Dl,n}^* \alpha_n^2} \left(\frac{\beta_r^{III} \alpha_r^2}{f^{III} \eta_r} + \frac{\beta_q^{II} \alpha_q^2}{f^{II} \eta_q} \right)}{\left(\frac{\alpha_p}{\alpha_n} - \frac{\alpha_s}{\alpha_n} \right) + \frac{1}{P_{ebl}^*} \left(\frac{\beta_p^I}{f^I} + \frac{\beta_s^{IV} \Gamma^{IV}}{f^{IV}} \right) + \frac{\eta_n}{15N_{Dl,n}^* \alpha_n^2} \left(\frac{\beta_p^I \alpha_p^2}{f^I \eta_p} + \frac{\beta_s^{IV} \alpha_s^2}{f^{IV} \eta_s} \right)}$	(B.6)	$\frac{F}{D} = \frac{\left(\frac{\alpha_r}{\alpha_n} - \frac{\alpha_q}{\alpha_n} \right) - \frac{\eta_n}{15N_{Dl,n}^* \alpha_n^2} \left(\frac{\beta_r^{III} \alpha_r^2}{f^{III} \eta_r} + \frac{\beta_q^{II} \alpha_q^2}{f^{II} \eta_q} \right)}{\left(\frac{\alpha_p}{\alpha_n} - \frac{\alpha_s}{\alpha_n} \right) + \frac{\eta_n}{15N_{Dl,n}^* \alpha_n^2} \left(\frac{\beta_p^I \alpha_p^2}{f^I \eta_p} + \frac{\beta_s^{IV} \alpha_s^2}{f^{IV} \eta_s} \right)}$	(B.12)

Because the feed volume must be positive, there is a minimum $N_{DL,n}^*$ for operation that can be determined using Eq. (B.6). The minimum $N_{DL,n}^*$ is derived and given in Eq. (B.13) in the general case.

$$N_{DL,nmin}^* = \frac{\frac{\eta_n}{15\alpha_n^2} \left(\frac{\beta_r^{III} \alpha_r^2}{\eta_r f^{III}} + \frac{\beta_q^{II} \alpha_q^2}{\eta_q f^{II}} \right)}{\left(\frac{\alpha_r}{\alpha_n} - \frac{\alpha_q}{\alpha_n} \right) - \frac{1}{P_{ebl}^*} \left(\frac{\beta_r^{III} \Gamma^{III}}{f^{III}} + \frac{\beta_q^{II} \Gamma^{II}}{f^{II}} \right)} \quad (B.13)$$

An $N_{DL,n}^*$ for maximum productivity can also be calculated by taking the derivative of Eq. (B.5) in terms of $N_{DL,n}^*$ that makes the derivative equal to zero. This assumes that the decay factors (β) are constant which is a reasonable approximation. When this is done, Eq. (B.14) is derived.

$$N_{DL,nmax}^* = \frac{\frac{2\eta_n}{15\alpha_n^2} \left(\frac{\beta_r^{III} \alpha_r^2}{\eta_r f^{III}} + \frac{\beta_q^{II} \alpha_q^2}{\eta_q f^{II}} \right)}{\left(\frac{\alpha_r}{\alpha_n} - \frac{\alpha_q}{\alpha_n} \right) - \frac{1}{P_{ebl}^*} \left(\frac{\beta_r^{III} \Gamma^{III}}{f^{III}} + \frac{\beta_q^{II} \Gamma^{II}}{f^{II}} \right)} \quad (B.14)$$

When Eq. (B.14) is substituted into Eq. (B.5), the resulting maximum dimensionless productivity is given in Eq. (B.15).

$$P_{R,max}^* = \frac{15 \left[(\alpha_q - \alpha_r) P_{ebl}^* + \alpha_n \left(\frac{\beta_r^{III} \Gamma^{III}}{f^{III}} + \frac{\beta_q^{II} \Gamma^{II}}{f^{II}} \right) \right]^2}{P_{ebl}^* \eta_n \left(\frac{\beta_r^{III} \alpha_r^2}{\eta_r f^{III}} + \frac{\beta_q^{II} \alpha_q^2}{\eta_q f^{II}} \right)} \quad (B.15)$$

As in the general case, the minimum $N_{DL,n}^*$ for operation can be calculated based on Eq. (B.12). In the diffusion limited case, the feed flow rate must still be a positive number. The results gives Eq. (B.16).

$$N_{DL,nmin}^* = \frac{\eta_n}{15\alpha_n^2 \left(\frac{\alpha_r}{\alpha_n} - \frac{\alpha_q}{\alpha_n} \right)} \left(\frac{\beta_r^{III} \alpha_r^2}{\eta_r f^{III}} + \frac{\beta_q^{II} \alpha_q^2}{\eta_q f^{II}} \right) \quad (B.16)$$

Similarly, the $N_{DL,n}^*$ for maximum productivity can be derived by taking the derivative of Eq. (B.11) with respect to $N_{DL,n}^*$ and setting the result equal to zero. This gives Eq. (B.17) seen below.

$$N_{DL,nmax}^* = \frac{2\eta_n}{15\alpha_n^2 \left(\frac{\alpha_r}{\alpha_n} - \frac{\alpha_q}{\alpha_n} \right)} \left(\frac{\beta_r^{III} \alpha_r^2}{\eta_r f^{III}} + \frac{\beta_q^{II} \alpha_q^2}{\eta_q f^{II}} \right) \quad (B.17)$$

Finally, the $N_{DL,n}^*$ can be substituted into Eq. (B.11) to give the maximum possible dimensionless productivity which can be seen in Eq. (B.18)

$$P_{R,max}^* = \frac{15(\alpha_r - \alpha_q)^2}{4\eta_n \left(\frac{\beta_r^{III} \alpha_r^2}{\eta_r f^{III}} + \frac{\beta_q^{II} \alpha_q^2}{\eta_q f^{II}} \right)} \quad (B.19)$$

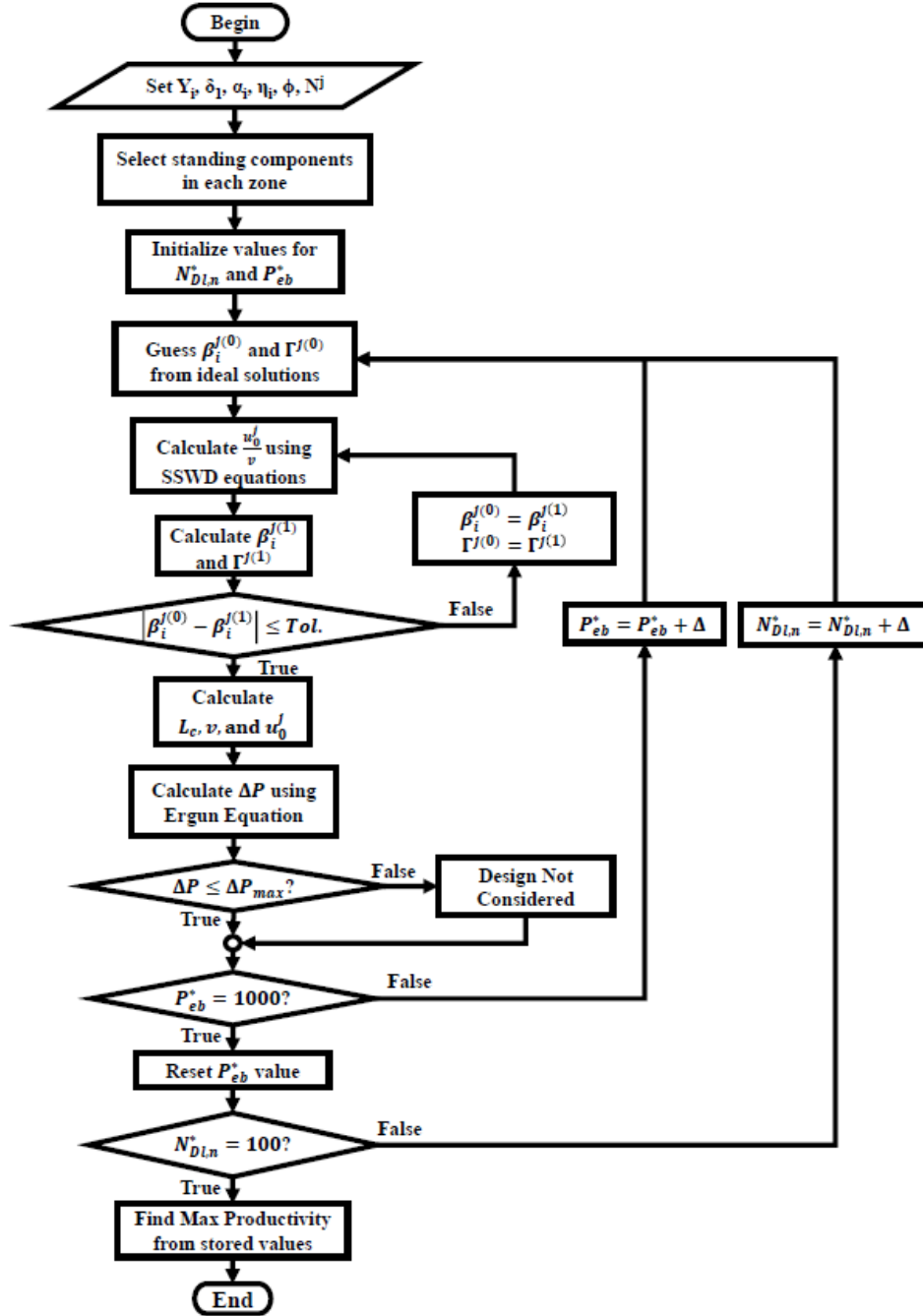


Figure. B.1. Implementation of SSWD for maximum productivity with set column configuration.

APPENDIX C. OPERATING CONDITIONS FOR THE CASE STUDIES

The operating conditions from both Ring 1 and Ring 2 of the case studies are given in Tables C1 and C2 respectively. These operating parameters were determined using the SSWD process. The parameters in Table C2 are the same in splits 1, 4b, and 5 because intrinsic parameters determine the ideal operating conditions. This is also the reason that the conditions for Splits 2, 3, and 4a are the same as well.

Table C1. Operating conditions for Ring 1 of Case Study

Split #	Switching time (min)	Port Velocity (cm/min)	Feed Flowrate (mL/min)	Desorbent Flowrate (mL/min)	Extract Flowrate (mL/min)	Raffinate Flowrate (mL/min)	Recycle Flowrate (mL/min)
1	5.51	1.680	19.98	558.17	548.10	30.06	61.22
2	15.9	0.580	39.05	142.70	125.96	55.78	22.26
3	15.1	0.613	40.17	134.42	129.20	45.93	36.50
4	12.2	0.758	58.83	201.52	199.98	60.38	28.88
5	5.8	1.595	19.23	58.95	51.89	26.29	58.75

Table C2. Operating conditions for Ring 2 of Case Study

Split #	Switching time (min)	Port Velocity (cm/min)	Feed Flowrate (mL/min)	Desorbent Flowrate (mL/min)	Extract Flowrate (mL/min)	Raffinate Flowrate (mL/min)	Recycle Flowrate (mL/min)
1	15.1	0.613	40.71	134.42	129.20	45.93	36.50
2	5.8	1.595	19.23	58.95	51.89	26.29	58.75
3	5.8	1.595	19.23	58.95	51.89	26.29	58.75
4a	5.8	1.595	19.23	58.95	51.89	26.29	58.75
4b	15.1	0.613	40.71	134.42	129.20	45.93	36.50
5	15.1	0.613	40.71	134.42	129.20	45.93	36.50

APPENDIX D. IMPLEMENTATION OF THE STANDING-WAVE DESIGN FOR NON-ISOCRATIC SYSTEMS

A summary of the iterative procedure required to solve the ideal SWD equations is given in Fig. D.1. Given column parameters, isotherm parameters, feed flow rate, and feed concentrations, the procedure shown in Fig. D.1. will yield the zone velocities, port velocity, and plateau concentrations. The initial guesses for $C_{s,1}$ and $C_{s,2}$ should be less than $C_{f,1}$ and $C_{f,2}$ respectively. After the initial guesses are made, the plateau concentrations are calculated using the Hodograph solutions. These concentrations can be used to calculate the retention factors. From there, the zone velocities can be determined. The velocities are then checked using the mass balances. If the hodograph solutions and the mass balance give the same results, the solution converges, otherwise the new concentrations are used as the initial guess and the process is repeated.

The procedure to solve the Standing-Wave Design equations in non-ideal systems is shown in Fig. D.2. The results from the ideal solution should be used as the initial guess in the non-ideal solution. This will decrease the required iteration times and improve chances of convergence. The process of solving for the zone velocities and plateau concentrations follows a similar pattern. In this case, the mass transfer parameters are needed to solve for the zone velocities, and the decay coefficients are also required. Otherwise, the zone velocities are calculated based on the retention factors, and the plateau concentrations are calculated using both the hodograph solutions and the mass balance similarly to the ideal case.

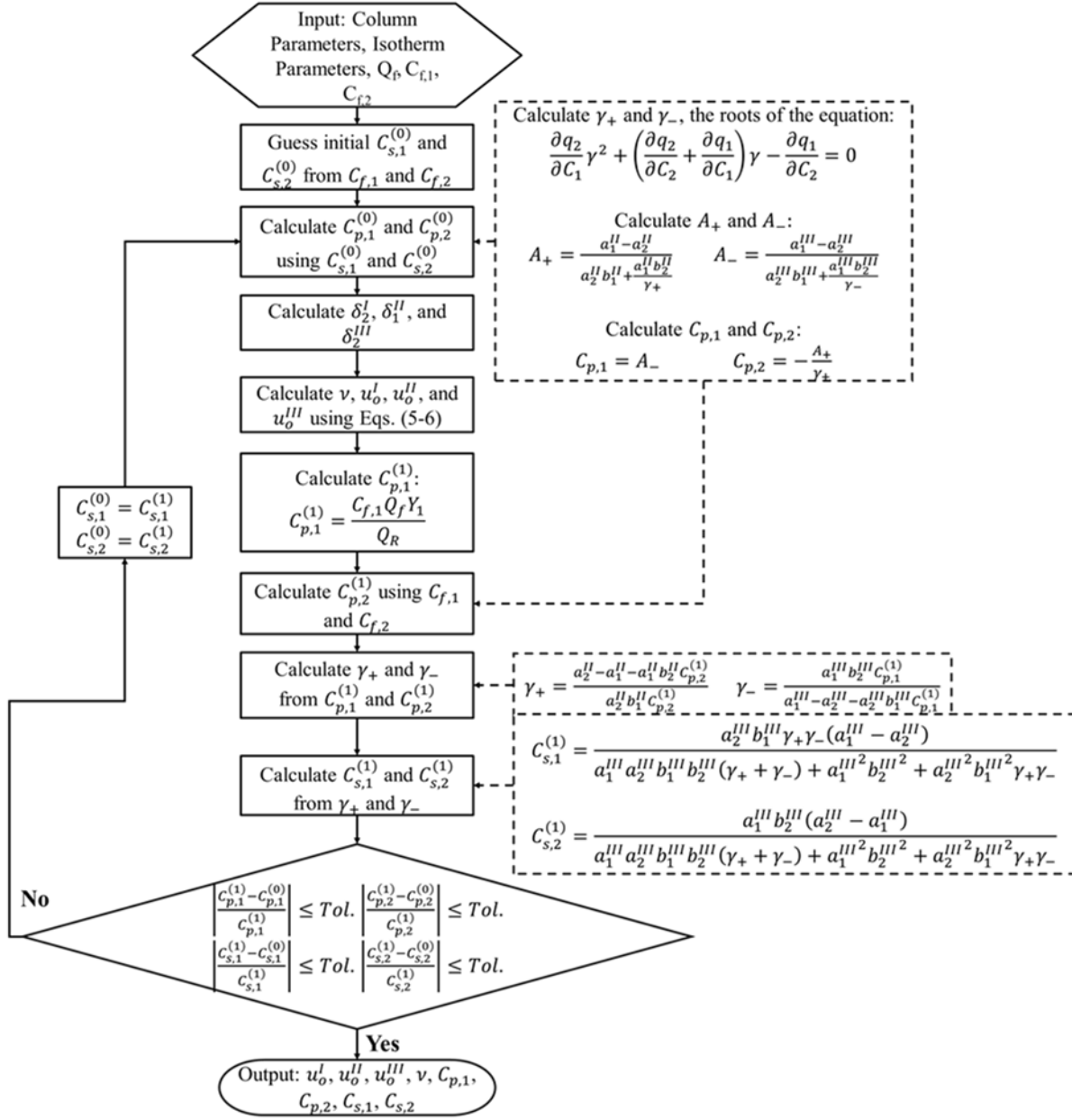


Figure D.1. Algorithm for the implementation of the non-isocratic SWD in ideal systems

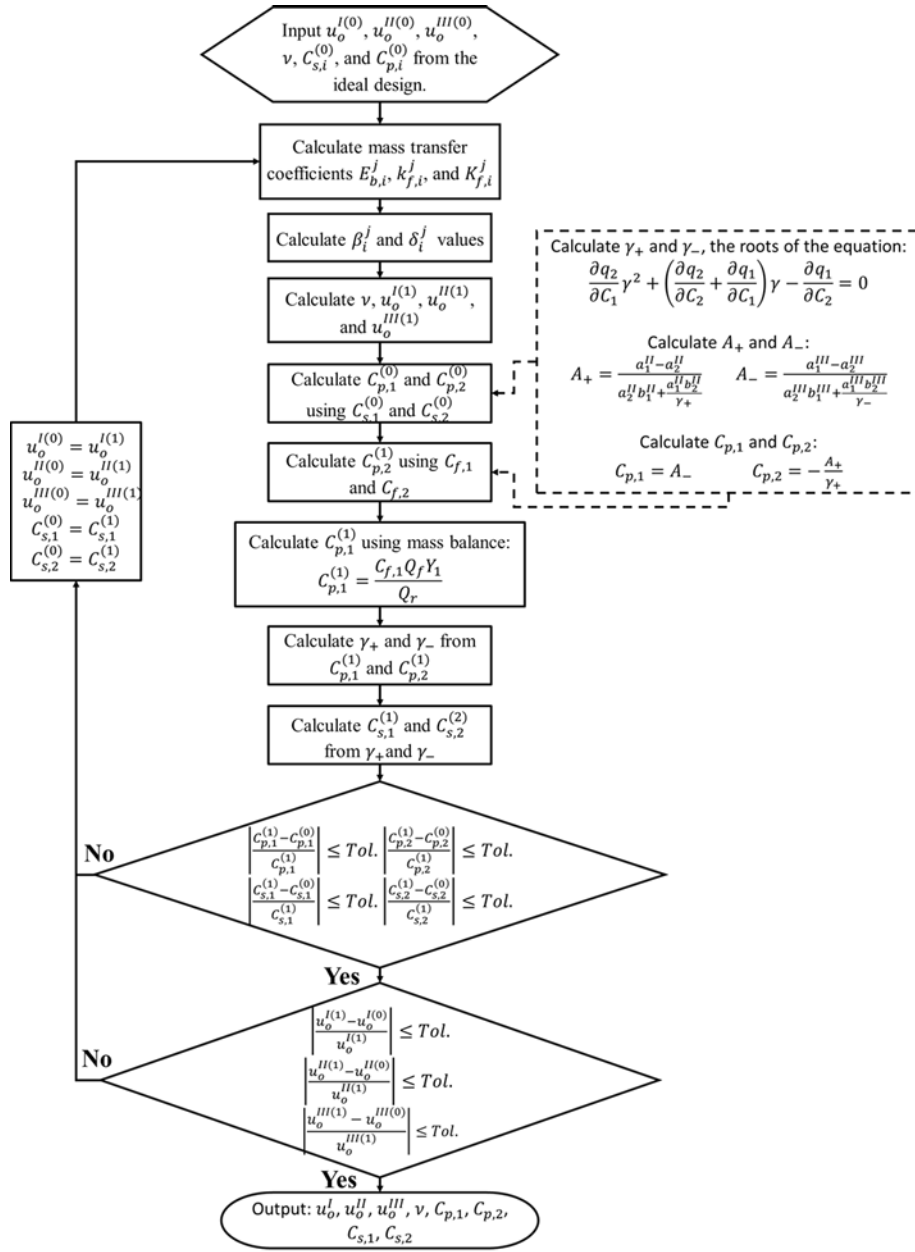


Figure D.2. Algorithm for the implementation of the non-isocratic SWD in non-ideal systems. The ideal solution is used as an initial guess in this system.

APPENDIX E. ASPEN CHROMATOGRAPHY MODEL

The mass balance equation used in the Aspen Chromatography simulations is as follows:

$$\varepsilon_b \frac{\partial C_i}{\partial t} + K_{se}(1 - \varepsilon_b)\varepsilon_p \frac{\partial \bar{C}_{i,pore}}{\partial t} + (1 - \varepsilon_b)(1 - \varepsilon_p)\rho_s \frac{\partial \bar{q}_l}{\partial t} + \varepsilon_b \frac{\partial (u_o^j C_i)}{\partial z} = \varepsilon_b (E_{b,i}^j) \frac{\partial^2 C_i}{\partial z^2} \quad (E.1)$$

Where ρ_s is the solid phase density, u_o^j is the mobile phase velocity within zone “j”, ε_b is the bed void fraction, ε_p is the particle porosity, $\bar{C}_{i,pore}$ is the average pore phase concentration. In Eq. (AF2.1), the $\frac{\partial \bar{q}_l}{\partial t}$ term is the linear lumped mass transfer parameter. In Example 1 it is:

$$\frac{\partial \bar{q}_l}{\partial t} = MTC_{s,i}(q_i^* - q_i) \quad (E.2)$$

Where $MTC_{s,i}$ is the mass transfer coefficient based on the solid phase concentration and q_i^* is the equilibrium solute concentration in the stationary phase

In Example 2 it is:

$$\frac{\partial \bar{q}_l}{\partial t} = MTC_{l,i}(C_i - C_i^*) \quad (E.3)$$

Where $MTC_{l,i}$ is the mass transfer coefficient based on the liquid phase concentration and C_i^* is the equilibrium mobile phase concentration. The axial dispersion coefficient was estimated using the Chung and Wen Correlations [36].

REFERENCES

- [1] D. Harvey, G. Weeden, N.H.L. Wang, Speedy standing wave design and simulated moving bed splitting strategies for the separation of ternary mixtures with linear isotherms, *J. Chromatogr. A.* 1530 (2017) 152–170. doi:10.1016/j.chroma.2017.10.050.
- [2] G.S. Weeden, N.L. Wang, Speedy standing wave design, optimization, and scaling rules of simulated moving bed systems with linear isotherms, *J. Chromatogr. A.* 1493 (2017) 19–40. doi:10.1016/j.chroma.2017.02.038.
- [3] F.H. Spedding, A.F. Voigt, E.M. Gladrow, N.R. Sleight, J.E. Powell, J.M. Wright, et al., The Separation of Rare Earths by Ion Exchange. II. Neodymium and Praseodymium, *J. Am. Chem. Soc.* 69 (1947) 2786–2792. doi:10.1021/ja01203a060.
- [4] D.B. Broughton, C.G. Gerhold, Continuous Sorption process employing fixed bed of sorbent and moving inlets and outlets, 2985589, 1961.
- [5] G.S. Weeden, L. Ling, N.H. Soepriatna, N.H.L. Wang, Size-exclusion simulated moving bed for separating organophosphorus flame retardants from a polymer, *J. Chromatogr. A.* 1422 (2015) 99–116. doi:10.1016/j.chroma.2015.09.064.
- [6] G.S. Weeden, N.H.L. Wang, Speedy standing wave design of size-exclusion simulated moving bed: Solvent consumption and sorbent productivity related to material properties and design parameters, *J. Chromatogr. A.* 1418 (2015) 54–76. doi:10.1016/j.chroma.2015.08.042.
- [7] Y. Xie, S. Mun, J. Kim, N.H.L. Wang, Standing wave design and experimental validation of a tandem simulated moving bed process for insulin purification, *Biotechnol. Prog.* 18 (2002) 1332–1344. doi:10.1021/bp025547r.
- [8] H. Heikkila, G. Hyöky, J. Kuisma, Method for the recovery of betaine from molasses, 5127957, 1992.
- [9] Y. Xie, C.Y. Chin, D.S.C. Phelps, C.H. Lee, K.B. Lee, S. Mun, et al., A five-zone simulated moving bed for the isolation of six sugars from biomass hydrolyzate, *Ind. Eng. Chem. Res.* 44 (2005) 9904–9920. doi:10.1021/ie050403d.
- [10] T.P. Binder, P.D. Bloom, G.B. Poppe, Applications of biobased glycol compositions, US 2008/013340 A1, 2008.

- [11] N.L. Mai, N.T. Nguyen, J. Il Kim, H.M. Park, S.K. Lee, Y.M. Koo, Recovery of ionic liquid and sugars from hydrolyzed biomass using ion exclusion simulated moving bed chromatography, *J. Chromatogr. A.* 1227 (2012) 67–72. doi:10.1016/j.chroma.2011.12.030.
- [12] R. Wooley, Z. Ma, N. Wang, A Nine-Zone Simulating Moving Bed for the Recovery of Glucose and Xylose from Biomass Hydrolyzate, *Ind. Eng. Chem. Res.* 37 (1998) 3699–3709. doi:Doi 10.1021/Ie9800896.
- [13] B.J. Hritzko, Y. Xie, R.J. Wooley, N.-H.L. Wang, Standing-wave design of tandem SMB for linear multicomponent systems, *AIChE J.* 48 (2002) 2769–2787. doi:10.1002/aic.690481207.
- [14] S. Mun, Y. Xie, J.-H. Kim, N.-H.L. Wang, Optimal Design of a Size-Exclusion Tandem Simulated Moving Bed for Insulin Purification, *Ind. Eng. Chem. Res.* 42 (2003) 1977–1993. doi:10.1021/ie020680+.
- [15] S. Mun, Y. Xie, N.H.L. Wang, Residence time distribution in a size-exclusion SMB for insulin purification, *AIChE J.* 49 (2003) 2039–2058. doi:10.1002/aic.690490814.
- [16] T. Masuda, T. Sonobe, F. Matsuda, M. Horie, United States Patent 5198120, 1993.
- [17] S. Imamoglu, *Modern Advances in Chromatography*, Springer Berlin Heidelberg, Berlin, Heidelberg, 2002. doi:10.1007/3-540-45345-8.
- [18] A. Rajendran, G. Paredes, M. Mazzotti, Simulated moving bed chromatography for the separation of enantiomers, *J. Chromatogr. A.* 1216 (2009) 709–738. doi:10.1016/j.chroma.2008.10.075.
- [19] G. Biressi, O. Ludemann-Hombourger, M. Mazzotti, R.M. Nicoud, M. Morbidelli, Design and optimisation of a simulated moving bed unit: Role of deviations from equilibrium theory, *J. Chromatogr. A.* 876 (2000) 3–15. doi:10.1016/S0021-9673(00)00191-6.
- [20] C. Migliorini, A. Gentilini, M. Mazzotti, M. Morbidelli, Design of Simulated Moving Bed Units under Nonideal Conditions, *Ind. Eng. Chem. Res.* 38 (1999) 2400–2410. doi:10.1021/ie980262y.
- [21] A.E. Rodrigues, L.S. Pais, Design of SMB chiral separations using the concept of separation volume, *Sep. Sci. Technol.* 39 (2004) 245–270. doi:Doi 10.1081/Ss-120027557.
- [22] D.C.S. Azevedo, A.E. Rodrigues, Design of a simulated moving bed in the presence of mass-transfer resistances, *AIChE J.* 45 (1999) 956–966. doi:10.1002/aic.690450506.

- [23] Z. Ma, N.-H.L. Wang, Standing Wave Analysis of SMB Chromatography: Linear Systems, *AICHE J.* 43 (1997) 2488–2508. doi:DOI 10.1002/aic.690431012.
- [24] K.B. Lee, R.B. Kasat, G.B. Cox, N.-H.L. Wang, Simulated Moving Bed Multiobjective Optimization Using Standing Wave Design and Genetic Algorithm, *AICHE J.* 54 (2008) 2852–2871. doi:10.1002/aic.11604.
- [25] F.G. Cauley, S.F. Cauley, K.B. Lee, Y. Xie, N.H.L. Wang, Standing Wave Annealing Technique: For the Design and Optimization of Nonlinear Simulated Moving Bed Systems with Significant Mass-Transfer Effects, *Ind. Eng. Chem. Res.* 45 (2006) 8697–8712. doi:10.1021/ie060300a.
- [26] F.G. Cauley, Y. Xie, N.-H.L. Wang, Optimization of SMB systems with linear adsorption isotherms by the Standing Wave Annealing Technique, *Ind. Eng. Chem. Res.* 43 (2004) 7588–7599. doi:10.1021/ie049842n.
- [27] K.B. Lee, S. Mun, F. Cauley, G.B. Cox, N.H.L. Wang, Optimal Standing-Wave Design of Nonlinear Simulated Moving Bed Systems for Enantioseparation, *Ind. Eng. Chem. Res.* 45 (2006) 739–752. doi:10.1021/ie0504248.
- [28] N. Soepriatna, N.H.L. Wang, P.C. Wankat, Standing Wave Design and Optimization of Nonlinear Four-Zone Thermal Simulated Moving Bed Systems, *Ind. Eng. Chem. Res.* 54 (2015) 10419–10433. doi:10.1021/acs.iecr.5b01296.
- [29] Y. Xie, C.A. Farrenburg, C.Y. Chin, S. Mun, N.H.L. Wang, Design of SMB for a Nonlinear Amino Acid System with Mass-Transfer Effects, *AICHE J.* 49 (2003) 2850–2863. doi:10.1002/aic.690491117.
- [30] N. Soepriatna, N.H.L. Wang, P.C. Wankat, Standing Wave Design of 2-Zone Thermal Simulated Moving Bed Concentrator (TSMBC), *Ind. Eng. Chem. Res.* 54 (2015) 12646–12663. doi:10.1021/acs.iecr.5b01296.
- [31] K.B. Lee, C.Y. Chin, Y. Xie, G.B. Cox, N.H.L. Wang, Standing-Wave Design of a Simulated Moving Bed under a Pressure Limit for Enantioseparation of Phenylpropanolamine, *Ind. Eng. Chem. Res.* 44 (2005) 3249–3267. doi:10.1021/ie049413p.
- [32] T. Mallmann, B.D. Burris, Z. Ma, N.H.L. Wang, Standing Wave Design of Nonlinear SMB Systems for Fructose Purification, *AICHE J.* 44 (1998) 2628–2646. doi:10.1002.

- [33] S. Mun, C. Chin, Y. Xie, N.H.L. Wang, Standing Wave Design of Carousel Ion-Exchange Processes for the Removal of Zinc Ions from a Protein Mixture, *Ind. Eng. Chem. Res.* 45 (2006) 316–329. doi:10.1021/ie050427k.
- [34] S. Mun, Y. Xie, N.-H.L. Wang, Robust Pinched-Wave Design of a Size-Exclusion Simulated Moving-Bed Process for Insulin Purification, *Ind. Eng. Chem. Res.* 42 (2003) 3129–3143. doi:10.1021/ie020992c.
- [35] S. Mun, N.H.L. Wang, Y.M. Koo, S.C. Yi, Pinched wave design of a four-zone simulated moving bed for linear adsorption systems with significant mass-transfer effects, *Ind. Eng. Chem. Res.* 45 (2006) 7241–7250. doi:10.1021/ie051033w.
- [36] S.F. Chung, C.Y. Wen, Longitudinal dispersion of liquid flowing through fixed and fluidized beds, *AIChE J.* 14 (1968) 857–866. doi:10.1002/aic.690140608.
- [37] S. Ergun, Fluid Flow through Packed Columns, *J. Chem. Eng. Prog.* 48 (1952) 89–94.
- [38] D. Wu, Y. Xie, Z. Ma, N. Wang, Design of simulated moving bed chromatography for amino acid separations, *Ind. Eng. Chem. Res.* 5885 (1998) 4023–4035. doi:10.1021/Ie9801711.
- [39] J.A. Berninger, R.D. Whitley, X. Zhang, N.H.L. Wang, A Versatile Model for Simulation of Reaction and Nonequilibrium Dynamics in Multicomponent Fixed-Bed Adsorption Processes, *Comput. Chem. Eng.* 15 (1991) 749–768. doi:10.1016/0098-1354(91)85020-U.
- [40] H.J. Lee, Y. Xie, Y.M. Koo, N.H.L. Wang, Separation of Lactic Acid from Acetic Acid Using a Four-Zone SMB, *Biotechnol. Prog.* 20 (2004) 179–192. doi:10.1021/bp025663u.
- [41] C.K.S. Ng, H. Osuna-Sanchez, E. Valéry, E. Sørensen, D.G. Bracewell, Design of high productivity antibody capture by protein A chromatography using an integrated experimental and modeling approach, *J. Chromatogr. B.* 899 (2012) 116–126. doi:10.1016/j.jchromb.2012.05.010.
- [42] Z. Ma, D. Tanzil, B.W. Au, N.H.L. Wang, Estimation of solvent-modulated linear adsorption parameters of taxanes from dilute plant tissue culture broth, *Biotechnol. Prog.* 12 (1996) 810–821. doi:10.1021/bp9600748.
- [43] S. Yamamoto, A. Kita, Rational design calculation method for stepwise elution chromatography of proteins, *Food Bioprod. Process.* 84 (2006) 72–77. doi:10.1205/fpb.05180.

- [44] S. Hjerten, O. Levin, A. Tiselius, Protein chromatography on calcium phosphate columns, *Arch. Biochem. Biophys.* 65 (1956) 132.
- [45] S. Yamamoto, T. Suehisa, Y. Sano, Preparative separation of proteins by gradient- and stepwise-elution chromatography: Zone-sharpening effect, *Chem. Eng. Commun.* 119 (1993) 221–230. doi:10.1080/00986449308936117.
- [46] C.K.S. Ng, F. Rousset, E. Valery, D.G. Bracewell, E. Sorensen, Design of high productivity sequential multi-column chromatography for antibody capture, *Food Bioprod. Process.* 92 (2014) 233–241. doi:10.1016/j.fbp.2013.10.003.
- [47] V. Warikoo, R. Godawat, K. Brower, S. Jain, D. Cummings, E. Simons, et al., Integrated continuous production of recombinant therapeutic proteins, *Biotechnol. Bioeng.* 109 (2012) 3018–3029. doi:10.1002/bit.24584.
- [48] E. Mahajan, A. George, B. Wolk, Improving affinity chromatography resin efficiency using semi-continuous chromatography, *J. Chromatogr. A.* 1227 (2012) 154–162. doi:10.1016/j.chroma.2011.12.106.
- [49] J. Pollock, G. Bolton, J. Coffman, S. V. Ho, D.G. Bracewell, S.S. Farid, Optimising the design and operation of semi-continuous affinity chromatography for clinical and commercial manufacture, *J. Chromatogr. A.* 1284 (2013) 17–27. doi:10.1016/j.chroma.2013.01.082.
- [50] R. Godawat, K. Konstantinov, M. Rohani, V. Warikoo, End-to-end integrated fully continuous production of recombinant monoclonal antibodies, *J. Biotechnol.* 213 (2015) 13–19. doi:10.1016/j.jbiotec.2015.06.393.
- [51] H. El-Sabbahy, D. Ward, O. Ogonah, L. Deakin, G.M. Jellum, D.G. Bracewell, The effect of feed quality due to clarification strategy on the design and performance of protein A periodic counter-current chromatography, *Biotechnol. Prog.* 34 (2018) 1380–1392. doi:10.1002/btpr.2709.
- [52] G. Carta, E.X. Perez-Almodovar, Productivity considerations and design charts for biomolecule capture with periodic countercurrent adsorption systems, *Sep. Sci. Technol.* 45 (2010) 149–154. doi:10.1080/01496390903423865.
- [53] M. V Ernest, J.P. Bibler, R.D. Whitley, N.H.L. Wang, Development of a Carousel Ion-Exchange Process for Removal of Cesium-137 from Alkaline Nuclear Waste, *Ind. Eng. Chem. Res.* 36 (1997) 2775–2788. doi:10.1021/ie960729+.

- [54] A.I. Liapis, D.W.T. Rippin, The simulation of binary adsorption in continuous countercurrent operation and a comparison with other operating modes, *AIChE J.* 25 (1979) 455–460. doi:10.1002/aic.690250310.
- [55] M. Angarita, T. Müller-Späth, D. Baur, R. Lievrouw, G. Lissens, M. Morbidelli, Twin-column CaptureSMB: A novel cyclic process for protein A affinity chromatography, *J. Chromatogr. A.* 1389 (2015) 85–95. doi:10.1016/j.chroma.2015.02.046.
- [56] D. Baur, M. Angarita, T. Müller-Späth, M. Morbidelli, Optimal model-based design of the twin-column CaptureSMB process improves capacity utilization and productivity in protein A affinity capture, *Biotechnol. J.* 11 (2016) 135–145. doi:10.1002/biot.201500223.
- [57] L. Aumann, M. Morbidelli, A Continuous Multicolumn Countercurrent Solvent Purification (MCSGP) Process, *Biotechnol. Bioeng.* 988 (2007) 1043–1055. doi:10.1002/bit.
- [58] T. Müller-Späth, L. Aumann, L. Melter, G. Ströhlein, M. Morbidelli, Chromatographic separation of three monoclonal antibody variants using multicolumn countercurrent solvent gradient purification (MCSGP), *Biotechnol. Bioeng.* 100 (2008) 1166–1177. doi:10.1002/bit.21843.
- [59] F. Steinebach, T. Müller-Späth, M. Morbidelli, Continuous counter-current chromatography for capture and polishing steps in biopharmaceutical production, *Biotechnol. J.* 11 (2016) 1126–1141. doi:10.1002/biot.201500354.
- [60] S. Abel, M. Mazzotti, M. Morbidelli, Solvent gradient operation of simulated moving beds, *J. Chromatogr. A.* 1026 (2004) 47–55. doi:10.1016/j.chroma.2003.11.054.
- [61] S. Abel, M. Mazzotti, M. Morbidelli, Solvent gradient operation of simulated moving beds - 2. Langmuir isotherms, *J. Chromatogr. A.* 1026 (2004) 47–55. doi:10.1016/j.chroma.2003.11.054.
- [62] C. Migliorini, M. Wendlinger, M. Mazzotti, M. Morbidelli, Temperature gradient operation of a simulated moving bed unit, *Ind. Eng. Chem. Res.* 40 (2001) 2606–2617. doi:10.1021/ie000825h.
- [63] B. Kelly, Industrialization of MAb production technology, *MAbs.* (2009) 443–452. doi:10.4161/mabs.1.5.9448.
- [64] M. Mazzotti, G. Storti, M. Morbidelli, Optimal operation of simulated moving bed units for nonlinear chromatographic separations, *J. Chromatogr. A.* 769 (1997) 3–24. doi:10.1016/S0021-9673(97)00048-4.

- [65] C.A. Martínez Cristancho, A. Seidel-Morgenstern, Purification of single-chain antibody fragments exploiting pH-gradients in simulated moving bed chromatography, *J. Chromatogr. A.* 1434 (2016) 29–38. doi:10.1016/j.chroma.2016.01.001.
- [66] I. Langmuir, THE ADSORPTION OF GASES ON PLANE SURFACES OF GLASS, MICA AND PLATINUM., *J. Am. Chem. Soc.* 40 (1918) 1361–1403. doi:10.1021/ja02242a004.
- [67] Y. Wang, A. Lomakin, R.F. Latypov, J.P. Laubach, T. Hideshima, P.G. Richardson, et al., Phase transitions in human IgG solutions, *J. Chem. Phys.* 139 (2013) 1–9. doi:10.1063/1.4811345.
- [68] C.K. Gupta, N. Krishnamurthy, Extractive metallurgy of rare earths, *Int. Mater. Rev.* 37 (1992) 197–248. doi:10.1179/imr.1992.37.1.197.
- [69] USGS, Rare Earths, 2019.
- [70] E. Vahidi, F. Zhao, Environmental life cycle assessment on the separation of rare earth oxides through solvent extraction, *J. Environ. Manage.* 203 (2017) 255–263. doi:10.1016/j.jenvman.2017.07.076.
- [71] G.G. Zaines, B.J. Hubler, S. Wang, V. Khanna, Environmental Life Cycle Perspective on Rare Earth Oxide Production, *ACS Sustain. Chem. Eng.* 3 (2015) 237–244. doi:10.1021/sc500573b.
- [72] F. Xie, T.A. Zhang, D. Dreisinger, F. Doyle, A critical review on solvent extraction of rare earths from aqueous solutions, *Miner. Eng.* 56 (2014) 10–28. doi:10.1016/j.mineng.2013.10.021.
- [73] L. Ling, N.H.L. Wang, Ligand-assisted elution chromatography for separation of lanthanides, *J. Chromatogr. A.* 1389 (2015) 28–38. doi:10.1016/j.chroma.2015.02.004.
- [74] H. Choi, D. Harvey, Y. Ding, N.H.L. Wang, Constant-pattern design method for the separation of ternary mixtures of rare earth elements using ligand-assisted displacement chromatography, *J. Chromatogr. A.* 1580 (2018) 49–62. doi:10.1016/j.chroma.2018.09.056.
- [75] H. Choi, D. Harvey, Y. Ding, N.L. Wang, Key parameters controlling the development of constant-pattern isotachic trains of two rare earth elements in ligand-assisted displacement chromatography, *J. Chromatogr. A.* 1563 (2018) 47–61. doi:10.1016/j.chroma.2018.05.057.

- [76] C.H. González, A.J.Q. Cabezas, M.F. Díaz, Preconcentration and determination of rare-earth elements in iron-rich water samples by extraction chromatography and plasma source mass spectrometry (ICP-MS), *Talanta*. 68 (2005) 47–53. doi:10.1016/j.talanta.2005.04.046.
- [77] F.H. Spedding, E.I. Fulmer, T.A. Butler, E.M. Gladrow, M. Gobush, P.E. Porter, et al., The Separation of Rare Earths by Ion Exchange. III. Pilot Plant Scale Separations, *J. Am. Chem. Soc.* 69 (1947) 2812–2818.
- [78] F.H. Spedding, A.F. Voigt, E.M. Gladrow, N.R. Sleight, The separation of rare earths by ion exchange; cerium and yttrium., *J. Am. Chem. Soc.* 69 (1947) 2777–2781. doi:10.1021/ja01203a060.
- [79] F.H. Spedding, E.I. Fulmer, T.A. Butler, J.E. Powerll, The separation of rare earths by ion exchange IV. Further investigations concerning variables involved in the separation of samarium, neodymium, and praseodymium, *J. Am. Chem. Soc.* 72 (1950) 2349–2354.
- [80] F. Spedding, J. Powell, The separation of rare earths by ion exchange. VII. Quantitative data for the elution of Neodymium, *J. Am. Chem. Soc.* 76 (1954) 2545–2550. doi:10.1021/ja01638a073.
- [81] F. Spedding, J. Powell, The Separation of Rare Earths by Ion Exchange. VIII. Quantitative Theory of the Mechanism Involved in Elution by Dilute Citrate Solutions, *J. Am. Chem. Soc.* 76 (1954) 2550–2557. doi:10.1021/ja01638a074.
- [82] D.B. James, J.E. Powell, F.H. Spedding, Cation-Exchange Elution Sequences--I Divalent and Rare-Earth Cations with EDTA HEDTA and Citrate, *J. Inorg. Nucl. Chem.* 19 (1961) 133–141.
- [83] R.E. Lindstrom, Separation of Rare-Earth Elements in Bastnasite by Ion Exchange, 1958.
- [84] B.R.E. Lindstrom, J.S. Berber, Effect of temperature in ion-exchange separation of rare-earth elements and recovery of EDTA from effluent solutions, Washington DC, 1961.
- [85] F. Helfferich, D.B. James, An Equilibrium Theory for Rare-Earth Separation by Displacement Development, *J. Chromatogr.* 46 (1970) 1–28.
- [86] B.W. Moore, L.J. Froisland, A.E. Petersen, Rapid separation of heavy rare-earth elements, 1995. <https://search.library.wisc.edu/catalog/999776393902121>.

- [87] Y. Ding, D. Harvey, N.-H.L. Wang, Two-zone ligand-assisted displacement chromatography for producing high-purity praseodymium, neodymium, and dysprosium with high yield and high productivity from crude mixtures derived from waste magnets, *Green Chem.* (2020). doi:10.1039/d0gc00495b.

VITA

David Harvey was born to Dennis and Karen Harvey on February 16, 1993 in Marion, IN. He graduated from Marion High School in May 2011. In August of 2011, he entered Rose-Hulman Institute of Technology where he graduated with his B.S. in Chemical Engineering and Chemistry in May 2015. He entered Purdue University in August of 2015 where he pursued his doctoral degree under the supervision of Prof. Nien-Hwa Linda Wang. He received his Ph.D. in Chemical Engineering in May 2020.

PUBLICATIONS

Harvey, D., Weeden, G., Wang, N.H.L., “Speedy Standing Wave Design and Simulated Moving Bed Splitting Strategies for the Separation of Ternary Mixtures with Linear Isotherms,” *J. Chromatogr. A*. Vol. 1530, 29, (2017), 152-170

Choi, H., Harvey, D., Ding, Y., and Wang, N.-H. L., “Key parameters controlling the development of constant-pattern isotachic trains of two rare earth elements in ligand-assisted displacement chromatography.” *J. Chromatogr. A*. Vol. 1563, 17, (2018), 47-61

Choi, H., Harvey, D., Ding, Y., and Wang, N.-H. L., “Constant-pattern design method for the separation of ternary mixtures of rare earth elements using ligand-assisted displacement chromatography.” *J. Chromatogr. A*. Vol. 1580, 14, (2018), 49-62

Harvey, D., Ding, Y., and Wang, N. -H., L., “Standing-Wave Design of Three-Zone Non-Isocratic SMB for Capture or Purification.” *BMC Chemical Engineering* Vol. 1, 17 (2019)

Y. Ding, D. Harvey, N.-H.L. Wang, Two-zone ligand-assisted displacement chromatography for producing high-purity praseodymium, neodymium, and dysprosium with high yield and high productivity from crude mixtures derived from waste magnets, *Green Chem.* (2020). doi:10.1039/d0gc00495b.